



TETRA TECH

Regional Groundwater Flow Model

Rosemont Copper Project

This report presents the results of a regional groundwater flow model developed for the Rosemont project. This geologically based, numerical flow model predicts the formation of a pit-lake within the proposed Rosemont Open Pit following the cessation of dewatering. Additionally, the pit-lake will be a hydraulic sink, meaning that water will flow into and not out of the pit due to the high evaporation rate of the area.



November 2010

Regional Groundwater Flow Model

Rosemont Copper Project

This report presents the results of a regional groundwater flow model developed for the Rosemont project. This geologically based, numerical flow model predicts the formation of a pit-lake within the proposed Rosemont Open Pit following the cessation of dewatering. Additionally, the pit-lake will be a hydraulic sink, meaning that water will flow into and not out of the pit due to the high evaporation rate of the area.

Prepared for:



4500 Cherry Creek South Drive, Suite #1040

Denver, Colorado 80246

(303) 300-0138

Fax (303) 300-0135

Prepared by:



3031 West Ina Road

Tucson, AZ 85741

(520) 297-7723

Fax (520) 297-7724

Tetra Tech Project No. 114-320874

November 2010

ROSEMONT COPPER PROJECT

REGIONAL GROUNDWATER FLOW MODEL

The following document has been prepared by the staff of Tetra Tech under the direct supervision of an Arizona Registered Professional Geologist, whose seal and signature appear below.

The INFORMATION presented here was prepared in accordance with generally accepted professional hydrogeologic practices.



Expires: 6/30/12

Michael Gabora, P.G.

TABLE OF CONTENTS

| | |
|--|-----------|
| ROSEMONT COPPER PROJECT | 2 |
| 1.0 INTRODUCTION..... | 5 |
| 1.1 Project Objectives | 5 |
| 1.2 Project Scope | 6 |
| 1.3 Approach | 6 |
| 1.4 Previous Studies | 7 |
| 1.5 Report Organization | 8 |
| 2.0 CONCEPTUAL GROUNDWATER MODEL | 10 |
| 2.1 Model Study Area Description | 10 |
| 2.2 Hydrogeology | 11 |
| 2.3 Stream Flow, Springs, and Riparian Vegetation..... | 13 |
| 2.3.1 Groundwater / Surface-Water Interactions..... | 14 |
| 2.3.2 Local and Regional Springs | 15 |
| 2.3.3 Riparian Vegetation..... | 17 |
| 2.4 Groundwater Flow System Boundaries | 18 |
| 2.5 Recharge..... | 18 |
| 2.6 Evapotranspiration | 19 |
| 2.7 Groundwater Pumping | 20 |
| 2.8 Groundwater and Surface-Water Fluctuations | 20 |
| 3.0 POTENTIAL IMPACTS..... | 22 |
| 3.1 Stream Flow | 22 |
| 3.2 Riparian Vegetation..... | 22 |
| 3.3 Water Quality..... | 23 |
| 3.4 Local and Regional Springs | 23 |
| 3.5 Groundwater System Changes | 23 |
| 4.0 HYDROGEOLOGIC FRAMEWORK..... | 25 |
| 4.1 Hydrogeologic Units | 25 |
| 4.1.1 Quaternary and Recent Alluvium (Qal)..... | 27 |
| 4.1.2 Late Tertiary and Quaternary Basin-Fill Deposits (QTg, QTg1, and QTg2) | 27 |
| 4.1.3 Early to Mid-Tertiary Sedimentary and Volcanic Rocks (Tsp)..... | 28 |
| 4.1.4 Upper Cretaceous and Early Tertiary Intrusive Rocks (KTi)..... | 28 |
| 4.1.5 Upper Cretaceous Volcanic and Sedimentary Rocks (Kv) | 28 |
| 4.1.6 Lower Cretaceous Sedimentary Rocks (Bisbee Group) (Ksd) | 28 |

| | | |
|------------|---|-----------|
| 4.1.7 | Paleozoic Sedimentary and Altered Sedimentary Rocks (Pz)..... | 29 |
| 4.1.8 | Precambrian Basement Rocks (pCb)..... | 30 |
| 4.2 | Hydrogeologic Framework Model..... | 30 |
| 4.2.1 | Approach..... | 30 |
| 4.2.2 | 3D Framework Model..... | 30 |
| 4.3 | Hydraulic Properties..... | 32 |
| 4.3.1 | Geologic Units..... | 32 |
| 4.3.2 | Short-Term Aquifer Test Analysis..... | 33 |
| 4.3.3 | Long-Term Pumping Test..... | 34 |
| 4.3.4 | Analysis Method Selection..... | 35 |
| 4.3.5 | Radial Flow Model Development..... | 36 |
| 4.3.6 | Aquifer Storage Properties..... | 42 |
| 4.3.7 | Hydraulic Property Summary..... | 43 |
| 5.0 | REGIONAL GROUNDWATER FLOW MODEL CONSTRUCTION..... | 45 |
| 5.1 | Modeling Approach..... | 45 |
| 5.2 | Model Code Selection..... | 45 |
| 5.3 | Model Domain..... | 46 |
| 5.4 | Horizontal and Vertical Model Grid..... | 46 |
| 5.5 | Hydrogeologic Framework..... | 47 |
| 5.6 | Recharge Distribution..... | 47 |
| 5.6.1 | Methodology..... | 48 |
| 5.6.2 | Mining-Phase Recharge..... | 49 |
| 5.6.3 | Post-Closure Recharge..... | 49 |
| 5.7 | Evapotranspiration..... | 51 |
| 5.8 | Stream Flow..... | 51 |
| 5.9 | Geologic Structures..... | 53 |
| 5.10 | External Model Boundaries..... | 53 |
| 5.11 | Existing Groundwater Use..... | 54 |
| 6.0 | STEADY-STATE MODEL CALIBRATION..... | 55 |
| 6.1 | Calibration Targets and Weights..... | 55 |
| 6.2 | Calibrated Model Parameter Values..... | 58 |
| 6.2.1 | Horizontal Hydraulic Conductivity..... | 59 |
| 6.2.2 | Vertical Hydraulic Conductivity..... | 59 |
| 6.2.3 | Hydraulic-Conductivity Scale Differences..... | 60 |

| | | |
|------------|--|-----------|
| 6.2.4 | Recharge | 60 |
| 6.2.5 | Evapotranspiration | 60 |
| 6.2.6 | Stream Flow | 61 |
| 6.2.7 | Quartz-Porphry Dike | 62 |
| 6.3 | Steady-State Calibration Statistics | 62 |
| 6.4 | Steady-State Mass Balance | 63 |
| 7.0 | TRANSIENT MODEL CALIBRATION | 65 |
| 7.1 | Storage Parameters | 65 |
| 8.0 | PREDICTIVE SIMULATIONS | 67 |
| 8.1 | Mining-Phase Pit-Dewatering Simulation | 67 |
| 8.1.1 | Pit Inflows | 68 |
| 8.1.2 | Predicted Groundwater Level Drawdown | 69 |
| 8.1.3 | Predicted Surface-Water Flows | 70 |
| 8.2 | Post-Closure Pit-Lake Simulation | 70 |
| 8.2.1 | Lake-Package Inputs | 71 |
| 8.2.2 | Stress Period Set-up | 72 |
| 8.3 | Post-Closure Phase Simulation Results | 73 |
| 8.3.1 | Predicted Groundwater Level Drawdown | 73 |
| 8.3.2 | Predicted Surface-Water Flows and Evapotranspiration | 75 |
| 8.4 | Predictive Model Mass Balance | 76 |
| 8.4.1 | Pit Lake Mass Balance | 78 |
| 9.0 | SENSITIVITY ANALYSES | 80 |
| 9.1 | Model Parameters | 80 |
| 9.2 | Steady-State Parameter Sensitivity | 81 |
| 9.2.1 | Steady-State Sensitivity Simulations | 82 |
| 9.2.2 | Vertical Hydraulic Conductivity by Zone | 83 |
| 9.2.3 | Vertical Hydraulic Conductivity by Rock Type | 84 |
| 9.2.4 | Recharge | 84 |
| 9.2.5 | Streambed Hydraulic Conductivity and Horizontal Flow Barrier | 84 |
| 9.3 | Western Flow Model Boundary | 84 |
| 9.3.1 | No-Flow Boundary | 84 |
| 9.3.2 | General Head Boundary | 85 |
| 9.4 | Mining-Phase Sensitivities | 85 |
| 9.4.1 | Basin-Fill Horizontal Hydraulic Conductivity | 86 |

| | | |
|-------------|--|------------|
| 9.4.2 | Bedrock Horizontal Hydraulic Conductivity..... | 86 |
| 9.4.3 | Basin-Fill Vertical Hydraulic Conductivity | 87 |
| 9.4.4 | Bedrock Vertical Hydraulic Conductivity..... | 87 |
| 9.4.5 | Quartz-Porphry Hydraulic Conductivity..... | 87 |
| 9.4.6 | Storage Parameters | 87 |
| 9.5 | Post-Closure Sensitivities..... | 88 |
| 9.5.1 | Pit Lake Sensitivity Analysis | 89 |
| 9.5.2 | Basin-Fill Horizontal Hydraulic Conductivity | 95 |
| 9.5.3 | Bedrock Horizontal Hydraulic Conductivity..... | 95 |
| 9.5.4 | Basin-Fill Vertical Hydraulic Conductivity | 95 |
| 9.5.5 | Bedrock Vertical Hydraulic Conductivity..... | 95 |
| 9.5.6 | Quartz-Porphry Dike Hydraulic Conductivity | 95 |
| 9.5.7 | Storage Parameters | 95 |
| 9.5.8 | Facility Area Recharge | 96 |
| 9.6 | Sensitivity Analysis Summary..... | 99 |
| 10.0 | DISCHARGE IMPACT AREA ANALYSIS | 100 |
| 10.1 | Analysis Approach..... | 100 |
| 10.2 | Mine Facilities and Changes in Hydrogeologic Conditions..... | 100 |
| 10.3 | Particle-Tracking Simulations..... | 101 |
| 10.3.1 | Particle-Tracking Model Input Parameters | 102 |
| 10.3.2 | Particle Starting Locations..... | 102 |
| 10.3.3 | Particle Tracking Simulation Results | 103 |
| 10.4 | Groundwater Quality Evaluation..... | 104 |
| 10.4.1 | Facilities Area Recharge Water Quality..... | 105 |
| 10.5 | Discharge Impact Analysis Conclusions..... | 107 |
| 11.0 | SUMMARY AND CONCLUSIONS | 108 |
| 11.1 | Open Pit | 108 |
| 11.2 | Stream Flows | 108 |
| 11.3 | Riparian Vegetation | 109 |
| 11.4 | Local and Regional Springs | 109 |
| 11.5 | Groundwater Quality | 109 |
| 11.6 | Conclusions..... | 110 |
| 12.0 | REFERENCES..... | 111 |

LIST OF TABLES

| | | |
|-----------|--|----|
| Table 2-1 | Flow Characteristics of Selected Springs in the Rosemont Project Area | 17 |
| Table 4-1 | Hydrogeologic Units used in the Hydrogeologic Framework Model | 26 |
| Table 4-2 | Hydraulic-Parameter Estimates for Observation Well PZ-5 from Long-Term Pumping in Well PC-5..... | 40 |
| Table 4-3 | Hydraulic-Parameter Estimates for Observation Well PC-2 from Long-Term Pumping in Well PC-5..... | 40 |
| Table 4-4 | Hydraulic-Parameter Estimates for Observation Well HC-1A from Long-Term Pumping in Well HC-1B..... | 41 |
| Table 4-5 | Hydraulic-Parameter Estimates for Observation Well HC-5B from Long-Term Pumping in Well HC-5A..... | 42 |
| Table 4-6 | Initial Hydrogeologic Unit Parameter Estimates for 3D Regional Groundwater Flow Model Calibration | 44 |
| Table 5-1 | Model Layer Elevations and Thicknesses | 47 |
| Table 5-2 | Summary of Monthly Mean Stream Flows..... | 52 |
| Table 6-1 | Weighting Criteria for Steady-State Calibration Water-Level Targets | 57 |
| Table 6-2 | Steady-State Calibration Stream-Flow Targets and Weights | 57 |
| Table 6-3 | Steady-State Model Initial and Calibrated Parameter Values | 58 |
| Table 6-4 | Simulated Pre-Mining Steady-State Stream Flows by Reach | 61 |
| Table 6-5 | Pre-Mining Steady-State Model Calibration Statistics | 63 |
| Table 6-6 | Mass Balance Summary for Pre-Mining Steady-State Model | 64 |
| Table 7-1 | Storage Parameter Values Simulated in the Mining-Phase and Post-Closure Predictive Simulations | 66 |
| Table 8-1 | Mining-Phase Simulation Stress Period Set-Up..... | 68 |
| Table 8-2 | Post-Closure Simulation Stress Period Set-Up | 73 |
| Table 8-3 | Mass Balance for Predictive Simulations | 77 |
| Table 8-4 | Simulated Pit-Lake Water Balance 1,000 Years after End of Operations | 79 |
| Table 9-1 | Final Hydrogeologic Unit Parameters Evaluated in the Sensitivity Analysis | 81 |
| Table 9-2 | Steady-State Model Composite Scaled Sensitivities for the Most Sensitive Parameters..... | 82 |
| Table 9-3 | Sensitivity Analysis Parameter Changes for the Pre-Mining Steady-State Model..... | 83 |
| Table 9-4 | Sensitivity Analysis Parameter Changes for the Mining-Phase Simulation..... | 86 |
| Table 9-6 | Pit-Lake Parameter Values used in the Sensitivity Analysis | 90 |
| Table 9-7 | Simulated Pit-Lake Stage and Groundwater Inflow Resulting from Pit-Lake Parameter Sensitivity Analysis | 90 |
| Table 9-7 | Simulated Pit-Lake Stage and Groundwater Inflow Resulting from Pit-Lake Parameter Sensitivity Analysis (continued) | 91 |

| | | |
|------------|--|-----|
| Table 9-8 | Cumulative Change in Stream Flow for Pit-Lake Parameter Sensitivity Simulations..... | 92 |
| Table 9-8 | Cumulative Change in Stream Flow for Pit-Lake Parameter Sensitivity Simulations (continued)..... | 93 |
| Table 9-9 | Simulated Change in Evapotranspiration Resulting from Pit-Lake Sensitivity Analysis..... | 93 |
| Table 9-10 | Simulated Change in Pit-Lake Stage and Groundwater Inflows Resulting from Recharge Sensitivity Analysis..... | 97 |
| Table 9-11 | Cumulative Change in Stream Flow for Recharge Sensitivity Simulation..... | 98 |
| Table 10-1 | Potential Mining-Related Sources of Groundwater Recharge..... | 101 |
| Table 10-2 | Particle Starting Locations..... | 102 |
| Table 10-2 | Particle Starting Locations (Continued)..... | 103 |
| Table 10-3 | Summary of Background Groundwater Quality Data..... | 105 |
| Table 10-4 | Summary of Water Quality Data for Project-Related Sources and Background Groundwater..... | 106 |

LIST OF FIGURES

| | |
|-------------|--|
| Figure 1-1 | Site Location Map |
| Figure 1-2 | Study Area Map |
| Figure 4-1 | Hydrogeologic Framework Model |
| Figure 4-2 | Hydrogeologic Framework Model Displayed in Section |
| Figure 4-3 | Comparison of Geologic Section A - A' with Hydrogeologic Framework Model |
| Figure 4-4 | Comparison of Geologic Section B - B' with Hydrogeologic Framework Model |
| Figure 4-5 | Location of Long-Term Tests |
| Figure 4-6 | Geologic Section for PC-2, PC-5, and PZ-5 |
| Figure 4-7 | Radial Flow Model Geologic Section from HC-1A to HC-1B |
| Figure 4-8 | Radial Flow Model Geologic Section from HC-5A to HC-5B |
| Figure 4-9 | Radial Flow Model Geologic Sections for PC-2 to PC-5 and PC-5 to PZ-5 |
| Figure 4-10 | Simulated Versus Observed Drawdown at PZ-5 (600) During Multi-Well Aquifer Test |
| Figure 4-11 | Simulated Versus Observed Drawdown at PZ-5 (1150) During Multi-Well Aquifer Test |
| Figure 4-12 | Simulated Versus Observed Drawdown at PZ-5 (1800) During Multi-Well Aquifer Test |
| Figure 4-13 | Simulated Versus Observed Drawdown at PC-2 During Multi-Well Aquifer Test |
| Figure 4-14 | Simulated Versus Observed Drawdown at HC-1A During Multi-Well Aquifer Test |
| Figure 4-15 | Simulated Versus Observed Drawdown at HC-5B During Multi-Well Aquifer Test |
| Figure 5-1 | Groundwater Flow Model Domain |
| Figure 5-2 | Groundwater Flow Model Grid |
| Figure 5-3 | Groundwater Flow Model Layers Vertical Discretization |
| Figure 5-4 | Estimated Recharge Distribution |
| Figure 5-5 | Post-Closure Recharge in Project Facility Area |
| Figure 5-6 | Post-Closure Recharge from Dry Stack Tailings Facility Drain-Down |
| Figure 5-7 | Maximum Simulated Evapotranspiration Rates |
| Figure 5-8 | Stream Gage Locations and Simulated Stream Flow Routing (SFR) Package Cells |
| Figure 5-9 | Geologic Map with Quartz-Porphyry Dike |

| | |
|-------------|--|
| Figure 5-10 | Quartz-Porphry Dike Simulated as a Horizontal Flow Barrier (HFB) |
| Figure 6-1 | Calibration Weights for Target Water Levels |
| Figure 6-2 | Observed Pre-Mining, Steady-State Potentiometric Surface Map and Upper Most Model Layer with Constant Head |
| Figure 6-3 | Observed and Simulated Hydraulic Conductivity Values |
| Figure 6-4 | Model Layer 1 Hydraulic Conductivity Distribution |
| Figure 6-5 | Model Layer 2 Hydraulic Conductivity Distribution |
| Figure 6-6 | Model Layer 3 Hydraulic Conductivity Distribution |
| Figure 6-7 | Model Layer 4 Hydraulic Conductivity Distribution |
| Figure 6-8 | Model Layer 5 Hydraulic Conductivity Distribution |
| Figure 6-9 | Model Layer 6 Hydraulic Conductivity Distribution |
| Figure 6-10 | Model Layer 7 Hydraulic Conductivity Distribution |
| Figure 6-11 | Model Layer 8 Hydraulic Conductivity Distribution |
| Figure 6-12 | Model Layer 9 Hydraulic Conductivity Distribution |
| Figure 6-13 | Model Layer 10 Hydraulic Conductivity Distribution |
| Figure 6-14 | Model Layer 11 Hydraulic Conductivity Distribution |
| Figure 6-15 | Model Layer 12 Hydraulic Conductivity Distribution |
| Figure 6-16 | Model Layer 13 Hydraulic Conductivity Distribution |
| Figure 6-17 | Model Layer 14 Hydraulic Conductivity Distribution |
| Figure 6-18 | Model Layer 15 Hydraulic Conductivity Distribution |
| Figure 6-19 | Model Layer 16 Hydraulic Conductivity Distribution |
| Figure 6-20 | Model Layer 17 Hydraulic Conductivity Distribution |
| Figure 6-21 | Model Layer 18 Hydraulic Conductivity Distribution |
| Figure 6-22 | Model Layer 19 Hydraulic Conductivity Distribution |
| Figure 6-23 | Model Layer 20 Hydraulic Conductivity Distribution |
| Figure 6-24 | Simulated Pre-Mining, Steady-State Recharge |
| Figure 6-25 | Weighted Water-Level Residuals for Calibrated Steady-State Model |
| Figure 6-26 | Unweighted Water-Level Residuals for Calibrated Steady-State Model |
| Figure 6-27 | Observed versus Simulated Water Levels |
| Figure 6-28 | Observed versus Unweighted Residuals |
| Figure 6-29 | Simulated versus Observed Potentiometric Surface Map |
| Figure 6-30 | Simulated Steady-State Stream Flows |
| Figure 8-1 | Simulated Drain-Cell Nodes in the Ultimate 2032 Pit Shell |
| Figure 8-2 | Simulated Progression of Open Pit Development |

LIST OF FIGURES

| | |
|-------------|--|
| Figure 1-1 | Site Location Map |
| Figure 1-2 | Study Area Map |
| Figure 4-1 | Hydrogeologic Framework Model |
| Figure 4-2 | Hydrogeologic Framework Model Displayed in Section |
| Figure 4-3 | Comparison of Geologic Section A - A' with Hydrogeologic Framework Model |
| Figure 4-4 | Comparison of Geologic Section B - B' with Hydrogeologic Framework Model |
| Figure 4-5 | Location of Long-Term Tests |
| Figure 4-6 | Geologic Section for PC-2, PC-5, and PZ-5 |
| Figure 4-7 | Radial Flow Model Geologic Section from HC-1A to HC-1B |
| Figure 4-8 | Radial Flow Model Geologic Section from HC-5A to HC-5B |
| Figure 4-9 | Radial Flow Model Geologic Sections for PC-2 to PC-5 and PC-5 to PZ-5 |
| Figure 4-10 | Simulated Versus Observed Drawdown at PZ-5 (600) During Multi-Well Aquifer Test |
| Figure 4-11 | Simulated Versus Observed Drawdown at PZ-5 (1150) During Multi-Well Aquifer Test |
| Figure 4-12 | Simulated Versus Observed Drawdown at PZ-5 (1800) During Multi-Well Aquifer Test |
| Figure 4-13 | Simulated Versus Observed Drawdown at PC-2 During Multi-Well Aquifer Test |
| Figure 4-14 | Simulated Versus Observed Drawdown at HC-1A During Multi-Well Aquifer Test |
| Figure 4-15 | Simulated Versus Observed Drawdown at HC-5B During Multi-Well Aquifer Test |
| Figure 5-1 | Groundwater Flow Model Domain |
| Figure 5-2 | Groundwater Flow Model Grid |
| Figure 5-3 | Groundwater Flow Model Layers Vertical Discretization |
| Figure 5-4 | Estimated Recharge Distribution |
| Figure 5-5 | Post-Closure Recharge in Project Facility Area |
| Figure 5-6 | Post-Closure Recharge from Dry Stack Tailings Facility Drain-Down |
| Figure 5-7 | Maximum Simulated Evapotranspiration Rates |
| Figure 5-8 | Stream Gage Locations and Simulated Stream Flow Routing (SFR) Package Cells |
| Figure 5-9 | Geologic Map with Quartz-Porphyry Dike |

| | |
|-------------|--|
| Figure 5-10 | Quartz-Porphry Dike Simulated as a Horizontal Flow Barrier (HFB) |
| Figure 6-1 | Calibration Weights for Target Water Levels |
| Figure 6-2 | Observed Pre-Mining, Steady-State Potentiometric Surface Map and Upper Most Model Layer with Constant Head |
| Figure 6-3 | Observed and Simulated Hydraulic Conductivity Values |
| Figure 6-4 | Model Layer 1 Hydraulic Conductivity Distribution |
| Figure 6-5 | Model Layer 2 Hydraulic Conductivity Distribution |
| Figure 6-6 | Model Layer 3 Hydraulic Conductivity Distribution |
| Figure 6-7 | Model Layer 4 Hydraulic Conductivity Distribution |
| Figure 6-8 | Model Layer 5 Hydraulic Conductivity Distribution |
| Figure 6-9 | Model Layer 6 Hydraulic Conductivity Distribution |
| Figure 6-10 | Model Layer 7 Hydraulic Conductivity Distribution |
| Figure 6-11 | Model Layer 8 Hydraulic Conductivity Distribution |
| Figure 6-12 | Model Layer 9 Hydraulic Conductivity Distribution |
| Figure 6-13 | Model Layer 10 Hydraulic Conductivity Distribution |
| Figure 6-14 | Model Layer 11 Hydraulic Conductivity Distribution |
| Figure 6-15 | Model Layer 12 Hydraulic Conductivity Distribution |
| Figure 6-16 | Model Layer 13 Hydraulic Conductivity Distribution |
| Figure 6-17 | Model Layer 14 Hydraulic Conductivity Distribution |
| Figure 6-18 | Model Layer 15 Hydraulic Conductivity Distribution |
| Figure 6-19 | Model Layer 16 Hydraulic Conductivity Distribution |
| Figure 6-20 | Model Layer 17 Hydraulic Conductivity Distribution |
| Figure 6-21 | Model Layer 18 Hydraulic Conductivity Distribution |
| Figure 6-22 | Model Layer 19 Hydraulic Conductivity Distribution |
| Figure 6-23 | Model Layer 20 Hydraulic Conductivity Distribution |
| Figure 6-24 | Simulated Pre-Mining, Steady-State Recharge |
| Figure 6-25 | Weighted Water-Level Residuals for Calibrated Steady-State Model |
| Figure 6-26 | Unweighted Water-Level Residuals for Calibrated Steady-State Model |
| Figure 6-27 | Observed versus Simulated Water Levels |
| Figure 6-28 | Observed versus Unweighted Residuals |
| Figure 6-29 | Simulated versus Observed Potentiometric Surface Map |
| Figure 6-30 | Simulated Steady-State Stream Flows |
| Figure 8-1 | Simulated Drain-Cell Nodes in the Ultimate 2032 Pit Shell |
| Figure 8-2 | Simulated Progression of Open Pit Development |

- Figure 8-3 Simulated Groundwater Inflow During Operations
- Figure 8-4 Simulated Water Table Along Row 105 at the End of Operations
- Figure 8-5 Predicted Groundwater Level Drawdown at End of Operations (Layer 17)
- Figure 8-6 Simulated Change in Stream Flows at End of Operations
- Figure 8-7 Predicted Groundwater-Level Drawdown at Simulated Observation Locations
- Figure 8-8 Lake Package Configuration for Bottom Cells
- Figure 8-9 Stage-Area Relationship in the Lake Package
- Figure 8-10 Predicted Groundwater Level Drawdown 20 Years After End of Operations (Layer 17)
- Figure 8-11 Predicted Groundwater Level Drawdown 50 Years After End of Operations (Layer 17)
- Figure 8-12 Predicted Groundwater Level Drawdown 150 Years After End of Operations (Layer 17)
- Figure 8-13 Predicted Groundwater Level Drawdown 1,000 Years After End of Operations (Layer 17)
- Figure 8-14 Comparison of Drawdown at 1,000 and 1,500 Years Post-Closure
- Figure 8-15 Simulated Change in Stream Flows 1,000 Years After End of Operations
- Figure 8-16 Simulated Pit-Lake Water Balance
- Figure 9-1 Horizontal Hydraulic Conductivity Sensitivity by Zone
- Figure 9-2 Horizontal Hydraulic Conductivity Sensitivity by Rock Type
- Figure 9-3 Vertical Hydraulic Conductivity Sensitivity by Zone
- Figure 9-4 Vertical Hydraulic Conductivity Sensitivity by Rock Type
- Figure 9-5 Recharge Sensitivity
- Figure 9-6 Streambed Hydraulic Conductivity and Horizontal Flow Barrier (HFB) Sensitivity
- Figure 9-7 Western Model Boundary as General Head Boundary with Results at End of Operations
- Figure 9-8 Western Model Boundary as General Head Boundary with Results at 150 Years Post-Closure
- Figure 9-9 Western Model Boundary as General Head Boundary with Results at 1,000 Years Post-Closure
- Figure 9-10 30 Percent Basin-Fill Horizontal Hydraulic Conductivity Decrease Model with Results at End of Operations
- Figure 9-11 30 Percent Basin-Fill Horizontal Hydraulic Conductivity Increase Model with Results at End of Operations
- Figure 9-12 10 Percent Bedrock Horizontal Hydraulic Conductivity Decrease Model with Results at End of Operations

- Figure 9-13 30 Percent Bedrock Horizontal Hydraulic Conductivity Increase Model with Results at End of Operations
- Figure 9-14 30 Percent Basin-Fill Vertical Hydraulic Conductivity Decrease Model with Results at End of Operations
- Figure 9-15 30 Percent Basin-Fill Vertical Hydraulic Conductivity Increase Model with Results at End of Operations
- Figure 9-16 10 Percent Bedrock Vertical Hydraulic Conductivity Decrease Model with Results at End of Operations
- Figure 9-17 30 Percent Bedrock Vertical Hydraulic Conductivity Increase Model with Results at End of Operations
- Figure 9-18 Order of Magnitude HFB Hydraulic Conductivity Decrease Model with Results at End of Operations
- Figure 9-19 Order of Magnitude HFB Hydraulic Conductivity Increase Model with Results at End of Operations
- Figure 9-20 Order of Magnitude Specific Storage Decrease Model with Results at End of Operations
- Figure 9-21 Order of Magnitude Specific Storage Increase Model with Results at End of Operations
- Figure 9-22 50 Percent Basin-Fill Specific Yield Decrease Model with Results at End of Operations
- Figure 9-23 50 Percent Basin-Fill Specific Yield Increase Model with Results at End of Operations
- Figure 9-24 Factor of 2 Bedrock Specific Yield Decrease Model with Results at End of Operations
- Figure 9-25 Factor of 2 Bedrock Specific Yield Increase Model with Results at End of Operations
- Figure 9-26 Comparison of Drawdown at 1,000 and 1,500 Years Post-Closure
- Figure 9-27 Comparison of End of Operations, 150 Years Post-Closure, and 1,000 Years Post-Closure Drawdown Contours
- Figure 9-28 30 Percent Pit-Lake Precipitation Decrease Model With Results at 150 Years Post-Closure
- Figure 9-29 30 Percent Pit-Lake Precipitation Decrease Model with Results at 1,000 Years Post-Closure
- Figure 9-30 30 Percent Pit-Lake Precipitation Increase Model with Results at 150 Years Post-Closure
- Figure 9-31 30 Percent Pit-Lake Precipitation Increase Model with Results at 1,000 Years Post-Closure
- Figure 9-32 20 Percent Pit-Lake Evaporation Decrease Model with Results at 150 Years Post-Closure
- Figure 9-33 20 Percent Pit-Lake Evaporation Decrease Model with Results at 1,000 Years Post-Closure

- Figure 9-34 20 Percent Pit-Lake Evaporation Increase Model with Results at 150 Years Post-Closure
- Figure 9-35 20 Percent Pit-Lake Evaporation Increase Model with Results at 1,000 Years Post-Closure
- Figure 9-36 20 Percent Pit-Wall Runoff Model with Results at 150 Years Post-Closure
- Figure 9-37 20 Percent Pit-Wall Runoff Model with Results at 1,000 Years Post-Closure
- Figure 9-38 40 Percent Pit-Wall Runoff Model with Results at 150 Years Post-Closure
- Figure 9-39 40 Percent Pit-Wall Runoff Model with Results at 1,000 Years Post-Closure
- Figure 9-40 30 Percent Basin Fill Horizontal Hydraulic Conductivity Decrease Model with Results at 150 Years Post-Closure
- Figure 9-41 30 Percent Basin Fill Horizontal Hydraulic Conductivity Decrease Model with Results at 1,000 Years Post-Closure
- Figure 9-42 30 Percent Basin Fill Horizontal Hydraulic Conductivity Increase Model with Results at 150 Years Post-Closure
- Figure 9-43 30 Percent Basin Fill Horizontal Hydraulic Conductivity Increase Model with Results at 1,000 Years Post-Closure
- Figure 9-44 10 Percent Bedrock Horizontal Hydraulic Conductivity Decrease Model with Results at 150 Years Post-Closure
- Figure 9-45 10 Percent Bedrock Horizontal Hydraulic Conductivity Decrease Model with Results at 1,000 Years Post-Closure
- Figure 9-46 30 Percent Bedrock Horizontal Hydraulic Conductivity Increase Model with Results at 150 Years Post-Closure
- Figure 9-47 30 Percent Bedrock Horizontal Hydraulic Conductivity Increase Model with Results at 1,000 Years Post-Closure
- Figure 9-48 30 Percent Basin Fill Vertical Hydraulic Conductivity Decrease Model with Results at 150 Years Post-Closure
- Figure 9-49 30 Percent Basin Fill Vertical Hydraulic Conductivity Decrease Model with Results at 1,000 Years Post-Closure
- Figure 9-50 30 Percent Basin Fill Vertical Hydraulic Conductivity Increase Model with Results at 150 Years Post-Closure
- Figure 9-51 30 Percent Basin Fill Vertical Hydraulic Conductivity Increase Model with Results at 1,000 Years Post-Closure
- Figure 9-52 10 Percent Bedrock Vertical Hydraulic Conductivity Decrease Model with Results at 150 Years Post-Closure
- Figure 9-53 10 Percent Bedrock Vertical Hydraulic Conductivity Decrease Model with Results at 1,000 Years Post-Closure
- Figure 9-54 30 Percent Bedrock Vertical Hydraulic Conductivity Increase Model with Results at 150 Years Post-Closure
- Figure 9-55 30 Percent Bedrock Vertical Hydraulic Conductivity Increase Model with Results at 1,000 Years Post-Closure

- Figure 9-56 Order of Magnitude HFB Hydraulic Conductivity Decrease Model with Results at 150 Years Post-Closure
- Figure 9-57 Order of Magnitude HFB Hydraulic Conductivity Decrease Model with Results at 1,000 Years Post-Closure
- Figure 9-58 Order of Magnitude HFB Hydraulic Conductivity Increase Model with Results at 150 Years Post-Closure
- Figure 9-59 Order of Magnitude HFB Hydraulic Conductivity Increase Model with Results at 1,000 Years Post-Closure
- Figure 9-60 Order of Magnitude Specific Storage Decrease Model with Results at 150 Years Post-Closure
- Figure 9-61 Order of Magnitude Specific Storage Decrease Model with Results at 1,000 Years Post-Closure
- Figure 9-62 Order of Magnitude Specific Storage Increase Model with Results at 150 Years Post-Closure
- Figure 9-63 Order of Magnitude Specific Storage Increase Model with Results at 1,000 Years Post-Closure
- Figure 9-64 50 Percent Basin Fill Specific Yield Decrease Model with Results at 150 Years Post-Closure
- Figure 9-65 50 Percent Basin Fill Specific Yield Decrease Model with Results at 1,000 Years Post-Closure
- Figure 9-66 50 Percent Basin Fill Specific Yield Increase Model with Results at 150 Years Post-Closure
- Figure 9-67 50 Percent Basin Fill Specific Yield Increase Model with Results at 1,000 Years Post-Closure
- Figure 9-68 Factor of 2 Bedrock Specific Yield Decrease Model with Results at 150 Years Post-Closure
- Figure 9-69 Factor of 2 Bedrock Specific Yield Decrease Model with Results at 1,000 Years Post-Closure
- Figure 9-70 Factor of 2 Bedrock Specific Yield Increase Model with Results at 150 Years Post-Closure
- Figure 9-71 Factor of 2 Bedrock Specific Yield Increase Model with Results at 1,000 Years Post-Closure
- Figure 9-72 Recharge at Steady-State Model Conditions with Results at 150 Years Post-Closure
- Figure 9-73 Recharge at Steady-State Model Conditions with Results at 1,000 Years Post-Closure
- Figure 9-74 Predicted Groundwater-Level Drawdown at Simulated Observation Locations for 20 Percent Pit-Lake Evaporation Decrease
- Figure 9-75 Predicted Groundwater-Level Drawdown at Simulated Observation Locations for Pre-Mining, Steady-State Recharge Simulation
- Figure 10-1 Project-Related Potential Sources of Groundwater Recharge

- Figure 10-2 Mining-Phase and Post-Closure Particle Tracks and Open Pit Groundwater Capture Zone Boundary in Project Area
- Figure 10-3 Mining-Phase and Post-Closure Particle Tracks and Open Pit Groundwater Capture Zone Boundary
- Figure 10-4 Background Groundwater Quality Wells and Spring

APPENDICES

- Appendix A Davidson Canyon Conceptual Model (Tetra Tech, 2010a)
- Appendix B Short-Term Hydraulic Test Analyses
- Appendix C Steady-State Target Water Levels

LIST OF ACRONYMS AND ABBREVIATIONS

ACRONYMS

| | |
|----------|---|
| 2D | 2-dimensional |
| 3D | 3-dimensional |
| Project | Rosemont Copper Project |
| ac | Acre |
| ac-ft/yr | Acre-feet per year |
| ADEQ | Arizona Department of Environmental Quality |
| ADWR | Arizona Department of Water Resources |
| APP | Aquifer protection permit |
| AZGS | Arizona Geological Survey |
| amsl | Above mean sea level |
| bgs | Below ground surface |
| cfs | Cubic feet per second |
| CN | Runoff Curve Number |
| CSS | Composite Scaled Sensitivity |
| DIA | Discharge Impact Area |
| DTW | Depth-to-water |
| EPM | Equivalent porous media |
| ET | Evapotranspiration |
| EVT | MODFLOW evapotranspiration package |
| gpm | Gallons per minute |
| GHB | General Head Boundary |
| GWSI | Groundwater Site Inventory |
| HFB | Horizontal Flow Barrier |
| HGU | Hydrogeologic unit |
| K_{xy} | Horizontal hydraulic conductivity |
| K_z | Vertical hydraulic conductivity |
| Ksd | Lower Cretaceous sedimentary units (Bisbee Group) |
| KTi | Upper Cretaceous and Early Tertiary intrusive |
| Kv | Upper Cretaceous volcanic rocks |
| M&A | Montgomery & Associates |
| mg/L | Milligrams per liter |
| MPO | Mine Plan of Operations |

| | |
|----------|--|
| NCDC | National Climatic Data Center |
| ND | Not detected |
| NED | National Elevation Dataset |
| Rosemont | Rosemont Copper Company |
| SOSWR | Sum of Square Weighted Residuals |
| S_s | Specific storage |
| S_y | Specific yield |
| OAW | Outstanding Arizona Water |
| PAG | Pima Association of Governments |
| PCG | Pre-Conditioned Conjugate Gradient |
| PWTS | Process Water Temporary Storage |
| PLS | Pregnant Leach Solution |
| Pz | Paleozoic sedimentary and metamorphic formations |
| Pz Pit | Paleozoic sedimentary and metamorphic formations near the Backbone Fault |
| pCb | Precambrian igneous and metamorphic crystalline formations |
| Qal | Quaternary and Recent alluvium |
| QTg | Late Tertiary to Early Quaternary basin-fill deposits – higher permeability |
| QTg1 | Late Tertiary to Early Quaternary basin-fill deposits – lower permeability |
| QTg2 | Late Tertiary to Early Quaternary basin-fill deposits – lowest permeability |
| QTg_TB | Tucson Basin Late Tertiary to Early Quaternary basin-fill deposits – higher permeability |
| Tsb | Early to Mid-Tertiary sedimentary and volcanic units (Pantano Formation) |
| UCL | Upper confidence limit |
| USDA | United States Department of Agriculture |
| USGS | United States Geological Survey |
| USDOI | United States Department of Interior |

EXECUTIVE SUMMARY

Rosemont Copper Company (Rosemont) is planning the development of an open-pit mining and mineral processing operation known as the Rosemont Copper Project (Project) located on the east side of the Santa Rita Mountains, approximately 30 miles southeast of Tucson, Arizona in Pima County. Operations will occur for approximately 22 years, during which time the Open Pit will be incrementally expanded and dewatered. Due to pit dewatering, geologically based, numerical flow models were developed to estimate potential impacts to water resources within the regional groundwater system. Specifically, potential effects on the surface-water and groundwater hydrology of Davidson Canyon and the Cienega Creek Basin were simulated. This included effects on groundwater levels, spring flows, surface-water flows, and riparian areas.

Numerical groundwater flow modeling was preceded by first developing conceptual and hydrogeologic framework models of the study area. The basis for these models was existing data and analyses completed for the Rosemont Project and from other independent studies. Additionally, the model domain was constrained to the area previously delineated by Montgomery & Associates (M&A) for their groundwater flow model simulations. The hydrogeologic framework model, which formed the foundation for the groundwater flow modeling simulations, was also based on existing horizontal hydrogeologic slices developed for the M&A flow model domain.

Three (3) numerical models were developed to simulate the different stages of the Project: pre-mining, mining-phase, and post-mining (post-closure). The pre-mining model was calibrated based on existing water-level measurements and stream flows. Results of the calibrated pre-mining model were subsequently used as the start of the mining-phase model. Conditions simulated at the end of the mining-phase model were used as the input to the post-closure model. All models used the finite-difference model code MODFLOW-SURFACT (MODFLOW). An additional MODFLOW package was added to simulate the pit-lake water balance in the post-closure simulation.

Geologic controls and hydrogeologic units were incorporated into the numerical models as appropriate. Due to the large size the model domain, the grid spacing within the numerical models limited the resolution of the smaller geologic features. Although cell sizes within posed limitations on delineating specific hydrogeologic features, the overall, regional flow system was appropriately simulated. Additionally, modeling was performed using an equivalent porous media assumption, which is inherent in MODFLOW. Although the groundwater flow system includes fractured geologic formations, at the regional scale it was assumed that the aquifers were accurately simulated as a porous media within MODFLOW.

Since a porous media assumption was used, the selected hydraulic properties used in the model simulations represented the average, bulk properties of the aquifers. The hydraulic connectivity associated with fractures yielding water to the pit, and throughout the broader hydrogeologic system, was likely over estimated due to this modeling approach. In practice, some fractures yielding flow to the Open Pit may initially have high flows, but then may have substantially reduced flows with time as storage is depleted and the rate of replenishment becomes lower than the hydraulic conductivity of the fracture(s). Lower than predicted inflows would equate to less pit capture and thus smaller impacts to the regional groundwater system.

Dewatering of the proposed Open Pit will result in groundwater levels being lowered to approximately 3,020 feet above mean sea level (amsl), which is about 2,200 feet below the pre-mining water level in the immediate Project area. The projected bottom of the pit is 3,050 feet amsl. Dewatering the pit will create drawdown in the regional groundwater system, propagating outward. Drawdown will be most dramatic in the vicinity of the Open Pit, the effects of which will decrease with increased distance from the pit. Although partial recovery of water levels within

the pit area are anticipated following the cessation of dewatering, water levels are anticipated to take hundreds of years to reach a new equilibrium condition.

Following the cessation of dewatering, the pit will naturally refill with water. The post-closure numerical groundwater flow model predicts the refilling process will take 700 to 1,000 years to reach an equilibrium or steady-state condition. At this point, the equilibrium lake stage is predicted to be 4,279 feet amsl. Due to the high evaporation rate in the Rosemont area, the pit-lake is predicted to be a hydraulic sink. A capture zone will exist around the Open Pit, perpetually drawing groundwater into the pit or pit-lake.

Flow-through conditions, or a non-terminal pit-lake, would exist should the lake stage reach an elevation of 4,680 feet amsl (groundwater divide). Sensitivity analyses were run on various model scenarios and model input parameters, such as changes in the evaporation rate and in groundwater recharge contributions from meteoric precipitation. None of the sensitivity model runs, however, caused the lake stage to reach the elevation of this groundwater divide.

The estimated groundwater-level drawdown associated with the pit or pit-lake 1,000 years into the post-closure period is shown on Illustration E-1. Historically, observed water-level fluctuations greater than five (5) feet have been recorded within the simulated five (5)-foot groundwater drawdown contour area shown on Illustration E-1. At the 1,000-year post closure time period, the steady-state groundwater inflow to the pit is anticipated to be 230 gpm. Inflows to the pit during active dewatering were estimated to be up to 500 gpm.

Drawdown due to the Project can only impact stream flows if there is a hydraulic connection between the stream channels and the regional groundwater system. The model employed a conservative approach whereby the base flows in Davidson Canyon and Cienega Creek were assumed to be hydraulically connected to the regional groundwater flow system. This was done even though studies indicate that stream flows in these areas are often associated with local geologic bedrock highs or constrictions of shallow, alluvial flow systems, and not the regional groundwater system. Predicted impacts to base flows in Davidson Canyon and Cienega Creek during operations were negligible and indiscernible compared to the accuracy of the model. Under post-closure conditions, a total decrease in average annual base flow along Cienega Creek, 1,000 years following the cessation of dewatering, was predicted to be 0.09 cubic feet per second (cfs), which was less than three (3) percent of the simulated base flow. The predicted change in Davidson Canyon flow was 0.01 cfs in the upper most reach after 1,000 years. However, no losses were predicted in the reach identified as an Outstanding Arizona Water.

The most significant riparian areas are near the Davidson Canyon and Cienega Creek stream channels. Based on the minimal predicted change in base flows in Davidson Canyon and Cienega Creek, and the anticipated groundwater drawdown shown on Illustration E-1, it is unlikely that riparian vegetation would be significantly affected.

Similar to base flows in Davidson Canyon or Cienega Creek, the effect on springs due to the Project will principally depend on the distance from the Open Pit and whether the spring is hydraulically connected to the regional groundwater flow system. For instance, Rosemont Spring will be covered by the Waste Rock Storage Area and will also be within the capture zone of the pit or pit-lake. Therefore, terminated flows are anticipated at this spring. Impacts to Questa Spring are not anticipated during the mining-phase but will likely have reduced or terminated flows in the post-closure period. Helvetia Spring, if it has a regional groundwater source, will also likely have reduced or terminated flows in the post-closure period. Nogales Spring and Little Nogales Spring will not be affected. It cannot be determined if Davidson Spring will be impacted. However, geologic evidence suggests that Davidson Spring is unlikely to be affected by the Project.

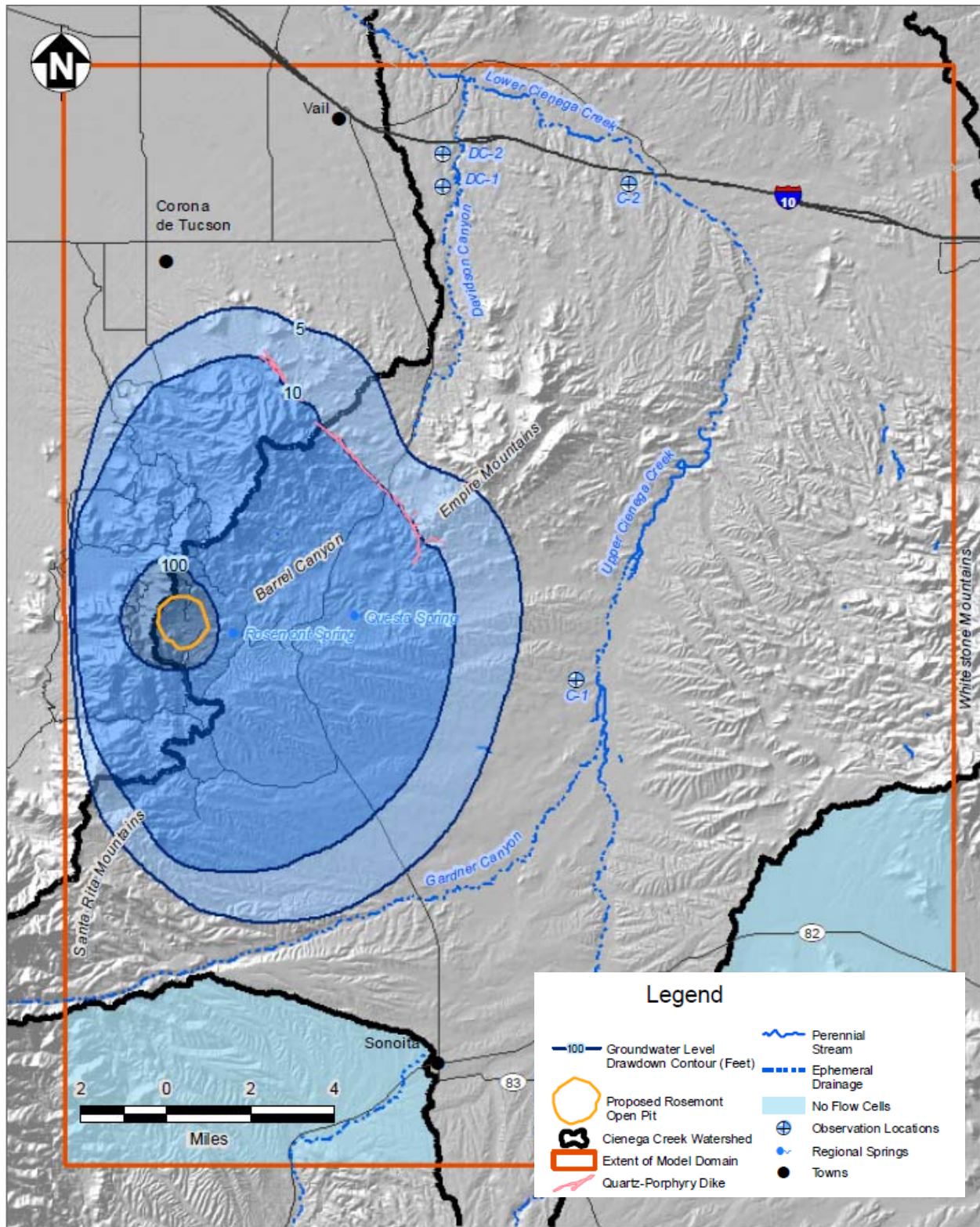


Illustration E-1 Predicted Groundwater Level Drawdown 1,000 Years after End of Operations

Based on pit dewatering and the formation of terminal pit-lake conditions during the post-closure period, the pit capture zone will extend underneath most of the Project facilities. Particle tracking simulations indicate that any seepage from facilities within the capture zone will flow back to the pit or pit-lake. Project facilities not within the predicted capture zone are anticipated to include part of the Dry Stack Tailings Facility and the flow-through drain system. The flow-through drain system passes stormwater from watershed areas up-gradient of the Project facilities to the down-gradient side, mainly passing underneath the Dry Stack Tailings Facility. Based on a volumetric basis, the water quality of the combined dry stack tailings seepage and potential infiltration due to the flow-through drain system was predicted to have a water quality with lower concentrations of all analyzed parameters than the background groundwater quality. Therefore, the Project is not anticipated to impact the quality of the down-gradient regional aquifer. Regardless, down-gradient groundwater monitoring will be performed as part of Arizona's aquifer protection permit (APP) program. Additionally, contingency plans will be developed should permit conditions be exceeded.

1.0 INTRODUCTION

Rosemont Copper Company (Rosemont) is planning the development of an open-pit mining and mineral processing operation known as the Rosemont Copper Project (Project) located on the east side of the Santa Rita Mountains, approximately 30 miles southeast of Tucson, Arizona in Pima County (Figure 1-1). Construction, mining operations, and post-closure activities will occur for approximately 25 to 30 years.

At the end of mining, final reclamation of the site will occur, including demolition and closure of the Plant Site facilities and final regrading and revegetation of the Rosemont Ridge Landform. The Rosemont Ridge Landform is the consolidated and contoured earthen structure consisting of waste rock from the Open Pit, a closed Heap Leach Facility encapsulated with waste rock, and a Dry Stack Tailings Facility, also encapsulated with waste rock. In addition to the Rosemont Ridge Landform, the Open Pit will remain following closure.

At the rim, the Open Pit dimensions will be approximately 6,500 feet north to south, 6,000 feet east to west, and about 1,800 to 2,900 feet deep (Westland Resources, 2007). The bottom elevation of the pit is projected to be 3,050 feet above mean sea level (amsl). The Open Pit will be advanced below the current groundwater table and will require dewatering during the approximately 22 years of mining operations. Once mining and mineral processing activities cease, dewatering of the pit will also be terminated.

When mining ceases and dewatering is discontinued, the Open Pit will naturally refill with water. This refilling process will take many years to reach an equilibrium or steady-state condition. It is expected that the pit will remain a hydraulic sink at this long-term equilibrium condition, i.e., groundwater will perpetually flow into the Open Pit, although at a much lower rate than during the dewatering process. This is due to the anticipated inflow rate of groundwater and surface water into the pit-lake versus removal of water from the lake due to the high evaporation rate of the Rosemont area.

1.1 Project Objectives

As part of the design and permitting process, Rosemont has undertaken detailed studies of the area resources. These resources include both surface water and groundwater and their interface. As part of these studies, numerical groundwater flow models were developed for the Project. These flow models simulated pre-mining steady-state conditions, active-mining (mining-phase) conditions, and post-mining (post-closure) conditions. These three (3) models are collectively termed the regional groundwater flow model (groundwater flow model).

The objective of developing a regional groundwater flow model for the Rosemont Project was to determine possible impacts to water resources in the model study area (model domain) due to the Rosemont operation (Figure 1-2). In addition to estimating down-gradient impacts, groundwater inflows to the Open Pit during the mining-phase and post-closure period were simulated to estimate pit dewatering and pit infill rates, respectively.

The assessment of potential impacts included perennial stream flow, perennial spring flow, and riparian area vegetation down-gradient of the Project. Davidson Canyon and Cienega Creek have perennial reaches and riparian vegetation as reported in several publications by the Pima Association of Governments (PAG, 2003a, 2003b, 2005). Groundwater level declines due to the Project could reduce surface flows and reduce vegetation density in these reaches. Perennial springs in the study area have also been identified by Tetra Tech (2010a).

The evaluation of the groundwater inflows to the Open Pit is important since the long-term, steady-state impact of the terminal pit-lake will be equal to the steady-state groundwater inflows.

Drawdown will propagate away from the pit until an equal rate of groundwater is captured from other sources.

1.2 Project Scope

The scope of the groundwater analysis was limited to those portions of the Project that may directly impact the surface-water and groundwater hydrology of Davidson Canyon and the Cienega Creek Basin. This included an analysis of the Project's effect on groundwater levels, spring flows, surface-water flows, and riparian areas.

Modifications to surface-water drainages will occur in the main Project or operations area. Other studies have been completed to address the specific issues related to stormwater management in the Project area (Tetra Tech, 2010b; Tetra Tech 2010c). Expected groundwater recharge changes due to the Project facilities (Tetra Tech, 2010c; Tetra Tech, 2010d) were incorporated into the post-closure groundwater flow model simulations.

The impact to the regional groundwater system caused by groundwater drawdown from pit dewatering was the primary focus of this groundwater impacts analysis. Predicted impacts to surface-water base flows and riparian area vegetation were limited to simulated changes in groundwater discharge based on the regional groundwater flow model. Groundwater discharges were simulated based on conditions without the Project and based on changes due to Open Pit dewatering and subsequent pit-lake formation.

Existing data and analyses completed for the Project, and from other independent studies in the region, formed the basis for the groundwater flow model. Aside from field observations in Davidson Canyon and of a quartz-porphyry dike (large-scale geologic feature) completed by Tetra Tech and Rosemont, no additional data were obtained. Existing data were evaluated and used in the analysis as appropriate.

Development of the flow model was constrained to the model domain previously developed by Montgomery & Associates (M&A, 2009b). A 3-dimensional (3D) hydrogeologic framework model, which formed the foundation of the numerical model, was based on the existing horizontal hydrogeologic slices developed for the M&A model domain (M&A, 2009b).

Additionally, due to the large area covered by the model domain, the number and size of the cells comprising the numerical model were also constrained. This limited the ability of the groundwater flow model to simulate hydrogeologic features smaller than the grid resolution. Therefore, hydrogeologic features smaller than the grid resolution were typically not explicitly simulated, and their geometries and distributions were approximated. Based on the role of these smaller scale hydrogeologic features on the localized groundwater flow system, predicting small magnitude changes in spring and stream flows, and small water-level changes at distant locations from the Open Pit, becomes more uncertain.

1.3 Approach

The approach used for evaluating potential impacts from future Project operations involved integrating the existing body of knowledge into a conceptual groundwater flow model followed by development of a regional-scale numerical flow model. In addition to field reconnaissance of the Project area and Davidson Canyon by Tetra Tech and Rosemont technical staff, numerous published studies provided data, analyses, and interpretations that were critical for developing an understanding and basis of the physical processes occurring in the model study area.

As indicated, three (3) flow models were constructed in order to simulate the current pre-mining steady-state conditions, mining-phase conditions, the post-closure conditions. These models were used to predict potential future impacts. Modeling methods varied depending on the

processes being simulated and available data. Each of the models was based on the hydrogeologic framework model defined through extensive geologic studies (Ferguson, 2009; Ferguson et al., 2001; M&A 2009b).

The current groundwater flow system in the Project area, and the majority of the model domain, was considered to be in a steady-state condition. This pre-mining or steady-state condition was defined by historical water-level, stream-flow, and hydraulic-property data. The pre-mining flow model was calibrated to the existing steady-state water-level data. These calibrated model parameters formed the basis for the subsequent transient flow models (mining-phase and post-closure models).

The mining-phase transient model simulated the step-wise deepening of the Open Pit and associated dewatering during the 22-year operational period. Dewatering of the Open Pit was simulated with drain cells, which removed water from the model when the water level reached a specified elevation below the bottom of the pit. The post-closure groundwater flow model used the LAK2 package (Council, 1999) to simulate the refilling of the pit following the end of dewatering.

The best available data and associated interpretations were used for construction and calibration of the groundwater flow model. Data sources used in this evaluation are summarized in Section 1.4, "Previous Studies", and comprehensively listed in Section 12.0, "References". Inputs to the groundwater flow model for geologic unit distribution and geometry, hydraulic properties, recharge estimates, stream flows, evapotranspiration (ET), and water levels were based on these data.

The groundwater flow models were developed with hydraulic properties considered to be the most appropriate and representative of the regional groundwater system. Understanding that uncertainties existed in these model inputs, a robust sensitivity analysis was completed. A range of potential impacts was developed through a sensitivity analysis process. Results of the sensitivity analysis are summarized in this report (Section 9.0) and are detailed in Tetra Tech (2010k).

1.4 Previous Studies

Numerous studies have been completed by Rosemont to assist in the Project's permitting process. Independent studies by other organizations and individuals have also been conducted in the region. The most critical data sources used in developing the groundwater flow model are summarized below.

In-depth hydrogeologic investigations involving baseline data collection, field testing, and modeling were completed by Montgomery & Associates (M&A):

- *Results of Phase 2 Hydrogeologic Investigations and Monitoring Program, Rosemont Project, Pima County, Arizona (M&A, 2009a);*
- *Groundwater Flow Modeling Conducted for Simulation of Proposed Rosemont Pit Dewatering and Post-Closure, Rosemont Project, Pima County, Arizona (M&A, 2009b);*
- *Analysis of Long-Term, Multi-Well Aquifer Test – November 2008 through January 2009, Rosemont Project, Pima County, Arizona (M&A, 2009c); and*
- *Comparison of Natural Fluctuation in Groundwater Level to Provisional Drawdown Projections, Rosemont Mine. (M&A, 2010b).*

Geologic mapping northeast of the Project area was completed by the Arizona Geological Survey (AZGS) (Ferguson et al., 2001; Ferguson, 2009).

As indicated, PAG completed several studies in Cienega Creek and Davidson Canyon including:

- *Contribution of Davidson Canyon to Baseflows in Cienega Creek* (PAG, 2003a);
- *Geologic Influence on the Hydrology of Lower Cienega Creek* (PAG, 2003b); and
- *Unique Waters Nomination – Davidson Canyon* (PAG, 2005).

Tetra Tech completed the following reports to address baseline and post-closure hydrology, infiltration modeling, and fate and transport modeling:

- *Site Water Management Update, Volumes 1-5* (Tetra Tech, 2010b);
- *Rosemont Infiltration Analysis* (Tetra Tech, 2010c);
- *Infiltration, Seepage, Fate and Transport Modeling Report – Revision 1* (Tetra Tech, 2010d);
- *Baseline Regulatory (100-Yr) Hydrology and Average-Annual Runoff, Rosemont Copper Project* (Tetra Tech, 2010e); and
- *Post-Mining Regulatory (100-Yr) Hydrology and Average-Annual Runoff, Rosemont Copper Project* (Tetra Tech, 2010f).

Analyses conducted by Tetra Tech in direct support of developing the groundwater flow model are provided in the following Technical Memorandums:

- *Davidson Canyon Hydrogeologic Conceptual Model and Assessment of Spring Impacts* (Tetra Tech, 2010a);
- *Hydraulic–Property Estimates* (Tetra Tech, 2010g);
- *Hydrogeologic Framework Model* (Tetra Tech, 2010h);
- *Groundwater Flow Model Construction and Calibration* (Tetra Tech, 2010i);
- *Predictive Groundwater Flow Modeling Results* (Tetra Tech, 2010j); and
- *Rosemont Groundwater Flow Model Sensitivity Analyses* (Tetra Tech, 2010k).

1.5 Report Organization

This report integrates and summarizes the results of previous Tetra Tech studies related to development of the regional groundwater flow model. The conceptual groundwater model used as the basis for development of the regional groundwater flow model is discussed in Section 2.0 and is provided in Appendix A (Tetra Tech, 2010a). This conceptual model provides an understanding of groundwater/surface-water interactions, recharge mechanisms, and the potential impacts to streams, springs, and riparian areas in the Project area as well as in Davidson Canyon and in Cienega Creek Basin.

Following a discussion of the conceptual groundwater model in Section 2.0, and possible impacts to area resources in Section 3.0, the 3D hydrogeologic framework model and the geologic units which form the basis for the regional groundwater flow model are discussed in Section 4.0. This discussion also included the selection of hydraulic properties for the hydrogeologic units (HGUs) within the model domain.

Section 5.0 presents details on the model grid, internal and external boundary conditions, and simulated hydrogeologic features. Similarities and differences between the pre-mining steady-state, mining-phase, and post-closure models are also discussed in this section.

The pre-mining steady-state model calibration section (Section 6.0) presents water-level targets, parameter values, calibration statistics, and simulation results. Details of the transient models, which are based on the pre-mining steady-state model, are described in Section 7.0. Results of the transient simulations for the mining-phase and post-closure periods are then presented (Section 8.0).

Sensitivity analysis results are presented in Section 9.0 and illustrate a range of potential impacts from the Project. Model parameter values for the pit-lake, hydraulic conductivity, storage, and external boundaries were varied in the sensitivity analysis. The most sensitive parameter changes and their impacts on streams, springs, and riparian vegetation are discussed in Section 9.0. Other simulations were also performed which may not have been sensitive to parameter changes. These simulations are presented in Tetra Tech (2010k).

Section 10.0 provides an assessment of the Discharge Impact Area (DIA). This assessment is required as part of the aquifer protection permit (APP) administered through the Arizona Department of Environmental Quality (ADEQ).

2.0 CONCEPTUAL GROUNDWATER MODEL

A conceptual groundwater model (conceptual model) was developed which provided a description of the hydrogeologic conditions and processes within the model study area. Existing data were used to form conclusions about the regional groundwater flow system, which in turn formed the framework for developing a regional groundwater flow model. The groundwater flow model developed for the Rosemont Copper Project is a numerical/mathematical representation of the conceptual model.

The components of the conceptual model are the general hydrogeology, groundwater/surface-water interactions, groundwater model boundaries, recharge, ET, groundwater pumping, and groundwater and surface-water fluctuations. The groundwater flow model incorporated this information and was used to predict the flow system's response to the development and dewatering of the Open Pit and to the ensuing formation of a pit-lake following the end of active dewatering.

The model study area for both the conceptual groundwater model, and the numerical flow models, encompassed the Project area, extended west to incorporate the full width of the northern Santa Rita Mountain range, extended north to incorporate Davidson Canyon and a small portion of the Tucson Basin (upper Santa Cruz), and extended south and east to incorporate most of the Cienega Creek Basin (Figure 1-2). Supporting data, analysis, and interpretations used to form the basis of the conceptual groundwater model are presented in the following sections.

2.1 Model Study Area Description

The Project is located in the upper Davidson Canyon watershed near the crest of the Santa Rita Mountains (Figure 1-2). The topography varies considerably within the watershed with elevations over 6,000 feet amsl in the upper portion of the watershed to an elevation of approximately 3,325 feet amsl where Davidson Canyon discharges to Cienega Creek, north of Interstate-10 (Figure 1-2). The Davidson Canyon watershed covers an approximate area of 32,920 acres (51 square miles). The upper portion of the watershed includes the sub-watersheds of McCleary Canyon, Wasp Canyon, and Barrel Canyon (Appendix A, Figure 1). Further northwards, Davidson Canyon drains the western flank of the Empire Mountains through a series of small sub-drainages. The distance from the confluence of upper Davidson Canyon with Barrel Canyon to the outlet of Davidson Canyon at Cienega Creek is approximately 14 miles.

The bedrock forming the Santa Rita Mountains consists of a metamorphic core flanked by a metamorphic shell of Paleozoic and Mesozoic-aged sedimentary rock including carbonates, shales, and limestones (Wardrop, 2005). These and similar rocks throughout the watershed are collectively termed bedrock. Permeability in the bedrock is primarily due to secondary fractures since the bulk rock is typically metamorphosed or highly consolidated with minimal porosity. This bedrock is typically covered by basin-fill deposits, recent alluvium, and unconsolidated deposits in the low lying surface-water drainage channels. These surficial deposits typically have higher storage and permeability and have the capacity to transmit more water than the underlying bedrock.

The central valley of adjacent Cienega Creek Basin is a high, semi-arid desert grassland with elevations of 3,000 to 5,000 feet amsl. The mountains surrounding the valley have elevations of 6,000 to 8,000 feet amsl. Cienega Creek Basin is bounded by the Santa Rita and Empire Mountains on the west, the Rincon Mountains on the north, the Whetstone and Mustang Mountains on the east, and the Canelo Hills and Patagonia Mountains on the south. Cienega

and Sonoita Creeks are the main surface water drainages in the Cienega Creek Basin (ADWR, 2010a). Sonoita Creek, however, was not included in the model study area since it lies on the other side of a surface-water divide selected as a model boundary.

Cienega Creek is primarily an ephemeral stream that drains towards the north into the Tucson Active Management Area (AMA). The creek can be divided into two (2) sections: 1) an upper section that drains the central valley; and 2) a lower section that flows through a narrow valley and empties into Pantano Wash (ADWR, 2010a). The upper and lower sections are separated by bedrock that form what locals call "the Narrows" (ADWR, 2010a). Bedrock at "the Narrows", and in several other places downstream, forces groundwater into Cienega Creek's streambed creating small perennial reaches. Other than perennial reaches in the lower section, most flow in Cienega Creek is runoff from local storm events (ADWR, 2010a). Similarly, surface water flows in Davidson Canyon generally occur only in response to rainfall within the drainage basin. However, springs and seeps within Davidson Canyon sustain some short intermittent and reportedly perennial flows in the lower stream reaches (PAG, 2005).

2.2 Hydrogeology

The geology within the model study area consists of mountain-forming pre-Tertiary bedrock and Tertiary to Quaternary age basin-fill geologic units. The bedrock units include Precambrian intrusive and metamorphic rocks, Paleozoic sedimentary rocks, Mesozoic sedimentary and volcanic rocks, and Laramide intrusive rocks (M&A, 2009b). Bedrock has low primary permeability and storage and only transmits significant quantities of water where it is faulted and fractured. The deeper Tertiary basin-fill units can be well cemented and deformed, while the youngest Quaternary sediments are flat lying and are generally not cemented.

The two (2) principal aquifers in the Cienega Creek Basin are the streambed alluvium and the basin-fill alluvium. The Pantano Formation and the bedrock complex of the surrounding fault-block mountains yield small amounts of water to wells and are considered only minor aquifers (ADWR, 2010a). In upper Cienega Creek, the streambed alluvium is a minor aquifer due to its limited areal extent and maximum thickness of only 200 feet (Boggs, 1980). The streambed alluvium is composed of sand and gravel deposited along Cienega Creek and its tributary washes (ADWR, 2010a). The main aquifer in upper Cienega Creek is the basin-fill alluvium that is composed of interbedded clay, silt, sand, and gravel layers that are deepest in the southern part of the model domain. The main aquifer in the lower Cienega Creek section is the streambed alluvium that consists of unconsolidated silt, sand, and gravel deposits. The basin-fill alluvium is a poor aquifer in the lower section and is composed of loosely-to-moderately lithified clay, silt, sand, and gravel to boulder-sized particles. The Pantano Formation, which consists of moderately-to-well lithified conglomerates, breccias, and fanglomerates, underlies the basin-fill in much of the lower Cienega Creek area (ADWR, 2010a).

In the regional flow system, groundwater levels vary from approximately 5,500 feet amsl to 2,600 feet amsl, which is a change of approximately 2,900 feet. This large water-level change results in steep gradients from the mountain top areas to the lower elevation stream channels and riparian areas. The most pronounced hydraulic gradients occur within the Davidson Canyon watershed.

The configuration and properties of the bedrock and surficial deposits leads to a groundwater system with two (2) primary flow components. The bedrock forms a deeper flow system with limited storage in which groundwater flow occurs primarily through fractures. The surficial deposits form spatially limited, shallow flow systems with greater storage (per unit area), with flows primarily through matrix materials. The degree to which these deep and shallow systems interact is highly variable and largely dependent on the location within the system. Water levels

east of the proposed Open Pit indicate downward gradients or recharging conditions. There are, however, deeper wells (e.g., PC-5 and PC-2, Figure 7, Appendix A) in the pit area that have upward hydraulic gradients with water levels at or near the land surface. These wells are likely monitoring localized conditions within the complex geology that have created locally confined conditions that are not representative of the overall regional flow system.

In the upper reaches of Davidson Canyon, near the proposed Open Pit, the regional groundwater table is typically 20 feet to over 100 feet below the ground surface (bgs). The shallowest depth-to-water (DTW) tends to occur in the alluvial drainages (RP-2 DTW = ~30 feet), while topographically higher wells, such as RP-4, had a DTW of approximately 181 feet. The observed DTW below the surface-water channels indicates that there is no persistent or direct connection between the surface-water flows and the regional groundwater system. However, the downward gradients indicate that recharge is occurring in the upper reaches of the watershed and through the stream channels.

The lower reaches of Davidson Canyon and Cienega Creek have similar conditions, with groundwater levels being persistently below the bottom of the stream channels (PAG, 1998). Streambed infiltration has been identified as a source of recharge along reaches of Cienega Creek and its tributaries (ADWR, 2010a).

2.2.1 Geologic Controls on Groundwater Flow

The Santa Rita and Empire Mountains are separated by the Davidson Canyon fault zone. The western fault trace is concealed by alluvium and the eastern fault is partially exposed in the northern piedmont of the Empire Mountains (Ferguson et al., 2001). Neither of the mapped primary fault traces directly underlie the channel alluvium in Davidson Canyon. These faults along Davidson Canyon, and around Davidson Spring, are poorly understood (Ferguson et al., 2001) and the hydraulic properties of the Davidson Canyon fault zone have not been tested. The faults are inferred over much of their extent, making field observations of properties (e.g., aperture, open versus closed, degree of fine grained material, etc.) difficult to determine. There may also be considerable lateral and vertical variability in the hydraulic properties of the fault zone.

The orientation of the Davidson Canyon fault zone and the surface water drainage direction are roughly parallel to the groundwater flow direction, suggesting that there is some potential for enhanced flow along this zone. The width of this enhanced flow zone, however, cannot be determined based on available information. A highly permeable and extensive fault zone would tend to drain groundwater from the upper parts of the Davidson Canyon watershed and the Project area. However, there is no conclusive evidence that groundwater flow along the fault zone is discharging at an “unnamed” spring identified by PAG (2005) in the lower reaches of Davidson Canyon. The low discharge at this spring, combined with the lack of any high-discharge, perennial springs in Davidson Canyon, suggests that the Davidson Canyon fault zone is not acting as a major, regional groundwater drain.

Based on a water-quality study by PAG (2003a), it was concluded that groundwater was not upwelling along the inferred western splay of the Davidson Canyon fault. This conclusion was supported further by low vegetation density around the fault zone, indicating a lack of available water.

Davidson Canyon is separated from the Project area by a series of northwest trending faults in the Upper Cretaceous Volcanics (Appendix A, Figure 6). The effect that these faults would have on the propagation of drawdown from Open Pit dewatering in the direction towards Davidson Canyon depends on the hydraulic properties of the faults. Faults can affect groundwater flow in two (2) ways: 1) by juxtaposing units with different hydrologic properties; and 2) by exhibiting

characteristics that are different from surrounding unfaulted rocks. Faults can therefore act as barriers to flow and/or as conduits for flow. If the fault zone core is filled with gouge, the fault can act as a barrier to flow (barrier faults). Alteration and mineral precipitation could also decrease the hydraulic conductivity by occluding pore spaces and filling connected fractures.

Geologic mapping and field observations, however, indicate that faults, fractures, and dikes play an important role in controlling groundwater flow. Evidence of their influence on groundwater flow was observed in upper Davidson Canyon, in the western pit area, and along a large mapped quartz-porphyry dike. Faults mapped by the AZGS in upper Davidson Canyon impede horizontal groundwater flow, as evidenced by the presence of several springs discharging where the faults daylight at land surface.

The degree to which faulting has resulted in compartmentalization of the groundwater flow system near the proposed Open Pit area remains uncertain. However, the occurrence of numerous springs along the northwest trending faults in the Upper Cretaceous Volcanics suggest that some faults are acting as barriers to groundwater flow. These faults are roughly perpendicular to groundwater flow and barrier faults can result in groundwater being forced to the surface.

Numerous quartz-porphyry dikes have formed in the Empire Mountains (Ferguson, C.A., 2009) and Mount Fagan areas (Ferguson et. al., 2001). Some of these dikes appear to have been formed by intrusion into existing faults (Drewes, 1972). These dikes are younger than the surrounding bedrock and therefore cut through the older bedrock. There is the potential that these dikes may create barriers to groundwater flow. A northwest-striking quartz-porphyry dike has been mapped on the Mount Fagan and Empire Ranch 7.5' quadrangles (Ferguson, 2009; Ferguson et al., 2001).

One of the longest and most continuous of these dikes intersects perpendicular to Davidson Canyon approximately 3,000 feet northeast of monitoring well RP-7 (Appendix A, Figure 6). This Tertiary age geologic feature is described in Ferguson (2009) as "*felsic porphyry containing 10-30% quartz and feldspar phenocrysts (1-3 mm) and sparse biotite in a fine-grained light-colored matrix, locally flow-foliated. Forms dikes and sills, and a plug-like stock in the northwest corner of the map area.*"

This quartz-porphyry dike strikes sub-perpendicular to groundwater flow in the Davidson Canyon area, is over four (4) miles long, and based on a field investigation, has a low fracture density and a thickness generally greater than 100 feet. The steep hydraulic gradient from the Open Pit area to Davidson Spring in Davidson Canyon is likely due, at least in part, to this quartz-porphyry dike. However, there has been no hydraulic testing of this dike to characterize its hydraulic properties and to confirm its influence on the groundwater flow system. The cross-cutting nature, width, and length of this dike, however, suggest that it restricts groundwater flow.

2.3 Stream Flow, Springs, and Riparian Vegetation

An objective of the regional groundwater flow model and supporting hydrologic studies was to estimate potential impacts to the regional groundwater flow system due to the proposed Open Pit dewatering and other relevant mining activities. Dewatering of the Open Pit will create drawdown in the regional aquifer that will be greatest near the pit and will decrease rapidly away from the pit. Stream flows, springs, and riparian vegetation that are directly supported by the regional groundwater flow system are most likely to be impacted. Close proximity to the Open Pit increases the likelihood of greater drawdown and thus likely impact, while features at greater distances from the pit are less likely to be impacted. The following subsections discuss the nature of the physical conditions that support stream flows, springs, and riparian vegetation.

2.3.1 Groundwater / Surface-Water Interactions

Persistent and direct groundwater/surface-water interactions occur when the groundwater table intersects the channel bottom or when there is a mechanism that causes deeper groundwater to flow to the surface (Appendix A, Figures 2 and 3). This results in groundwater discharging to the stream channel alluvium and an increase in surface-water flows. Streams supported by regional groundwater tend to have persistent base flows over distances of several hundred feet to miles. Base flows tend to be consistent since regional groundwater level fluctuations are typically small and are less influenced by short-term or seasonal changes in precipitation and evapotranspiration. Precipitation and stormwater runoff events tend to increase stream flows by contributing more water to the groundwater base flow.

Discharging groundwater can occur anywhere in the stream channels. However, in semi-arid environments such as Southern Arizona, this is most likely to occur in the major, incised channels that drain the basins or in the lower reaches of stream drainages.

Shallow bedrock can be a mechanism for forcing groundwater to the surface and causing stream flow and spring discharge. However, shallow bedrock alone is not sufficient for creating perennial stream flow conditions. Gravity surveys were analyzed with respect to perennial stream flow and depth to bedrock and not all shallow bedrock occurrences resulted in perennial stream flow (Roudebush, 1996).

Cienega Creek is an example of a drainage with groundwater inflows that contribute to sustaining surface flows in some reaches (i.e., gaining reaches). Within Davidson Canyon, the lower reaches (Reaches 2, 3, and 4, Appendix A, Figure 4) would be the most likely to have gaining conditions. These lower reaches of Davidson Canyon typically have the shallowest DTW, and the water table can approach land surface, particularly near the confluence with Cienega Creek.

Groundwater/surface-water interactions in the lower Cienega Creek section, and in the lowest reach of Davidson Canyon, have been documented by PAG (1998). Local, shallow, unconsolidated alluvial aquifer conditions in close proximity to the flowing reaches were found to influence stream flows. Depth to water (DTW) in the unconsolidated stream channel deposits was generally 13 to 30 feet bgs. Although these depths were likely below the stream channel bottoms, channel elevations were not provided (PAG, 1998). Water levels in the streambed alluvium were reported to range from four (4) to 51 feet bgs by the Arizona Department of Water Resources (ADWR) (2010a). Additional studies by Tetra Tech on the potential for groundwater/surface-water interactions within Davidson Canyon (Attachment A) also concluded that the available information suggests minimal hydraulic connection, except in the lowest reaches of the canyon.

These findings indicate that the regional groundwater table is generally disconnected from the Davidson Canyon and Cienega Creek alluvial stream channels. Groundwater level declines in the vicinity of these hydraulically disconnected reaches would not be expected to impact stream flow. However, if the surface flows are hydraulically connected to the regional groundwater flow system, groundwater level declines in the area of the stream could result in a decrease in surface flows. This could occur from either less groundwater discharging to the stream or from more surface water discharging to the groundwater system as a result of lower groundwater levels in the vicinity of the stream.

2.3.1.1 Geologic Controls on Surface-Water Flow

Although most of Davidson Canyon is a dry channel under normal conditions, an “unnamed” spring and sections of the lower reaches have been designated as an Outstanding Arizona Water (OAW) by the ADEQ (ADEQ, 2008; PAG, 2005). It has been suggested that stream flow

is perennial or intermittent where the volume of channel alluvium is restricted by bedrock, forcing groundwater to the surface (PAG, 2005). In contrast, where the width or depth of the alluvium increases, stream flow becomes intermittent or ephemeral (PAG, 2005). These observations have also been made in the lower Cienega Creek section (PAG, 2003b).

Geology in the lower reaches of Davidson Canyon is comprised of steeply dipping Turney Ranch Formation of the Bisbee Group (Upper Cretaceous) (Appendix A, Figures 6 and 16). The more resistant quartz sandstone beds periodically form fins that extend into the channel, which could constrict subsurface flow and create upward vertical gradients or temporarily pond surface water (PAG, 2005; Appendix A, Photograph 11).

The Davidson Canyon channel is narrow (i.e., less than a 100 feet) and the depth of the alluvium is unknown, but also probably limited in the vicinity of the “unnamed” spring (Appendix A, Photograph 12). The “unnamed” spring may be connected to upstream alluvial material that stores stormwater that subsequently flows through the shallow subsurface and discharges at the spring due to shallow bedrock (PAG, 1998).

Restricted channel conditions and shallow bedrock exist at the outlet of Davidson Canyon to Cienega Creek (Appendix A, Photograph 18), along perennial reaches of lower Cienega Creek (PAG, 2003b), and at the Narrows in upper Cienega Creek (PAG, 1998). Subsurface bedrock highs are likely forcing groundwater flow to the surface, resulting in observable flow in Cienega Creek (PAG, 2003b). Bedrock outcrops and channel constriction north of Escondido Spring likely influence the seasonal base flows in this area (Appendix A, Figure 4).

In lower Cienega Creek, the termination of surface-water flow was correlated with faults cross-cutting the stream channel (PAG, 2003b). Higher hydraulic conductivity bedrock zones that increase water infiltration could be due to higher fracture density, fault breccias, or a juxtaposition of less consolidated materials. The density and extent of vegetation did not change near these faults, indicating that the water available to plants did not increase or decrease. This suggests that there is no upwelling of groundwater in the Davidson Canyon fault splay beneath the trace of Davidson Canyon (PAG 2003a, 2003b). Stream flow may be recharging the groundwater system in areas where there is a downward hydraulic gradient. The recharge rate would be enhanced in areas with permeable faults and fractures.

The basin-fill alluvium in upper Cienega Creek is composed of interbedded clay, silt, sand, and gravel layers with unconfined aquifer conditions. However, confining conditions occur near the stream channel in upper Cienega Creek (Township 19 South, Range 17 East) where several deep exploration wells flow under artesian pressure (Geraghty and Miller, 1970). In this area, clay layers in the upper fine-grained portion of the alluvium separate the unconfined aquifer from a lower leaky, confined aquifer whose areal extent is unknown. Confining conditions also existed near the Santa Rita Mountains where, in 1987, water levels ranged from 31 feet above land surface to 406 feet bgs (ADWR, 2010a). These leaky confined conditions could potentially result in the deeper, basin-fill aquifer supplying water to the shallow stream-channel alluvial aquifer in some areas.

2.3.2 Local and Regional Springs

Springs occur when groundwater discharges at the ground surface. In the Davidson Canyon watershed and Cienega Creek Basin, springs can receive water from shallow, local, or perched sources or from deeper, regional groundwater sources. The source of the discharging water is important since it will determine which springs are likely to be impacted due to the Project. Local, or perched, springs are not hydraulically connected to the regional groundwater system under normal conditions. Therefore, they would not be impacted by potential declines in the regional water table (Appendix A, Figure 9).

Characteristics of local springs include variable temperature, intermittent flow, and short residence time. These springs are fed by precipitation that infiltrates into the ground, flows a relatively short distance, and is discharged to the surface. Regional springs tend to have perennial flow, consistent flow rates, and consistently warmer water temperatures. Flow paths and residence times for regional springs also tend to be longer than those of local springs. In general, water temperatures and chemistry from regional springs typically reflect those observed in deep groundwater. The determination of whether a spring was regional or local was largely made on the basis of the water chemistry, geology, and water-level elevation. Water temperature data was not used as the data were considered unreliable, i.e., all water temperature measurements were consistent with the ambient air temperature.

Based on the available data, both regional and local springs occur in the model study area. All observed springs had minor discharge with flows less than one (1) gallon per minute (gpm) being common as shown in Table 2-1. On a regional scale, these springs are not significant to the water balance, and the observed discharges are too low to be simulated with a regional-scale flow model.

Spring flows and physical parameters for 20 springs in the upper reach of Davidson Canyon have been reported by M&A (2009a). Based on the conditions observed (i.e., dry, wet and flowing) at the springs during the monitoring program, flow conditions were generalized into three (3) categories:

- Intermittent Seep: visible wet areas observed on occasion, but flow has not been observed;
- Intermittent: visible flow observed on occasion; and
- Perennial: flow has been observed on all site visits during the monitoring period.

Helvetia Spring and Rosemont Spring (Appendix A, Figure 8) were classified by Tetra Tech (2010a) as potentially perennial. Based on the low discharge rates and intermittent or absent flows, most springs classified as intermittent seeps or intermittent appear to be fed by shallow water sources that are strongly influenced by seasonal precipitation variations.

Questa Spring is likely fed by the deeper, regional groundwater flow system. This spring's water chemistry is consistent with nearby well RP-9 and its carbon-14 data are representative of water that is possibly thousands of years old. Although very low flows and dry conditions have been reported at Questa Spring, these observations may not accurately reflect field conditions. During a January 2010 site visit, Tetra Tech observed low or no-flow conditions at several springs, including only dripping water at the spring tank at Questa Spring. A short distance down-gradient (less than 50 feet) from the Questa Spring tank, however, water was observed to be discharging at several gallons per minute. Recorded spring discharge and water temperatures were likely measured at the spring tank rather than in the natural spring discharge channel. Therefore, it is likely that the recorded data at Questa Spring underestimates the discharge and the flow conditions.

Helvetia Spring, Rosemont Spring, and Questa Spring are the only springs that could be considered regional springs in the Project vicinity. Each of these springs are within the expected long-term drawdown area and are therefore likely to have decreased or terminated flows due to the Project. Local springs are likely to be impacted if their locations or catchment areas are physically disturbed by Project activities.

Nogales Spring and Little Nogales Spring are regional springs located along a fault zone at the western base of the Whetstone Mountains (Pima County, 2000). Nogales Spring had elevated water temperature and was considered a thermal spring, which is indicative of a deep

groundwater source. Discharge at Nogales Spring was measured as 7.3 gpm in May 2005. This rate was considered a minimum due to the five (5) years of previously recorded drought conditions (USDOI, 2008). Additionally, the water chemistry of Nogales Spring contained carbonate minerals obtained from Paleozoic limestone (Grahn, 1995). Little Nogales Spring was reported as being very similar to Nogales Spring in discharge and is located only a few hundred yards to the west (USDOI, 2008). These springs are located east of Cienega Creek and are not at risk of being impacted by the Project.

Table 2-1 Flow Characteristics of Selected Springs in the Rosemont Project Area

| Spring Name | Source ¹ | Flow Conditions | Discharge (gpm) ² | |
|-----------------------|---------------------|-------------------|------------------------------|---------|
| | | | Minimum | Maximum |
| Barrel Spring | Local | Intermittent | 0.00 | 0.20 |
| Crucero Spring | Local | Intermittent | 0.00 | 0.61 |
| Deering Spring | Local | Intermittent | 0.00 | 1.00 |
| Fig Tree Spring | Local | Intermittent seep | 0.00 | 0.10 |
| Helvetia Spring | Regional (?) | Perennial | 0.18 | 1.59 |
| Locust Spring | Local | Intermittent seep | 0.00 | 0.00 |
| Lower Mulberry Spring | Local | Intermittent seep | 0.00 | 0.08 |
| MC-1 | Local | Intermittent | 0.00 | 1.00 |
| MC-2 | Local | Intermittent | 0.00 | 0.74 |
| McCleary Dam | Local | Intermittent | 0.03 | 10.00 |
| Mulberry Spring | Local | Intermittent | 0.00 | 0.08 |
| Papago Spring | Local | Intermittent | 0.00 | 1.70 |
| Peligro Adit | Local | Intermittent | 0.00 | 0.02 |
| Questa Spring | Regional (?) | Intermittent | 0.00 | 0.32 |
| Rosemont Spring | Regional (?) | Perennial | 0.00 | 0.79 |
| Ruelas Spring | Local | Intermittent seep | 0.00 | 0.00 |
| SC-2 | Local | Intermittent seep | 0.00 | 0.00 |
| Scholefield Spring | Local | Intermittent seep | 0.00 | 0.00 |
| SW | Local | Intermittent seep | 0.00 | 0.00 |
| Sycamore Spring | Local | Intermittent | 0.00 | 1.00 |

¹ Source: Local = water likely derived from shallow, localized source that is not consistently connected to the regional water table; Regional = water derived from deeper, regional groundwater system.

² Spring discharge data presented is from M&A (2009a).

2.3.3 Riparian Vegetation

Riparian vegetation in the model study area were mapped as part of the Sonoran Desert Conservation Plan (Harris Environmental Group et al., 2000). Additional mapping by WestLand Resources, Inc. (WestLand) in the Rosemont area was presented in a report titled *Onsite Riparian Habitat Assessment* (WestLand, 2010). This mapping indicated a significant reduction in riparian areas from those presented in the Sonoran Desert Conservation Plan.

Research on riparian evapotranspiration (ET) rates suggests that they may vary depending on factors that include, but are not limited to, vegetation composition and density, groundwater depth, weather conditions, and season. There is significant spatial and temporal variability of ET measurements, making them difficult to quantify.

Decreasing groundwater levels can reduce water availability and result in vegetation canopy dieback. Different riparian vegetation species react differently to declines in groundwater-level

elevations. Riparian trees can also react differently depending on the DTW conditions in which they were established (Horton et al., 2001). Trees established in deeper groundwater conditions tend to adjust better to changes in DTW. The rate of groundwater level declines also impacts whether plants can adapt to changes by increasing their root depth.

The Horton study (2001) determined that there are thresholds for increasing plant stress. Based on the distances from the Project site to known riparian vegetation areas, and on the long periods over which the potential impacts would materialize (e.g., hundreds of years), any imposed stress on these communities by the Project is anticipated to be low. Potential impacts may also be within the range of natural groundwater-level fluctuations.

2.4 Groundwater Flow System Boundaries

The model study area boundary was initially established by M&A to encompass the Project area and areas that could potentially be impacted by the Project. Areas of primary concern included Cienega Creek and Davidson Canyon, which have surface-water flow and riparian vegetation.

In the southwest and southeast portions of the model study area, the Cienega Creek Basin boundary forms a groundwater divide. As a result, no flow into or out of the model study area was expected in this area. Groundwater divides located at large distances from the applied hydraulic stresses are often simulated as no flow boundaries.

The west model boundary is the closest boundary to the Open Pit and is located on the west edge of the Precambrian granodiorite (pCb) hydrogeologic unit (HGU), which comprises the core of the Santa Rita Mountains. The very low permeability pCb HGU was expected to limit the flux of groundwater through the mountains. Conceptually, the groundwater divide in the Santa Rita Mountains limits how far drawdown impacts can migrate to the west.

The flow system boundaries to the east, which are in a large part bounded by the Whetstone Mountains, are poorly understood. Conceptually, inter-basin flows are limited by the permeability of the bedrock and the water levels between the adjoining basins.

The northern model study area boundary is within the Cienega Creek Basin, but distant to the Project site. Groundwater will either discharge to Cienega Creek or through the northwest part of the model study area boundary.

Simulation of the flow model boundaries is discussed further in Section 5.0, "Groundwater Flow Model Construction".

2.5 Recharge

Recharge is precipitation that infiltrates and reaches the groundwater table. In semi-arid areas such as Davidson Canyon and the Cienega Creek Basin, recharge can occur in a number of ways. Mountain top or high-elevation recharge occurs when precipitation infiltrates through fractures and fault zones within the bedrock. This recharge mechanism can be relatively limited due to the steep slopes, low permeability bedrock, and a high percentage of runoff.

Precipitation occurring in the higher, mountain bedrock areas tends to runoff and collect in drainages where it then proceeds to flow down-gradient. Run-on and precipitation on flatter slopes having higher permeability surficial deposits are more likely to result in groundwater recharge. These conditions are commonly found at the slope breaks along mountain fronts and within surface-water drainages filled with unconsolidated materials. Streambed infiltration has been identified as a source of recharge along the reaches of Cienega Creek and its tributaries (M&A, 1985; ADWR, 2010a).

The low permeability of the bedrock, and the steep topography in much of the Davidson Canyon watershed and higher elevations of Cienega Creek Basin, likely results in most of the precipitation being redistributed and routed to ephemeral channels. Focused flow in dry channels having permeable alluvium typically results in rapid infiltration. This usually starts to occur at the contact between the mountain block and the alluvial fan, where a change in slope and presence of more permeable deposits result in increased infiltration rates (Wilson and Guan, 2004).

Several studies have estimated annual recharge in and around the model study area. These recharge estimates vary considerably depending on the specific areas included and the methods used. Some recharge estimates include upper and lower Cienega Creek, but omit the Sonoita Creek section. Although streambed infiltration is a source of recharge along Cienega Creek reaches and its tributaries, most investigators did not include streambed infiltration in their total basin recharge estimates (ADWR, 2010a). M&A (1985) estimated streambed infiltration along Cienega Creek to be between 1,600 and 6,000 ac-ft/yr. ADWR (2010a) reported an average of the annual recharge estimates of 12,700 and 16,600 ac-ft/yr, but it was unclear which studies were included in these averages.

Annual recharge for the Cienega Creek Basin, without the Sonoita Creek section, was estimated to range from 6,900 to 19,500 ac-ft/yr by M&A (1985), and 8,500 to 25,500 ac-ft/yr was reported by ADWR (1994). The Anderson (1995) recharge method applied by M&A (2009) to the U.S. Geological Survey (USGS) delineation of the Cienega Creek Basin, estimated a recharge rate of 10,426 ac-ft/yr. Freethy and Anderson (1986) estimated an annual recharge rate of 11,000 ac-ft/yr, which included the Sonoita Creek area. For the upper Cienega Creek Basin, Knight (1996) estimated an annual recharge rate of 12,000 ac-ft/yr, and Bota (1997) estimated an annual recharge rate of 15,000 ac-ft/yr. The annual recharge rate in lower Cienega Creek Basin has been estimated to range from 3,200 to 9,000 ac-ft/yr (M&A, 1985).

2.6 Evapotranspiration

Although riparian areas along Cienega Creek and Davidson Canyon are the most significant source of ET, evaporation of open water and shallow groundwater also occurs. Evapotranspiration was estimated to be 2,400 ac-ft/yr in upper Cienega Creek Basin and 900 ac-ft/yr in lower Cienega Creek Basin for a total of 3,300 ac-ft/yr for the entire basin (M&A, 1985). Evapotranspiration in the upper Cienega Creek Basin was estimated by Knight (1996) and Bota (1997) to be 2,897 ac-ft/yr. Lower Cienega Creek Basin ET, as used in the calibrated Chong-Diaz (1995) groundwater model, was 2,200 ac-ft/yr.

M&A (2009b) further analyzed ET for the model study area. The ET rates developed by M&A (2009b) were adopted for use in Tetra Tech's regional groundwater flow model. Riparian areas, plant types, plant cover density, and riparian plant distributions were estimated from aerial photograph interpretations, previous vegetation mapping by Harris et al. (2000), and from field visits by M&A personnel.

The M&A (2009b) analysis method included dividing the model study area's riparian vegetation into plant functional groups (PFGs). These are groupings of plants that have similar responses to environmental conditions and have similar impacts on ecosystem processes (Maddock and Baird, 2003). Annual groundwater consumption for each PFG was estimated based on desert southwest ET measurements obtained by Leenhouts et al. (2006) and Maddock and Baird (2003). Groundwater discharge due to riparian evapotranspiration was estimated to be 3,100 ac-ft/yr in upper Cienega Creek, 1,030 ac-ft/yr in lower Cienega Creek, and 115 ac-ft/yr in Davidson Canyon, for a total of 4,240 ac-ft/yr in the model study area. Additional details of how these ET estimates were obtained are provided in M&A (2009b).

2.7 Groundwater Pumping

All water use within the Cienega Creek Basin is from groundwater sources with no recorded surface-water diversions (ADWR, 2006). Average-annual water demand in the Cienega Creek Basin was 1,250 acre-feet (ac-ft) between 2001-2006, which included 600 ac-ft of municipal demand, 150 ac-ft of industrial demand, and 500 ac-ft of agricultural demand (ADWR, 2009). Municipal, industrial, and agricultural groundwater use has remained fairly consistent since 1991. Approximately 170 acres of vineyards have been reported in the Cienega Creek Basin, with most vineyards being located in the Elgin area (ADWR, 2006). These estimates do not include pumping in the Davidson Canyon watershed, which is outside of the ADWR Cienega Creek Basin boundary.

Groundwater pumping in the upper Cienega Creek Basin was estimated by Knight (1996) to be 400 to 500 ac-ft/yr. Most of the pumping was from wells in the Sonoita-Elgin area. Groundwater pumping at Empirita Ranch, in the lower Cienega Creek Basin, was estimated by M&A (1985) to be 340 ac-ft/yr; however, Empirita Ranch pumping was retired in 1991 when Pima County purchased the Empirita Ranch properties.

Domestic groundwater users are likely tapping the regional groundwater system in the Davidson Canyon watershed to supply water to their homes, ranches, and small businesses. The ADWR well registry database indicates that there are over 300 wells (monitoring wells excluded) within the Davidson Canyon watershed (Appendix A, Figure 11). As of 2005, there were 1,874 registered wells within Cienega Creek Basin with a pumping capacity of less than or equal to 35 gpm and 169 wells with a pumping capacity of more than 35 gpm (ADWR, 2006). In the absence of actual discharge rates from these wells, the magnitude and spatial distribution of impacts on the hydrologic system due to this pumping cannot be accurately assessed.

Although available data does not allow withdrawals to be accurately determined, the cumulative withdrawal from these wells could be 300 gpm to 1,500 gpm (480 to 2,400 ac-ft/yr) assuming the range of average discharge is from one (1) gpm to five (5) gpm. This range of groundwater withdrawal is expected to be greater than the pumping expected due to dewatering the Open Pit or from evaporative losses during the steady-state, post-closure pit-lake condition.

2.8 Groundwater and Surface-Water Fluctuations

Natural climatic variations can also impact groundwater resources within the Davidson Canyon watershed and Cienega Creek Basin. The shallow groundwater system, spring, and surface flows can be sensitive to drought and changing climatic conditions. The "Unique Water Nomination for Davidson Canyon" application filed by PAG (2005) indicated that drought conditions had decreased flows at the "unnamed" spring.

Surface-water flows in the model study area show considerable natural variation. The beginning of a flow location within the Jungle Road site, for example, varied from 500 to 1,370 feet over a three (3) year monitoring period. The percent flow over three (3) sites ranged from zero to 100 percent (dry to continuous flow over the reach) (PAG, 1998). Cienega Creek, near Pantano stream gage (USGS station ID 09484560), had a minimum estimated annual flow of 608 ac-ft/yr (0.84 cfs), a median flow of 1,408 ac-ft/yr (1.9 cfs), and a maximum flow of 4,496 ac-ft/yr (6.2 cfs). Davidson Canyon is typically dry, but an estimated peak flood flow of 38,000 cfs occurred on August 11, 1958 (USGS data reported by Pima County Department of Transportation and Flood Control District, 1993). Water-level data reported by PAG (1998) also indicated significant natural groundwater level variations in lower Cienega Creek of six (6) to nineteen (19) feet over a three (3) year monitoring period (PAG, 1998).

An analysis of water levels in the Project area was performed by M&A (2010b). Water levels measured for the Rosemont groundwater monitoring program indicated that recent (2007-2009), short-term (2 to 3 years) groundwater level fluctuations ranged from 0.71 to 33.07 feet at 52 wells, with an average fluctuation of 7.1 feet. Long-term groundwater-level data were obtained from the Anamax groundwater monitoring program for the period 1975 through 1982, from the Rosemont groundwater monitoring program for the period 2006 through 2009, and from historic monitoring data obtained from the ADWR Groundwater Site Inventory (GWSI) database (ADWR, 2010b). The long-term (37 to 55 years) groundwater-level fluctuations ranged from 0.70 to 69.04 feet at 14 wells, with an average fluctuation of 19.7 feet. Groundwater fluctuations in the Davidson Canyon area have been observed to range from four (4) to 25 feet (M&A, 2010b).

The water-level and stream flow fluctuations observed in the available data likely underestimate actual fluctuations. Measurements are intermittent, inconsistent, and have occurred over relatively short periods of time. Extreme water-level and flow conditions have likely not been observed due to the incomplete data record.

3.0 POTENTIAL IMPACTS

The long-term impacts to the water resources in Davidson Canyon and in the Cienega Creek watershed need to be evaluated in the context of long-term pit inflows associated with the anticipated terminal pit-lake. The reduction of water to the regional groundwater flow system cannot exceed the steady-state groundwater inflow to the pit. Pit-inflow estimates will be highest following the cessation of pit dewatering and will gradually decrease to a steady-state condition. As the pit-lake level stabilizes at an equilibrium level, so will groundwater inflows. The cone-of-depression associated with an open pit having a terminal pit-lake will extend away from the pit until an equal volume of water is captured from the flow system and a new equilibrium is established. Estimates of groundwater inflows associated with the Rosemont Open Pit are presented in Section 8.0, "Predictive Simulations".

3.1 Stream Flow

Water-level data and stream channel elevations indicate that stream flow is largely disconnected from the groundwater flow system. However, the hydrologic conditions are highly variable and can change over short stream reaches. Stream flow recharges the groundwater system in some reaches, while leaky confined, basin-fill aquifer conditions likely supply the stream channel alluvium with groundwater. Overall, available data indicate that a persistent hydraulic connection does not exist between the stream channels and the regional groundwater system in the model study area. Groundwater-level declines are therefore not likely to significantly impact stream flows.

It has been estimated that the surface area affected by the Project comprises about 16 percent of the entire Davidson Canyon watershed. Stormwater flow patterns in the Project area will be altered by the Project facilities. However, construction of flow-through drains is anticipated as part of the Project which are designed to pass stormwater from the up-gradient side of the facilities to the down-gradient side. During average annual conditions, stormwater entering these flow-through drains will result in infiltration and ultimately recharge to the groundwater system or to the pit-lake. This will increase the lake stage and reduce the long-term, down-gradient drawdown associated with the steady-state terminal, pit-lake. Storms resulting in higher than average annual precipitation conditions could also generate runoff through the flow-through drains, which would supply stormwater to vegetation in the lower reaches of Davidson Canyon.

3.2 Riparian Vegetation

Water-level declines in stream channel reaches with riparian vegetation could result in reductions in plant health, density, and distribution. The regional water table would have to be lowered beyond the root depths to cause canopy dieback in vegetation that is dependent on groundwater. Since the greatest drawdown would be observed close to the Open Pit, the limited riparian vegetation in the upper reaches of Davidson Canyon would be the most likely to be impacted. However, based on the depth to groundwater measurements at the Project site, it is unlikely that these plants are tapping the regional groundwater table in this area.

Riparian vegetation in the lower reaches of Davidson Canyon, lower Cienega Creek, and upper Cienega Creek are located approximately eight (8) to 15 miles from the Open Pit. Drawdown at these distant locations would be expected to occur slowly over a period of hundreds of years as the cone of depression propagates from the Open Pit. This gradual increase in DTW over a long-period of time would be a favorable condition, allowing plants to adapt and increase their root depths.

3.3 Water Quality

Down-gradient water-quality impacts due to the Project are not expected to occur due to the anticipated terminal hydraulic sink. The anticipated hydraulic sink condition has the potential to provide tertiary containment for most of the mine operations and prevent groundwater in the operations areas from flowing down-gradient to wells, springs, and riparian areas. The geometry of the capture zone of the hydraulic sink determines which sources of potentially impacted waters would be captured by the pit. An assessment of this capture zone is provided in Section 10.0, "Discharge Impact Area Analysis".

3.4 Local and Regional Springs

Springs are the most likely groundwater resources to be impacted by the Project. Springs near the Open Pit will likely be impacted by pit dewatering and by Project disturbance. The springs located nearest the pit are McCleary, MC-1, MC-2, Fig Tree, Sycamore, Helvetia, Peligro Adit, Ruelas, SW, Locust, and Deering Springs (Appendix A, Figure 8). If the source areas that supply water to these springs are disturbed by pit development or associated Project facilities, they would likely experience decreased or terminated flows. Long-term pit dewatering is expected to reduce water levels in the low storage bedrock forming the crest of the Santa Rita Mountains, but would not be expected to alter the local flow system.

The anticipated reduction in discharge at the springs indicated above is based solely on their proximity to the pit. Papago, Mulberry, Crucero, Lower Mulberry, Scholefield, SC-2, and Barrel Springs (Appendix A, Figure 8) appear to be fed by local recharge. Since these springs are not likely connected to the deeper, regional groundwater flow system, and are at a sufficient distance from the pit, they are not expected to be impacted by the Project.

Questa Spring (Appendix A, Figure 8) is likely fed by the regional groundwater flow system. Pit dewatering and alteration of the recharge mechanisms may affect flows at this spring. Rosemont Spring will be buried by waste rock. Additionally, its proximity to the pit makes it likely to have terminated flows.

Davidson Spring, the "unnamed" or Reach 2 Spring, and Escondido Spring are located in the lower reach of Davidson Canyon (Appendix A, Figure 8) at distances of nine (9) to 14 miles from the proposed pit. Davidson Spring is likely fed by recharge from the Empire Mountains and is likely disconnected from the upper reaches of Davidson Canyon. No data are available to conclusively determine the source of water to Davidson Spring. Evidence suggests that the "unnamed" or Reach 2 Spring and Escondido Spring are fed largely by summer recharge from surface-water flows and not by regional groundwater. The lack of a persistent hydraulic connection between the Reach 2 Spring and Escondido Spring, and surface flows to the regional groundwater flow system makes it unlikely that they will be impacted by Project activities.

3.5 Groundwater System Changes

Dewatering of the Open Pit and the subsequent formation of a pit-lake will result in groundwater lowering in the vicinity of the Project facilities. The magnitude of these changes will evolve and change through time with the various operational phases and after the cessation of pit dewatering and formation of a terminal pit-lake. Impacts near the Open Pit will be most pronounced near the end of the mining when the pit is fully dewatered. In contrast, the effects of a lowered groundwater table in the Project area may not fully develop for hundreds of years down-gradient of the site, at which time small water-level declines could materialize.

At large distances from the Open Pit, however, the complexity of the flow system and the numerous variables that cause water-level declines on a regional scale make it technically challenging to distinguish impacts due only to the Project. In reality, distal impacts to groundwater elevations from dewatering of the Open Pit may be indiscernible from natural and other man-induced regional water-table fluctuations.

Large groundwater fluctuations have been observed in the Davidson Canyon and (M&A, 2010b), lower Cienega Creek areas (PAG, 1998;. M&A, 2010b). Changing weather and climate conditions, or other stresses, including groundwater pumping in Davidson Canyon, in the Cienega Creek Basin, and potentially in the Tucson Basin, could impact water levels in the model study area. Drawdown due to the Project in riparian and stream channel areas would need to approach the magnitude of these natural fluctuations to be distinguishable from other causes.

4.0 HYDROGEOLOGIC FRAMEWORK

The hydrogeologic units (HGUs), their spatial distribution, the 3D hydrogeologic framework model, and the hydraulic properties that supported development of the regional groundwater flow model are presented in this section. The 3D hydrogeologic framework model was used to define the distribution of HGU zones in the groundwater flow model. These HGU zones were then assigned initial hydraulic properties based on an evaluation of available hydraulic testing data. During the calibration process, the hydraulic properties of the HGUs were modified as needed to improve the model's fit to observed water levels and stream flows. For example, the Paleozoic HGU zone near the Open Pit was subdivided to better represent the Backbone Fault and the near vertically dipping beds. The other HGUs, however, honored the original distribution of geologic units.

The fundamental geologic and hydrogeologic data used in creating the 3D hydrogeologic framework model was created by the AZGS, USGS, Rosemont geologists, and M&A geologists. Rosemont geologists developed several detailed geologic cross sections and maps in the proposed Open Pit area based on mineral exploration borehole data. M&A reviewed these geologic sections and maps and modified them based on hydrologic investigation boreholes (wells) completed by M&A. Cienega Creek Basin geology was also evaluated by M&A using studies by the USGS (Finnell, 1971; Drewes, 1972), the AZGS (Johnson and Ferguson, 2007; Spencer et al., 2001; Ferguson et al., 2001; Ferguson, 2009; Ferguson et al., 2009), and geologic and drillers' logs from selected wells in the model study area. The hydrogeologic cross sections and horizontal slices that extended across the model study area, i.e., model domain, were developed by M&A (2009a) and M&A (2009b).

4.1 Hydrogeologic Units

The geologic units within the model study area were grouped into ten (10) HGUs based on similar lithology, age, areal extent, and material properties (M&A, 2009b). A brief description of each HGU within the 3D hydrogeologic framework model, and their abbreviation, is provided in Table 4-1.

Table 4-1 Hydrogeologic Units used in the Hydrogeologic Framework Model

| Hydrogeologic Unit Abbreviation | Brief Description | Geologic Units |
|--|---|--|
| Qal | Quaternary and Recent alluvium | Unconsolidated sand, gravel, and silt deposits along ephemeral wash channels or occurring as a thin veneer of unsaturated sediment overlying older rock units in the upland areas. |
| QTg | Late Tertiary to Early Quaternary basin-fill deposits - higher permeability | Basin-fill deposits, less cemented |
| QTg1 | Late Tertiary to Early Quaternary basin-fill deposits - lower permeability | Older basin-fill deposits, cemented, with larger clay content |
| QTg2 | Late Tertiary to Early Quaternary basin-fill deposits - lowest permeability | Basin-fill deposits, cemented, not substantially fractured or faulted |
| Tsp | Early to Mid-Tertiary sedimentary and volcanic units | Pantano Formation |
| KTi | Upper Cretaceous and Early Tertiary intrusive rocks | Quartz Monzonite Porphyry |
| Kv | Upper Cretaceous volcanic rocks | Salero Formation, Hilton Ranch Conglomerate, Fort Crittenden Formation |
| Ksd | Lower Cretaceous sedimentary units (Bisbee Group) | Bisbee Group (Turney Ranch Formation, Shellenberger Canyon Formation, Apache Canyon Formation, Willow Canyon Formation, and Glance Conglomerate) |
| Pz | Paleozoic sedimentary and metamorphic formations | Naco Group (Permian and Pennsylvanian), Black Prince Limestone (Mississippian or Pennsylvanian), Escabrosa Limestone (Early Mississippian), Martin Limestone (Late Devonian), Abrigo Formation (Middle to Late Cambrian), and Bolsa Quartzite (Middle Cambrian). The Naco group is subdivided into: Rain Valley Formation (Permian), Concha Limestone (Permian), Scherrer Formation (Permian), Epitaph Formation (Permian), Colina Limestone (Permian), Earp Formation (Pennsylvanian/Permian), and the Horquilla Limestone (Pennsylvanian). |
| pCb | Precambrian igneous and metamorphic crystalline formations | Continental Granodiorite, Pinal Schist |

HGU descriptions from M&A (2009b) are provided in the following subsections for reference. Detailed geologic descriptions are available from the original data sources (Finnell, 1971; Drewes, 1972a; Drewes 1971; Johnson and Ferguson, 2007; Spencer et al., 2002; Ferguson et al., 2001; Ferguson, 2009; and Ferguson et al., 2009). The original hydrogeologic unit distributions, used as the basis for the 3D geohydrologic framework model, are presented at 200-foot intervals between the elevations of 5,400 to 2,400 feet amsl in M&A (2009b).

4.1.1 Quaternary and Recent Alluvium (Qal)

The Quaternary and recent alluvium (Recent alluvium) generally consists of unconsolidated sand, gravel, and silt deposits along ephemeral wash channels or occurs as a thin veneer of unsaturated sediment overlying older rock units in upland areas. When water is present during or after storm runoff, these deposits provide short-term storage of water which infiltrates downward into older rocks and/or which migrates downstream through the Recent alluvium. In the lower Cienega Creek section south of and adjacent to Interstate-10, a thick coarse-grained zone of Recent alluvium is present in an area of shallow groundwater. In this area, the Recent alluvium is an important aquifer and has the largest known hydraulic conductivity in the model study area. Groundwater occurs in the Recent alluvium along much of upper Cienega Creek. The Recent alluvium along other drainage channels, including Davidson Canyon and Barrel Canyon, is intermittently or ephemerally saturated (M&A, 2009b).

4.1.2 Late Tertiary and Quaternary Basin-Fill Deposits (QTg, QTg1, and QTg2)

The Late Tertiary and Quaternary basin-fill deposits comprise a principal aquifer in the Cienega Creek and Tucson Basins. Aquifer hydraulic parameters in these sediments are highly variable.

The deepest Tertiary sediments in the model study area included some well-cemented, older, deformed units deposited prior to the formation of the basin, but younger than the Pantano Formation. Above these Tertiary sediments are progressively younger, less deformed sediments deposited in conjunction with down-faulting that occurred during formation of the regional basins. The younger sediments tend to be less cemented and have higher permeability. Therefore, aquifer permeability within the basin-fill deposits tends to be highest in the younger, shallower sediments and tends to decrease with depth. Aquifer permeability can also be lower in basin-fill deposits where the silt and clay content is large. Sediments deposited in areas with low relief and flatter topography tend to have proportionately larger silt and clay contents. This condition is more common toward the interior of an alluvial basin where sediments are typically deposited under low energy conditions.

For purposes of modeling, the basin-fill deposits in the model study area were subdivided into three (3) different hydrogeologic units. These divisions were based on inferred or known permeabilities. The younger and more permeable basin-fill deposits were designated as QTg on the surface and subsurface maps. Sequences of basin-fill deposits with a lower permeability than QTg were designated as QTg1. These sediments include older, cemented basin-fill, or basin-fill with large clay contents. Basin-fill sediments occurring in the southeast part of the pit area, designated as QTg2, are more strongly cemented than QTg1 sediments due to age and their proximity to Paleozoic carbonate rocks. The cemented QTg2 sediments were deposited mostly after faulting and mountain-building activity in the area. These sediments are not substantially fractured or faulted, contributing to their low hydraulic conductivity.

The depth of basin-fill deposits in the upper and lower Cienega Creek Basin and in the Tucson Basin was interpreted from two (2) basic sources of information: site-specific geologic and lithologic data obtained from drilling and regional depth-to-bedrock maps developed from gravity data. Where drilling data were available and considered reliable, well logs were used to infer the thickness of basin-fill deposits (and alluvium) and the depth to underlying bedrock. Drilling information, where available, was used to refine the interpretations of gravity data obtained from the depth to bedrock map developed by Oppenheimer and Sumner (1980), and from gravity mapping of the lower Cienega Creek Basin (Ellett, 1994).

4.1.3 Early to Mid-Tertiary Sedimentary and Volcanic Rocks (Tsp)

The Early to Mid-Tertiary sedimentary and volcanic rocks are mostly associated with the Pantano Formation in the model study area. The Pantano Formation either directly underlies much of lower Cienega Creek or underlies younger sediments near the creek. Besides the lower Cienega Creek Basin and Davidson Canyon area, small exposures of Pantano Formation are found in the northern Santa Rita Mountains, east of the Rosemont Project area, and in the southwest part of the Whetstone Mountains. Except for the area around the lower Cienega Creek Basin to the north and northeast of the Empire Mountains, the Pantano Formation is not considered hydrogeologically significant in the model study area. The low permeability of the shallow Pantano Formation in the lower Cienega Creek Basin forces overlying groundwater to the surface.

4.1.4 Upper Cretaceous and Early Tertiary Intrusive Rocks (KTi)

The Upper Cretaceous and Early Tertiary (Laramide) intrusive rocks are generally restricted to the northern Santa Rita and Empire Mountains. These units have very low primary porosity and permeability, but will store and transmit small quantities of water where fractured or faulted. The Laramide intrusive rocks consist of quartz monzonites, granodiorites, quartz latite porphyries, and diorites.

4.1.5 Upper Cretaceous Volcanic and Sedimentary Rocks (Kv)

The Upper Cretaceous volcanic and sedimentary rocks are an important unit in the northeast part of the Santa Rita Mountains but are relatively uncommon in other parts of the model study area. These rocks are well-lithified and have very low primary porosity and permeability, except where fractured or faulted. The Upper Cretaceous volcanic and sedimentary sequence consists of the Salero Formation, the Hilton Ranch conglomerate, and the Fort Crittenden Formation. There is a substantial unconformity between the Upper Cretaceous sediments and the underlying Lower Cretaceous Bisbee group sediments. The Fort Crittenden Formation is the basal unit of the Upper Cretaceous sequence. It consists of boulder conglomerate and pebbly sandstone. The Fort Crittenden Formation is not found at all locations in the model study area and is not present in the vicinity of the proposed Rosemont Project area. The Hilton Ranch conglomerate, found in the Empire Mountains, is considered correlative with the Fort Crittenden Formation (Shafroth, 1968). The Fort Crittenden Formation is overlain by volcanic breccias of the Salero Formation, without any apparent break in deposition (Ferguson et al., 2001). The Salero Formation in the Santa Rita Mountains consists of a basal unit of andesitic to dacitic lava and breccia, overlain by a thick sequence of silicic ash-flow tuff and welded tuff called the Mt. Fagan Rhyolite. In approximately 75 percent of the area where it occurs, the Mt. Fagan Rhyolite contains very large lithic blocks composed of older units, including rocks of the Bisbee Group, the Fort Crittenden Formation, and basal andesite. The Mt. Fagan Rhyolite grades upward into a sequence of sedimentary and tuffaceous rocks which are mapped as part of the Salero Formation (Drewes, 1971).

4.1.6 Lower Cretaceous Sedimentary Rocks (Bisbee Group) (Ksd)

Rocks of the Bisbee Group tend to have very low primary porosity and permeability. An exception to this is the Glance Conglomerate, which locally appears to have moderate primary permeability. Bisbee Group rocks are deformed over much of the model study area, but less so than the Paleozoic rocks. In some areas, they are locally fractured, providing secondary permeability.

The Bisbee Group is a mixture of non-marine and marginal marine sedimentary units. The Bisbee Group is made up of five (5) formations in the model study area. These are, from youngest to oldest, the Turney Ranch Formation, Shellenberger Canyon Formation, Apache Canyon Formation, Willow Canyon Formation, and Glance Conglomerate (Schafroth, 1968). The Turney Ranch Formation is an intercollated sequence of thin to thick bedded sandstones, siltstones, and shales. The Shellenberger Canyon Formation consists of arkosic sandstone, thin-bedded siltstones, and shales. The Apache Canyon Formation is made up of thin bedded, organic-rich limestones, siltstones, and shales. The Willow Canyon Formation is primarily an arkosic sandstone and arkosic sandstone conglomerate. In the Rosemont Project area, the Willow Canyon Formation includes a local andesite unit which can be a few tens of feet up to a few hundred feet thick. The Glance Conglomerate has two (2) facies, one (1) of which is comprised of eroded Paleozoic carbonate rock, while the other is comprised largely of Precambrian granitic rock fragments.

Bisbee Group rocks, particularly the Willow Canyon Formation, were penetrated by a minimum of eight (8) wells in the vicinity of the proposed Rosemont Project (on the east side of the Santa Rita Mountains). Aquifer testing showed that hydraulic conductivities in these wells varied by more than three (3) orders of magnitude. Because rocks of the Bisbee Group have little to no primary permeability, the variation in hydraulic conductivity is attributed to the degree of faulting and fracturing present at the completed depth in each well. Similar variations in permeability were apparent from aquifer testing conducted at wells completed in Paleozoic units and in the Salero Formation.

The Bisbee Group rocks outcrop extensively along the eastern and northern slopes of the Santa Rita Mountains. They cover a large area around the Empire Mountains and in the west-central part of the Whetstone Mountains. In addition, Bisbee Group rocks are known to underlie the basin-fill deposits in much of the upper Cienega Creek and Tucson Basins.

4.1.7 Paleozoic Sedimentary and Altered Sedimentary Rocks (Pz)

Paleozoic sedimentary rocks outcrop in all of the mountain ranges within the model study area. These units have little to no primary porosity and permeability, but will store and transmit water where fractured or faulted and tend to be much more deformed and fractured than younger rocks. Early Mesozoic rock units are rare and outcrop over very small areas in the model study area. Because these units occur with the Paleozoic rock and tend to have similar hydraulic characteristics, the Paleozoic and Early Mesozoic rocks were grouped into the same HGU.

The Paleozoic rocks in the model study area include limestone, dolomitic limestone, and dolomite, along with lesser amounts of sandstone, conglomerate, shale, and siltstone. Many of the limestone rocks in the Project area have been altered and/or metamorphosed to skarn or marble. The Paleozoic Formations present in the model study area, from youngest to oldest are: the Naco Group (Permian and Pennsylvanian); Black Prince Limestone (Mississippian or Pennsylvanian); Escabrosa Limestone (Early Mississippian); Martin Limestone (Late Devonian); Abrigo Formation (Middle to Late Cambrian); and Bolsa Quartzite (Middle Cambrian). The Naco group is subdivided into: Rain Valley Formation (Permian); Concha Limestone (Permian); Scherrer Formation (Permian); Epitaph Formation (Permian); Colina Limestone (Permian); Earp Formation (Pennsylvanian/Permian); and the Horquilla Limestone (Pennsylvanian).

Paleozoic rocks outcrop occur within and north of the Project area, along the eastern slopes of the Santa Rita Mountains, where they are extensively faulted and are steeply dipping at angles typically in the range of 60 to 80 degrees. Limestone units of the Naco group, particularly the Horquilla Limestone, are the host rock for copper mineralization in the Rosemont area. Mineralizing fluids severely altered the Paleozoic rocks in the vicinity of the intrusion that

created the orebody. Paleozoic rocks are also abundant in the Empire, Whetstone, and Mustang Mountains, and in the northern part of the Canelo Hills.

4.1.8 Precambrian Basement Rocks (p€b)

The Precambrian basement rocks are the oldest rock units known to occur in the model study area. They were heavily eroded in the Late Precambrian era and were exposed when the earliest Paleozoic marine rocks were deposited. These crystalline rocks have little to no primary porosity or permeability and are generally considered a barrier to groundwater movement, except where fractured or faulted. The primary Precambrian rock units in the model study area are the Continental Granodiorite and the Pinal Schist (Drewes, 1980). The Continental Granodiorite is the principal Precambrian rock unit in the model study area. It outcrops extensively on the western slopes of the Santa Rita Mountains near the Project area. The Continental Granodiorite also outcrops in the pediment area north of the Empire Mountains and in the northern part of the Whetstone Mountains. The Pinal Schist is less abundant in the model study area. It is present in small areas on the west side of the Santa Rita Mountains, the Whetstone Mountains, and in the northern part of the Empire Mountains.

4.2 Hydrogeologic Framework Model

A 3D hydrogeologic framework model is a representation of the extent and geometry of the hydrogeologic units. Development of a hydrogeologic framework model was a necessary step toward creating a geologically-based numerical flow model. As indicated, the hydrogeologic framework model scope was limited to the original M&A model domain (M&A, 2009b) and the existing horizontal hydrogeologic slices developed by M&A (2009b). No additional field investigation or geologic interpretation was completed by Tetra Tech.

4.2.1 Approach

The 3D hydrogeologic framework model was constructed using the Mining Visualization System (MVS) software package (CTech, 2010) and was based on hydrogeologic data represented on horizontal slices taken at 200-foot intervals between elevations 5,400 and 2,400 feet amsl. These horizontal slices, or 2-dimensional (2D) layers, represent the subsurface hydrogeologic units (M&A, 2009b). These hydrogeologic slices were created from a combination of publically available surface geology maps, borehole lithology data, and cross sections. Additional details of the 3D hydrogeologic framework model can be found in the Technical Memorandum titled *Hydrogeologic Framework Model* (Tetra Tech, 2010h).

4.2.2 3D Framework Model

The process utilized to transform the 2D data sets into the 3D model consisted of three (3) steps:

- Step 1. Data sampling** – Convert horizontal slices from GIS shapefile polygon format to a grid with approximately 400-meter horizontal spacing.
- Step 2. Hydrogeologic Unit Interpolation** – Define the HGUs in the regional groundwater flow model grid utilizing indicator kriging and interpolation methods.
- Step 3. Consistency Check** – Perform Quality Assurance/Quality Control check of the resulting 3D hydrogeologic framework model to ensure consistency with the source horizontal (2D) layers. The hydrogeologic framework model was corrected where statistical interpolation resulted in conceptually inconsistent rock types.

4.2.2.1 Data Sampling

The conceptual hydrogeologic model developed by M&A was visualized in 2D horizontal slices (M&A, 2009b). These slices were provided in polygon-format GIS shapefiles, one (1) shapefile for each of the 16 horizontal slices (5,400 to 2,400 feet amsl with a 200-foot vertical spacing).

The bottom of the proposed pit was at an elevation of 3,050 feet amsl. The 3D hydrogeologic framework model was extended to an elevation of 1,000 feet amsl to allow simulation of deep groundwater flow in the regional groundwater flow model. Two (2) additional horizontal slices were therefore created at elevations 2,000 and 1,600 feet amsl. These slices were constructed to be conceptually consistent with the existing 2,400 feet amsl layer by continuing previous trends to a depth of 1,000 feet amsl. However, the lack of vertical boreholes at these depths prevented confirmation of the interpolated geology.

The horizontal slices were sampled on a grid that produced a sufficient data density to minimize the extent of spatial statistical interpolation used to identify the most probable rock type. The grid data were then converted into 3D boring logs, which were used in the MVS software package (CTech, 2010) to create the 3D hydrogeologic framework model.

The grid data captured the major HGU features found in the original data (M&A, 2009b). Exceptions included areas where the scale of the feature was smaller than the 400-meter grid spacing, such as the Upper Cretaceous and Early Tertiary intrusive unit (KTi) near the pit. This KTi unit was therefore manually defined in the 3D hydrogeologic framework model.

4.2.2.2 Hydrogeologic Unit Interpolation

The hydrogeologic framework model grid was matched to the regional groundwater flow model grid, which is discussed in detail in Section 5.0, "Groundwater Flow Model Construction". Indicator kriging within the groundwater flow model layers was used to assign the highest probability hydrogeologic unit to each individual flow model cell. The 3D hydrogeologic framework model was then processed using the interpolation module to populate the final variable-thickness of the groundwater flow model grid. This resulted in a final 3D hydrogeologic framework model resolution that was matched to the groundwater flow model layers and cells.

4.2.2.3 Consistency Check

The 3D hydrogeologic framework model was examined for consistency with the conceptual hydrogeologic model provided by M&A (2009b). Inconsistencies are typically the result of scale issues or transitions between hydrogeologic units. As indicated, the 400-meter spaced grid could not capture small-scale, detailed features when the spacing was larger than the feature.

The transition between steeply dipping materials in two (2) horizontal hydrogeologic slices, or where the geology in one (1) slice was significantly different from the geology in the slices above or below, typically results in alternating HGUs near the contact. Inconsistencies that would significantly impact the regional groundwater flow model results were corrected, but other minor discrepancies were not edited.

The primary corrections included refining the Upper Cretaceous and Early Tertiary intrusive unit (KTi) present to the north of the pit and refining the distribution of the Recent alluvium (Qal) where the groundwater flow model layers intersected the land surface. The final 3D hydrogeologic framework model is shown on Figure 4-1.

A set of hydrogeologic sections in the form of a fence diagram was created to illustrate the internal hydrogeologic framework (Figure 4-2). Hydrogeologic sections A-A' and B-B' from the M&A's groundwater flow modeling report (M&A, 2009b) were compared to sections at the same locations in the 3D hydrogeologic framework model (Figures 4-3 and 4-4). A horizontal grey line

was added to the sections created using the MSV software to denote the maximum depth of the M&A hydrogeologic slices. Interpolation was performed below this elevation to extend the 3D hydrogeologic framework model to an elevation of 1,000 feet amsl. The 3D hydrogeologic framework model sections generally agreed well with the M&A sections. However, there were areas where the M&A section lines intersected a small portion of an HGU that was not manually drawn on the sections, but was included in the 3D hydrogeologic framework model. Examples of these areas are illustrated on Figures 4-3 and 4-4.

4.3 Hydraulic Properties

Short-term aquifer-test data and long-term test simulated data were evaluated to estimate hydraulic properties in the Project area. These hydraulic-property estimates were used to guide and constrain development of the regional groundwater flow model. The scope was limited to existing testing completed by M&A as documented in the following reports. No additional field investigations or hydraulic testing was completed by Tetra Tech.

- Short-term aquifer tests performed from 5/15/2007 to 6/1/2007 (Results of Drilling, Construction, and Testing of Four Pit Characterization Wells, Rosemont Project, M&A, 2009b);
- Short-term aquifer tests performed from 6/18/2008 to 10/23/2008 (Results of Phase 2 Hydrogeologic Investigations and Monitoring Program, M&A, 2009a, Volume 2); and
- Long-term aquifer tests completed between 11/19/2008 and 1/21/2009 (Analysis of Long-Term, Multi-Well Aquifer Test November 2008 through January 2009, M&A, 2009c).

The approach selected to determine the initial hydraulic properties representing the rock units in the groundwater flow model was to conduct a quality-assurance evaluation of M&A's aquifer test analyses, perform a re-analysis of select short-term aquifer test data, and develop a method for analyzing the 30-day aquifer-test data. A range of hydraulic-property parameter values was then developed for the tested geologic formations and hydrogeologic units located within the groundwater flow model.

4.3.1 Geologic Units

Hydrologic testing results were analyzed by geologic units and then grouped into the hydrogeologic units presented in Table 4-1. The geologic unit descriptions are as follows (modified from Johnson and Ferguson, 2007):

Willow Canyon Formation (Lower Cretaceous): A succession of medium- to coarse-grained feldspathic to argillaceous sandstone with vuggy, silty mudstone. There is a volcanoclastic conglomerate interval near the middle of the unit below a sequence of mafic lava flows. This unit is up to 7,200 feet thick.

Glance Conglomerate (Upper Jurassic and/or Lower Cretaceous): A massive to very thick-bedded, clast-supported conglomerate containing pebble- to boulder-sized clasts reflecting the composition of underlying units (Proterozoic through Permian). The unit is at least 720 feet thick at the HC-1 well cluster.

Concha Limestone (Permian): A grey, medium- to thick-bedded, massive to planar-laminated, amalgamated, cherty limestone (locally dolomitic) with poorly formed chert nodules that locally form lenses. The Concha Limestone is mostly micritic and is about 650 to 820 feet thick.

Scherrer Formation (Permian): Generally light grey to pink, fine-grained, massive quartzose sandstone with rare laminations. The upper portion is locally differentiated as a transitional interval consisting of cream-colored, medium-bedded, dolomitic with poorly preserved siltstone and argillaceous carbonate rocks. The unit is about 330-490 feet thick.

Epitaph Formation (Permian): A mixed siliciclastic-carbonate unit. The siliciclastic units are purple to reddish, thin- to medium-bedded siltstone and silty mudstone, and a fine-grained laminated sandstone. These units are often metamorphosed to a light orange-pink or greenish hornfels. The carbonate units are light grey to pink micritic carbonates. The Epitaph Formation is about 250 to 390 feet thick.

Colina Limestone (Permian): A light grey to white, medium- to thick-bedded, amalgamated, commonly dolomitic, micritic carbonate and skeletal wackestone that is about 165 to 260 feet thick.

4.3.2 Short-Term Aquifer Test Analysis

Short-term aquifer tests were completed by M&A in 2007 and 2008 (M&A, 2009a and M&A 2009d). These constant-rate pumping tests were conducted for 12- or 24-hours. M&A analyzed these tests using the Cooper-Jacob (1946) and Theis (1935) type curve matching methods. A number of tests were re-analyzed as a quality assurance measure by Tetra Tech to determine if differences in test interpretation would result in significant differences in parameter values.

Short-term aquifer tests that were amenable to standard straight-line solutions were re-analyzed. These aquifer tests were selected to meet the requirements of the Cooper-Jacob or Theis Recovery solutions as closely as possible. This constraint eliminated the observation well data, since the observation wells were not screened at the same depth intervals as the pumped wells. Re-analysis results for the pumped well data sets, and a comparison to the M&A results for the same pumped well data sets, are provided in Appendix B.

The pumped wells were selected for analysis based on the following constraints:

- In cases where a packer was used in a pumped well, the pumped well was selected if there was little or no drawdown above the packer, indicating that the packer was effectively isolating the pumped interval.
- The measured drawdown in the observation well was at least a few inches, and the water level recovered when pumping was stopped. This indicated that the measured response was due to pumping and not due to other influences.
- If multiple pumping rates were used, only the drawdown for the first rate in the pumped well was analyzed, and recovery data were not analyzed. Multiple pumping rates were defined as persistent changes in rate that produced an obvious and sudden effect on the drawdown in the pumped well, so that fitting a single straight line was not feasible. The recovery data were not re-analyzed since the aquifer was affected by multiple pumping rates and durations.
- If multiple straight lines were observed in the data, the one least likely to correspond to borehole storage (early-time data), or a possible boundary condition (very late-time data), was selected for the curve match.
- Tests in which drawdown anomalies occurred near the end of the pumping period were analyzed using the earlier drawdown data only. Recovery data were not re-analyzed.

In summary, the hydraulic conductivity values obtained from the re-analysis of the short-term aquifer test data using the Cooper-Jacob (1946) and Theis (1935) methods were similar to the

results of M&A's original analyses (M&A, 2009a). The geometric mean of the original analysis (0.08 feet/day [ft/d]) and the re-analyzed data set (0.06 ft/d) are nearly identical. The hydraulic conductivity values M&A obtained ranged from 0.0004 to 761 ft/d. M&A's upper hydraulic conductivity value of 761 ft/d was from Tucson Basin well RC-2 that monitored the Upper Tinaja Beds, which pinch out to the east and are not present in the model study area. Several wells within the model study area in lower Cienega Creek's stream channel were completed in Recent alluvium and had high hydraulic conductivity estimates that ranged from 101 to 516 ft/d. The re-analyzed results from wells within the model domain were consistent with M&A's estimated range for the same wells.

4.3.3 Long-Term Pumping Test

A long-term pumping test was conducted by M&A from November 2008 to January 2009 (M&A, 2009c). Five (5) pumping wells (test wells) (PC-5, RP-6, HC-1B, HC-5A, and RP-3B) were pumped simultaneously, although with staggered starting dates. The longest duration of pumping was 30 days in PC-5 and all five (5) wells were pumped simultaneously for only 12 of the 30 days. Pumping in well RP-3B was terminated before the other wells due to excessive drawdown at a pumping rate of 27.8 gpm. Average pumping rates for all five (5) test wells varied from 27.8 to 47.2 gpm.

Since the five (5) test wells were pumped simultaneously, a drawdown analysis at the observation wells was performed to determine any interference or combined effects. If a water-level response was observed, the pumped well inducing the response was identified.

Pumping wells HC-5A and PC-5 were located approximately 3,500 feet apart, which was the closest spacing between the pumped wells (Figure 4-5). The drawdown analysis indicated that neither of these test wells, nor their nearby observation wells, hydraulically responded to the well's pumping. The other remaining pumping wells were at least one (1) mile from the next closest pumped well and no interference between the wells was observed. The drawdown analysis indicated that the observation wells only responded to pumping of the closest test well, and that many observation wells did not respond to pumping at all (Figure 4-5).

For example, the drawdown observed at observation well PC-6 did not change slope in response to pumping in test well HC-5A, indicating that only test well PC-5 induced a drawdown response at observation well PC-6. As a result of this analysis, each pumping well was considered to be a separate test for the subsequent analyses. This interpretation is in contrast to M&A's interpretation that the observed drawdown in observation well PC-6 was due to pumping at test wells PC-5 and HC-5A (M&A, 2009c).

4.3.3.1 Responses to Long-term Pumping

The long-term tests involved pumping from 12 to 30 days and the pumping rates were relatively low, ranging from 27.8 to 47.2 gpm. Five (5) observation wells had drawdown associated with pumping in test well PC-5. The observed maximum drawdown and distance from test well PC-5 (corrected for trends) for the observation wells are summarized as follows:

- PC-7: 1.45 feet of drawdown at a distance of 3,541 feet;
- PZ-7: 1.81 feet of drawdown at a distance of 3,490 feet;
- PC-6: 1.26 feet of drawdown at a distance of 2,195 feet;
- PC-2: 2.38 feet of drawdown at a distance of 1,371 feet; and
- PZ-5: 13.31 feet of drawdown at a distance of 61 feet.

Definitive responses to pumping from the other test wells in the observation wells occurred at much closer distances. Drawdown from test wells HC-1B and HC-5A was observed only in the nearest observation well within the well cluster. The observed maximum drawdown and distance from test wells HC-1B and HC-5A (corrected for trends) for observation wells HC-1A and HC-5B are summarized as follows:

- Pumping well HC-1B: 16.88 feet of drawdown in observation HC-1A at 30 feet; and
- Pumping well HC-5A: 6.95 feet of drawdown in observation HC-5B at 32 feet;

Although observation well RP-3A had an apparent response to pumping in nearby test well RP-3B, the drawdown data were deemed unreliable for analysis. Responses to pumping in other observation wells were not definitive and minor water-level changes could be attributable to other influences. There was no response in any of the observation wells to pumping in test well RP-6. M&A conducted an independent evaluation of these tests and in some cases came to different conclusions regarding which observation wells had drawdown and which pumping wells contributed to the drawdown (M&A, 2009b and M&A, 2009c).

The scale of these hydraulic tests, i.e., distance from pumped wells to observation wells, was from tens of feet to a few thousands of feet. The scale of the regional groundwater flow model, however, is on the order of tens of miles. At the relatively small scale of the tests, there are numerous hydrogeologic complexities such as faults, fractures, dikes, and lithologic changes that may have contributed to the observed responses. Distinct responses to flow barriers, however, were not observed in the hydraulic test data. In some cases, water levels did not return to pre-testing levels after pumping. These observations could be due to several factors, including a declining regional groundwater level trend.

4.3.4 Analysis Method Selection

Analytical and numerical methods can be used for analyzing the long-term hydraulic testing data to determine estimated hydraulic properties. Analytical methods are best suited for simple geology and testing conditions that are consistent with the method assumptions. Numerical models are better suited to more complex geology and test conditions, including multiple formations, multiple screen intervals, and varying discharge. As such, numerical models were deemed more appropriate for analyzing the long-term test data since they can better simulate the geologic and well configuration complexities.

Numerical models can be constructed as 2D and 3D representations of the flow system. Vertical, 2D radial flow models were considered for this analysis due to several positive attributes:

- A 2D radial flow model is an appropriate tool for simulating geologic heterogeneities present within a borehole or within a short distance between wells that neither an analytical solution nor a larger scale 3D regional groundwater flow model could accurately simulate.
- Vertical hydraulic gradients can be simulated in a 2D radial flow model, which is not possible in an analytical model. The 2D radial flow model allows for vertical and horizontal hydraulic conductivity estimates.
- Large variations in horizontal hydraulic gradients near a well can be accurately simulated in a 2D radial flow model due to the refined grid near the pumping well, whereas a 3D regional model grid cannot.

- Screen intervals of the pumping well and observation well(s) can be explicitly simulated in a 2D radial flow model due to the refined grid in the vertical direction, whereas a 3D regional flow model cannot.
- Since there was no interference observed between the five (5) pumping wells during the 30-day aquifer test, different 2D radial flow models can be created for each aquifer test to represent changes in lithologies with depth, well screen intervals, and well spacing, whereas this is not possible with a 3D regional flow model.

However, a radial flow assumption presents limitations on the geology that can be accurately simulated. A radial flow model grid represents cylinders or concentric shells around the borehole. A radial flow model is capable of representing different rock layers if those layers are laterally extensive on all sides of the borehole. A radial flow model, however, would not appropriately represent flow barriers (e.g., vertical dike, fault, or intrusive body) present on one side of the borehole, but not on the other.

Although a 3D numerical model could also be used to analyze the long-term test data and obtain aquifer properties, this approach was not taken in this study. There are two (2) basic 3D numerical model approaches that could have been used to simulate the long-term test data. The first approach would have been to analyze the data using the regional-scale model grid. The 3D regional groundwater flow model developed in MODFLOW for the model domain has 200 foot by 200 foot grid cells in the immediate pit area and 800 foot by 800 foot grid cells in the surrounding area. The relatively large cell sizes and layer thicknesses in the regional model result in simplifications of the hydrogeologic features that control the localized pumping responses. Additionally, the large cell sizes resulted in the pumping well and the closest observation well being located in the same model cell. An exception was pumping well RP-6, which did not have nearby observation wells. Although it is possible to interpolate drawdown to observation wells in the same model cell as the pumping well, the results are less accurate than if a finer grid were used.

The second potential 3D numerical model approach to simulating the long-term test data would be to create a refined “daughter” grid for the specific test area. The refined horizontal and vertical grid would allow for a more accurate representation of the geologic complexity and well configurations. A refined model would also require more detailed geologic data, such as orientations and spatial distributions of faults, fractures, and lithologic heterogeneities. Assuming that an approximation of the detailed geology was possible, the hydraulic properties from the refined, calibrated model would ultimately need to be incorporated into the regional model grid to simulate potential impacts from the Project. However, the geologic detail necessary to obtain a good calibration to the long-term pumping tests in a refined model could not be retained in the regional-scale model since MODFLOW-SURFACT (HydroGeoLogic, 2010) does not support embedded refined daughter models. Hydraulic properties would have to be scaled to the regional model (likely by averaging), which would obscure the distinct properties that were necessary to calibrate to the observed test responses. Therefore, the benefit of the refined grid would likely be lost.

Based on the benefits and limitations of the various long-term test analysis methods, 2D radial flow models were selected. Details of the 2D radial flow model construction, including estimates of the vertical and horizontal hydraulic conductivity and specific storage obtained from the models, are discussed in the following section.

4.3.5 Radial Flow Model Development

As an alternative to the long-term test analyses completed by M&A (2009c), 2D numerical radial groundwater flow models were used to analyze the long-term tests. The radial-model method

can accommodate pumping and observation wells screened at different depth intervals in the same or different geologic formations. Additionally, radial flow models allow the simulation of well completion data and greater geologic complexity than could be included in traditional analytical solutions. Another benefit of using a numerical model is that hydraulic properties can be optimized using automated parameter estimation (Doherty, 2010).

The long-term pumping tests were analyzed using the MODFLOW-96 numerical model code in a 2D, radial coordinate system (r - z ; *radial distance – vertical distance*). This analysis provided estimates of horizontal and vertical hydraulic conductivity (K_{xy} and K_z) and specific storage (S_s). Estimation of these hydraulic parameters was used to guide the selection of hydraulic properties in the 3D regional groundwater flow model.

The radial models were defined with the pumping well located at the $r = 0$ boundary. Lithologic information was incorporated into the model grid with the lithologic layers assumed to be perpendicular to the well axis. The screened intervals of the test and monitoring wells were incorporated into the model grid based on their locations relative to the lithology and distance relative to the center of the pumping well. A zero-drawdown boundary condition was located at a large radial distance (r) beyond the expected zone of influence of the pumping well. Recharge was assumed to be zero.

Details of the steps required for radial model construction, calibration, and post-processing methods can be found in the Technical Memorandum titled *Hydraulic-Property Estimates* (Tetra Tech, 2010g). Preprocessors and post-processors used in the radial modeling are also discussed in this Technical Memorandum.

4.3.5.1 Long-term Test Configurations

The test configuration for each of the five (5) pumping wells, including the observation wells, is discussed in this section. Well completion information, monitored geologic unit(s), and compatibility with radial flow modeling are presented. No packers were used in the pumping or observation wells during the long-term test; therefore, the responses are representative of the screened intervals. The configuration for each of the individual pumping wells is summarized as follows:

- **Pumping well PC-5:** All zones of PC-5 (109 to 2,001 feet) were open to pumping during the long-term test. The average pumping rate was 43.1 gpm. Water levels in observation wells PC-2, PC-6, PZ-7/PC-7, and PZ-5 (Figure 4-5) responded to pumping in test well PC-5. Observation well PC-1 may also have responded, but the response was not clear since no recovery was observed when pumping in test well PC-5 ceased. Available boring logs, geologic maps, and published and unpublished geologic sections provided by Rosemont and M&A were used to define the geology between PC-5 and each monitoring well that responded to pumping in PC-5. Each of the geologic sections between pumping well PC-5 and the observation wells are discussed below:

The geology of the section between PC-5, PZ-5, and PC-6 was based on Rosemont's unpublished geologic maps. This section contained multiple faults, truncated near-vertically dipping geologic beds, and younger units overlain on top of the truncated geologic units. Although a radial-model would be suitable for representing hydraulic conductivity differences between laterally-homogeneous geologic layers, it would not be suitable for representing the level of lateral heterogeneity found in this section. Therefore, this section was determined to be too geologically complex for representation and simulation in the radial-model analysis.

The geology between PC-5, PC-7, and PZ-7 crosses the proposed pit location, which has been subjected to a high degree of faulting and alteration. This section was also determined to be too geologically complex for representation and simulation in the radial-model analysis.

The geology between PC-2, PC-5, and PZ-7 is illustrated on Figure 4-6. The Willow Canyon, Concha Limestone, Scherrer Formation, Epitaph Limestone, and Colina Limestone are present in this section. Since this section lies along strike, the geologic units have no apparent dip along the section. However, the geologic units near PC-5 dip approximately 75-degrees based on geologic maps (Johnson and Ferguson, 2007). The units on either side of the steeply-dipping fault have the same dip and are part of the same hydrogeologic units, but bedding planes have been truncated. Although this potentially presents lateral heterogeneity, quantifiable drawdown was measured at PC-2 indicating that the fault was not a significant barrier to groundwater flow. Therefore, the geology present in this section was sufficiently amenable to the simplifying assumptions and was selected for analysis using the radial-model methodology.

- Pumped well RP-6: No observation wells responded to pumping in well RP-6 (47.2 gpm), so this data set was not amenable to radial-model analysis. Hydraulic properties for this test were estimated by M&A (2009b).
- Pumped well HC-1B: The entire screened interval (480-700 feet; 760-980 feet) of HC-1B was pumped at an average rate of 43.0 gpm. Observation well HC-1A, which is 30 feet from HC-1B, responded to pumping. Since these wells were completed in different depth intervals of the Glance Conglomerate with no faulting, the data set was analyzed using the radial-model analysis method. The configuration of these wells is illustrated on Figure 4-7.
- Pumped well HC-5A: The entire screened interval (100-540 feet) of HC-5A was pumped at an average rate of 39.7 gpm. Observation well HC-5B, located 32 feet from HC-5A with a screened interval from 580-960 feet, responded to pumping. The static potentiometric surface changed by 50 feet over the 32 foot distance between these wells, which is a 60-degree angle. This steep hydraulic gradient would be difficult to simulate with horizontal layers, such as in a 3D regional groundwater flow model. However, the Willow Canyon and Epitaph Formations located between these wells also have a 60-degree dip (Johnson and Ferguson, 2007). Setting the model layers parallel to the formation dip and the potentiometric surface allowed the response between HC-5A and HC-5B to be simulated with a radial flow model. The configuration for these wells is illustrated on Figure 4-8.
- Pumped well RP-3B: RP-3B was pumped at an average rate of 27.8 gpm and observation well RP-3A appeared to respond. However, anomalous, post-test data adjustments were not reproducible, so the response was not considered reliable. This well was therefore not analyzed using a radial flow model.

Three (3) other locations, PZ-8/PC-8 well cluster, HC-3 well cluster, and well 1445 (Figure 4-5), were identified by M&A (2009c) as having potential responses or responses to the long-term pumping test. These wells, however, were not analyzed using the radial-model method. The apparent 1-2 inches of response in the PZ-8/PC-8 well cluster was within the range of measurement error and non-pumping related influences. Therefore, this small response was not sufficiently reliable to warrant further analysis.

The HC-3 well cluster and well 1445 had less than one (1) foot of water-level change over the duration of the long-term test. There was no water-level recovery when pumping ceased, indicating that the water-level changes were likely due to factors unrelated to the long-term pumping test. Additionally, the HC-3 well cluster and well 1445 had ten (10) feet of water-level fluctuation during non-pumping periods in 2008 (M&A, 2009a). Therefore, the less than one (1) foot of drawdown during testing was within this magnitude of natural water-level fluctuations. Also, the lack of a pumping response in these wells was to be expected since the HC-3 well cluster was located about 3,600 feet from the nearest pumping well (PC-5) and well 1445 was located about 6,800 feet from the nearest pumping well (HC-1B).

Based on these test conditions, radial-models were constructed and calibrated for pumping wells PC-5, HC-1B, and HC-5A. These models provided values for vertical hydraulic conductivity (K_z), horizontal hydraulic conductivity (K_{xy}), and specific storage (S_s).

4.3.5.2 PC-5 Radial-Model

The numerical model grid used for simulating responses due to pumping at PC-5 consisted of 100 rows and 55 columns with the column spacing determined using a radial space multiplier of 1.25. The row, or vertical, spacing was based on lithologic changes and screened intervals from the lithologic logs of wells PC-2, PC-5, and PZ-5 as shown on the geologic cross section (Figure 4-6). The average pumping rate in test well PC-5 was 43.1 gpm, with variations from approximately 42 to 49 gpm. Seven (7) stress periods were used to more accurately represent the pumping rates during the 30-day pumping phase. A single stress period was used to represent the 30-day recovery phase for a total of eight (8) stress periods.

Responses in observation wells PZ-5 and PC-2 were simulated under two (2) scenarios to better represent geologic variations. Scenario one (1) simulated the geology between pumping well PC-5 and PZ-5 (Figure 4-9). Scenario two (2) simulated the geology between pumping well PC-5 and PC-2 (Figure 4-9). Although a radial model could have been used to represent the entire section simultaneously, the ability to resolve hydraulic properties for the three (3) Permian formations (Concha Limestone, Scherrer Formation, and Epitaph/Colina Limestone) near PC-5 (Figure 4-9) would have been lost. The material property values obtained for the individual Permian formations provided a range of property values for the Paleozoic (Pz) HGU, which was useful in the 3D regional flow model calibration.

The first scenario matched pumping responses to the three (3) PZ-5 piezometer depths (600, 1150, and 1800) to separately estimate the material properties of the Concha, Scherrer, and Epitaph/Colina. The match between the observed and simulated drawdown are shown on Figures 4-10, 4-11, and 4-12. As shown on these figures, the radial flow model under predicted drawdown and over predicted recovery; however, the match was within one (1) foot for most observations and two (2) feet for all observations. The parameter values resulting from the first radial flow model analysis of the PC-5 pumping test are provided in Table 4-2.

**Table 4-2 Hydraulic-Parameter Estimates for Observation Well PZ-5
from Long-Term Pumping in Well PC-5**

| Formation | Horizontal Hydraulic Conductivity (K_{xy}) (ft/day) | Vertical Hydraulic Conductivity (K_z) (ft/day) | Specific Storage (S_s) (1/ft) |
|--|---|--|-----------------------------------|
| Willow Canyon (Ksd) | 1.6×10^{-1} | $2.8 \times 10^{+0}$ | 7.0×10^{-7} |
| Concha Limestone (Pz) | 6.0×10^{-2} | 3.5×10^{-1} | 4.0×10^{-3} |
| Scherrer Formation (Pz) | 7.0×10^{-2} | 1.3×10^{-1} | 1.5×10^{-7} |
| Epitaph Limestone with Interfingered Colina Limestone (Pz) | 1.7×10^{-4} | 3.5×10^{-1} | 2.2×10^{-6} |

The second scenario matched pumping responses only to observation well PC-2, combining all the Permian formations as a single HGU (Pz). The Concha, Scherrer, and Epitaph/Colina formations near pumping well PC-5 were combined with the Epitaph formation near PC-2 as a single Pz unit. The match between the observed and simulated drawdown in PC-2 was excellent as shown on Figure 4-13. The parameter values resulting from this analysis are presented in Table 4-3.

**Table 4-3 Hydraulic-Parameter Estimates for Observation Well PC-2
from Long-Term Pumping in Well PC-5**

| Formation or HGU | Horizontal Hydraulic Conductivity (K_{xv}) (ft/day) | Vertical Hydraulic Conductivity (K_z) (ft/day) | Specific Storage (S_s) (1/ft) |
|---|---|--|-----------------------------------|
| Willow Canyon (Ksd) | 1.0×10^{-1} | 6.0×10^{-3} | 6.6×10^{-3} |
| Concha, Scherrer, and Epitaph/Colina (Pz) | 5.7×10^{-1} | 1.3×10^{-3} | 1.5×10^{-7} |

Steeply dipping formations and faults are present in the western portion of the pit area based on unpublished Rosemont geologic maps and cross sections. The formations near pumping well PC-5 had higher estimated vertical hydraulic conductivities than horizontal (Table 4-2), while the formations between PC-5 and observation well PC-2 had overall higher estimated horizontal conductivities than vertical (Table 4-3). Geologic units near PC-5 dip approximately 75-degrees based on geologic maps (Johnson and Ferguson, 2007). In the vicinity of PC-5, the direction of highest conductivity is along the bedding planes that are nearly vertical. These bedding planes are also likely present in observation well PZ-5 that is located 60 feet away. The higher vertical conductivity estimated for PZ-5 is therefore conceptually and geologically reasonable.

Faulting between pumping well PC-5 and observation well PC-2 truncated the bedding planes and offset the geologic units between these wells. This has resulted in a lateral heterogeneity that does not strictly meet the radial-flow model assumptions regarding homogeneous and laterally extensive units. Using a radial flow model in this case would introduce uncertainty in the hydraulic estimates. However, the faulting does not appear to be a significant barrier to flow. Therefore, the radial-flow model results were considered representative of hydraulic properties in an equivalent porous media (EPM) between PC-5 and PC-2. These results were considered appropriate for guiding development of the 3D regional groundwater flow model, which also

simulates an EPM. The EPM concept states that fluid flow through the fractured bedrock over sufficiently large volumes will be similar to that of porous media. The evaluation of hydraulic properties based on aquifer testing data usually assumes the concept of a representative elementary volume (REV) (Bear, 1972). The REV of a fractured rock mass is the smallest volume over which the studied parameter (e.g., hydraulic conductivity) yields a consistent result (Long et al., 1982). Therefore, the assumption inherent in up-scaling the 2D radial flow model values to the 3D regional groundwater flow model is that hydraulic testing was at the scale of a REV and resulted in EPM hydraulic properties.

The relatively high vertical hydraulic conductivity estimates from the radial-flow model between pumping well PC-5 and observation well PZ-5 likely represent enhanced permeability due to higher fracture density, faults, or partings along bedding planes associated with nearly vertical orientations. Horizontal hydraulic conductivity values from the PC-5/PZ-5 model, and both hydraulic conductivity values from the PC-5/PC-2 model, represent reasonable bulk permeability estimates.

4.3.5.3 HC-1B Radial-Model

The grid for the pumping well HC-1B radial-model consisted of 24 rows and 45 columns with the column spacing determined using a radial space multiplier of 1.26. The row, or vertical spacing was based on the screened intervals in observation well HC-1A (260-440 feet) and screened intervals in HC-1B (480-700 feet and 760-980 feet). The Glance Conglomerate lithology was consistent between these two (2) wells which are located 30 feet apart (Figure 4-7). The pumping rate in test well HC-1B was fairly consistent at 43 gpm; therefore, only one (1) stress period was used to represent the 25-day pumping phase of the test. A single stress period was also used to represent the 32-day recovery phase, for a total of two (2) stress periods.

The match between observed and simulated drawdown data in observation well HC-1A is illustrated on Figure 4-14. The model matches drawdown very well and over predicts the recovery data by less than two (2) feet. Due to the secondary porosity effects inherent in fractured rock systems, it was not possible to precisely match the recovery data. The parameter values resulting from the radial flow model analysis of the HC-1B pumping test are presented in Table 4-4. The Glance Conglomerate is part of the Lower Cretaceous age sedimentary rocks of the Bisbee Group (Ksd HGU) and was therefore included with the Willow Canyon Formation material property values to obtain a range of Ksd values for calibrating the 3D regional groundwater flow model.

Table 4-4 Hydraulic-Parameter Estimates for Observation Well HC-1A from Long-Term Pumping in Well HC-1B

| Formation | Horizontal Hydraulic Conductivity (K_{xy}) (ft/day) | Vertical Hydraulic Conductivity (K_z) (ft/day) | Specific Storage (S_s) (1/ft) |
|---------------------|---|--|-----------------------------------|
| Glance Conglomerate | 6.0×10^{-2} | 2.0×10^{-3} | 1.0×10^{-6} |

4.3.5.4 HC-5A Radial-Model

The grid for the pumping well HC-5A radial-model consisted of 26 rows and 40 columns with the column spacing determined using a radial space multiplier of 1.25. The row, or vertical spacing, was based on lithology changes and the screened intervals of HC-5A (100-540 feet) and observation well HC-5B (580-960 feet). There was an approximate 60-degree formation dip between the two (2) wells and a matching 60-degree slope of the potentiometric surface (Figure

4-8). The model was tilted 60-degrees to allow representation of a flat potentiometric surface and flat-lying geologic bedding planes. The distance between the wells was adjusted to be measured along dip. HC-5A's pumping rate varied from approximately 36 to 43 gpm and six (6) stress periods were used to represent the 23-day pumping phase of the test. A single stress period was used to represent the 32-day recovery phase, for a total of seven (7) stress periods.

Initially, the pumping well HC-5A radial flow model was constructed with the Willow Canyon as a single material property zone. However, a good calibration was not possible. Further inspection of the observation well HC-5B lithologic log indicated the presence of andesite and/or shale in the deeper parts (680-710 feet; 750-780 feet; 820-900 feet) of the predominately sandstone Willow Canyon Formation. Also, the short-term aquifer test when HC-5B was the pumping well was terminated after four (4) hours of pumping at an average rate of 0.8 gpm due to excessive drawdown (i.e., over 250 feet). Due to the dramatically different geologic and hydraulic properties within the Willow Canyon Formation, the HC-5A radial flow model was split into two (2) zones: Zone 1 (sandstones above 680 feet bgs) and Zone 2 (andesite and shales below 680 feet bgs) (Figure 4-8). Simulating the Willow Canyon Formation as two (2) material property zones in the radial-flow model made it possible to more closely match the observed drawdown data at observation well HC-5B. The parameter values resulting from the radial flow model analysis of the HC-5A pumping test are presented in Table 4-5. The lower hydraulic conductivity values estimated for the Willow Canyon Zone 2 are due to the presence of the low-conductivity shale and andesite. The upper portion (Zone 1) of the Willow Canyon is predominately sandstone and has an overall higher hydraulic conductivity.

The match between observed and simulated drawdown data in observation well HC-5B is shown on Figure 4-15. The model slightly under predicts drawdown and over predicts recovery by two (2) to 2.5 feet. Due to the secondary porosity effects inherent in fractured rock systems, it was not possible to precisely match the recovery data. A dual-porosity model would be required to better match the fracture-flow response. Material property values obtained from the radial flow model provided a range of values for calibration of the 3D regional groundwater flow model.

Table 4-5 Hydraulic-Parameter Estimates for Observation Well HC-5B from Long-Term Pumping in Well HC-5A

| Formation | Horizontal Hydraulic Conductivity (K_{xy}) (ft/day) | Vertical Hydraulic Conductivity (K_z) (ft/day) | Specific Storage (S_s) (1/ft) |
|---|---|--|-----------------------------------|
| Willow Canyon Zone 1 (Sandstone) | 2.5×10^{-1} | 5.5×10^{-1} | 3.3×10^{-4} |
| Willow Canyon Zone 2 (Andesite and Shale) | 2.4×10^{-4} | 5.0×10^{-4} | 3.3×10^{-4} |
| Epitaph Limestone (Pz) | 4.7×10^{-3} | 4.7×10^{-3} | 3.3×10^{-4} |

4.3.6 Aquifer Storage Properties

Specific yield (S_y) and Specific storage (S_s) estimates from studies in similar and nearby geologic settings were used to guide the initial alluvial storage estimates. Specific yield is the volume of water that an unconfined aquifer releases from storage per unit surface area of the aquifer per unit decline in the water table. Specific storage applies to confined aquifers and is the volume of water released from storage under a unit decline in hydraulic head. Many of the available storage estimates were based on calibrated groundwater flow model parameter values. A groundwater flow model for the Upper San Pedro Basin utilized a specific storage of 6.56×10^{-5} per foot for interbedded Upper Basin-Fill (Pool and Dickinson, 2007), which is

equivalent to the Qal, QTg, QTg1, and QTg2 HGUs in the groundwater flow model. The specific yield of the near surface basin-fill varied spatially with higher hydraulic conductivity zones having higher specific yields that ranged from five (5)-percent to 15 percent.

In the Santa Cruz Basin, M&A (2009e) simulated a storage coefficient of 1×10^{-4} per foot for the entire model domain. The average specific yield for the upper Santa Cruz Basin was estimated to be approximately 15-percent by Anderson (1972). Travers and Mock (1984) assigned a range of specific yield in the upper Santa Cruz Basin and in the vicinity of the M&A (2009e) model study area, in which the simulated specific yield varied from three (3)- to 17-percent. The M&A (2009e) model simulated specific yield from 0.08 to 0.18 in Model Layers 1 and 2 and from 0.05 to 0.09 in the deeper Model Layer 3. The Tucson AMA regional groundwater flow model assigned bedrock (Pantano Formation) specific yield values of 0.07 to 0.09 and basin-fill specific yield values of 0.10 to 0.13 (Mason and Bota, 2006).

Storage coefficients in the Empire Ranch area were reported to range from 7×10^{-5} to 1.9×10^{-2} per foot, based on a long-term pumping and recovery test conducted at well EP-1 (Harshbarger and Associates, 1975). A specific yield of approximately 0.05 was estimated by Harshbarger and Associates (1975) and the Arizona Water Commission (1972). Specific yields in the upper Cienega Creek basin-fill deposits were estimated to be between 0.01 to 0.1 by Boggs (1980) and Bota (1997). The Recent alluvium along the stream channel in lower Cienega Creek had specific yield estimates of 0.04 to 0.33 (M&A, 1985).

Basin-fill deposits have been hydraulically tested more than other units and the storage estimates indicate a high degree of variability. Specific yield estimates for the basin-fill deposits ranged from 0.01 to 0.33, with most estimates in the 0.05 to 0.15 range. Storage-coefficient estimates, which are the specific storage multiplied by the aquifer thickness for the basin-fill, ranged from 1.9×10^{-2} to 7×10^{-5} .

Less data are available for the bedrock storage properties. In a Tucson AMA model (Mason and Bota, 2006), the bedrock specific yield was specified as 0.07 to 0.09. Specific storage estimates for the bedrock units were not available.

4.3.7 Hydraulic-Property Summary

The results of hydraulic testing and 2D radial modeling provided a range of estimated hydraulic conductivity and specific storage values to guide the development of the groundwater flow model. Based on the available data, the horizontal hydraulic conductivities for wells within the model domain ranged from 1.7×10^{-4} ft/day to 516 ft/day. Additionally, the 2D radial flow models indicated that vertical hydraulic conductivities ranged from 5.0×10^{-4} ft/day to 2.8×10^{-0} ft/day.

The specific storage of the alluvial materials was spatially highly variable due to the observed variation in lithologic facies. Estimates from studies in similar geologic settings (Pool and Dickinson, 2007) were used to guide the initial alluvial specific-storage estimate of 6.56×10^{-5} per foot.

The bedrock specific storage estimates obtained from the radial flow modeling ranged from 7×10^{-7} to 4×10^{-3} per foot, with a geometric mean of 9.84×10^{-6} per foot. The geometric mean from the multiple Willow Canyon specific storage values was obtained first to prevent over-representing that unit. The Willow Canyon's geometric mean was then used in the subsequent bulk geometric mean calculation. The specific storage (9.84×10^{-6} per foot) estimate obtained from the calibrated radial flow models was used for all bedrock units in the transient (mining-phase and post-closure period) 3D regional groundwater flow modeling effort. These specific storage estimates were the most reliable estimates available for bedrock units in the region.

An initial specific yield estimate of 0.01 was used for the bedrock units. This value was less than the Tucson AMA value (Mason and Bota, 2006) but was considered reasonable for the fractured bedrock in the model study area. This relatively low specific yield estimate, however, likely resulted in conservative drawdown estimates within the 3D regional groundwater flow model.

The initial hydraulic conductivity and storage estimates used in the groundwater flow model are provided in Table 4-6. Final hydraulic-property values for the calibrated flow model are discussed in Section 6.0, "Steady-State Model Calibration."

Table 4-6 Initial Hydrogeologic Unit Parameter Estimates for 3D Regional Groundwater Flow Model Calibration

| Zone | HGU | Initial Horizontal Hydraulic Conductivity (ft/day) | Initial Vertical Hydraulic Conductivity (ft/day) | Initial Specific Storage (ft ⁻¹) | Initial Specific Yield |
|------|------|--|--|--|------------------------|
| 1 | Qal | $2.39 \times 10^{+2}$ | $2.39 \times 10^{+1}$ | 6.56×10^{-5} | 0.15 |
| 2 | QTg | 8.86×10^{-1} | 8.86×10^{-2} | 6.56×10^{-5} | 0.10 |
| 3 | QTg1 | 2.00×10^{-2} | 2.00×10^{-3} | 6.56×10^{-5} | 0.05 |
| 4 | QTg2 | 2.00×10^{-3} | 2.00×10^{-4} | 6.56×10^{-5} | 0.05 |
| 5 | Tsp | 1.71×10^{-2} | 1.71×10^{-3} | 9.84×10^{-6} | 0.01 |
| 6 | Kti | 3.28×10^{-3} | 3.28×10^{-3} | 9.84×10^{-6} | 0.01 |
| 7 | Kv | 2.39×10^{-2} | 2.39×10^{-3} | 9.84×10^{-6} | 0.01 |
| 8 | Ksd | 1.28×10^{-1} | 1.31×10^{-1} | 9.84×10^{-6} | 0.01 |
| 9 | Pz | 2.89×10^{-2} | 6.89×10^{-2} | 9.84×10^{-6} | 0.01 |
| 10 | PEb | 2.82×10^{-3} | 2.82×10^{-3} | 9.84×10^{-6} | 0.01 |

5.0 REGIONAL GROUNDWATER FLOW MODEL CONSTRUCTION

Dewatering of the Open Pit during the mining-phase, and pit-lake formation during the post-closure period, will result in drawdown that will propagate through the regional groundwater flow system. The objective of the groundwater flow modeling effort was to estimate the impact of the drawdown to area water resources. Of particular interest were potential impacts to Cienega Creek, Davidson Canyon, and regional spring flows.

As previously indicated, development of the regional groundwater flow model was constrained to the M&A (2009b) model domain. The 3D hydrogeologic framework model, which formed the foundation of the groundwater flow model, was based on the existing horizontal hydrogeologic slices developed for the M&A flow models (M&A, 2009b and M&A, 2010a). Except for a limited field investigation in Davidson Canyon and of the quartz-porphyry dike, no additional geologic interpretation was completed as part of Tetra Tech's 3D hydrogeologic framework or groundwater flow modeling tasks.

The large aerial extent of the regional flow model domain limited the size of the finite-difference model grid cells which comprise the numerical model. Hydrogeologic features that were smaller than the grid resolution were typically not explicitly simulated, i.e., their geometries and distributions were approximated. Due to the uncertain role these smaller hydrogeologic features have on the localized groundwater flow system, the prediction of small magnitude changes in spring and stream flows, including small water-level changes, become more uncertain at distant locations from the Open Pit.

5.1 Modeling Approach

Modeling methods vary depending on the processes being simulated and available data. Groundwater flow models were constructed for each phase of the Project: pre-mining steady state conditions; dewatering during active mining; and 1,000 years into the post-closure phase. The pre-mining condition was based on historical water level, stream-flow, and hydraulic-property data. The pre-mining flow model was calibrated to the steady-state water-level and stream flow data, forming the basis for the subsequent transient flow models.

The mining-phase transient model simulated the step-wise deepening of the Open Pit and dewatering during the 22-year operational period. Dewatering of the Open Pit was simulated with drain cells, which removed water from the model when water levels reached a specified elevation below the bottom of the pit.

The post-closure model used the LAK2 package (Council, 1999) to simulate the refilling of the pit following the end of dewatering. Other minor differences between the simulation approaches are discussed in detail in the following sections.

The three (3) distinct flow models used to simulate the different project phases were linked to create a continuous simulation period. Steady-state water levels were used as the starting condition for the mining-phase model. Water levels at the end of mining, when the ultimate pit shell was completely dewatered, were used as the starting condition for the post-closure model.

5.2 Model Code Selection

Simulation of the hydrogeologic conditions within the model domain posed several numerical challenges, both in model setup and execution. Steep hydraulic gradients occur in the model domain as a result of the natural water-level elevation change of over 2,800 feet and due to dewatering of the 2,000-foot to 2,500-foot deep Open Pit. Relatively thin flow model layers were used to more accurately simulate these steep hydraulic gradients. Smaller water-level changes

between model layers reduce numerical errors, instability, and computational time. However, the long-simulation periods (up to 1,000 years post-closure), pit dewatering, pit-lake formation, and tight convergence criteria contributed to long model execution times.

Due to these complexities, the finite-difference model code, MODFLOW-SURFACT (HydroGeoLogic, 2010) was selected for use over the traditional MODFLOW model code due to the following capabilities: 1) the code allows modeling of free movement of the water table in unconfined layers (while satisfying flow-continuity requirements), which is important for modeling a steep water table in multiple layers, such as in a pit dewatering simulation; 2) improved and faster solvers (Pre-Conditioned Conjugate Gradient (PCG) solvers PCG4 and PCG5); and 3) adaptive time-stepping and output control package (ATO4) that reduces simulation time.

5.3 Model Domain

The model domain encompasses a 457 square-mile area (Figure 5-1), following the same M&A groundwater flow model domain (M&A, 2009b; M&A, 2010a). The selected northern, eastern, and southern model boundaries were far enough away from the Open Pit to minimize potential boundary effects in the mining-phase and post-closure simulations. The western model boundary was set to the western extent of the Precambrian igneous and metamorphic crystalline formations (pCb HGU) located at the western base of the Santa Rita Mountains. These pCb HGUs have low hydraulic conductivity, which limited the propagation of drawdown west of the Open Pit.

In addition to modeling the effects of dewatering and pit refilling within the immediate Project area, the model domain was also selected to evaluate potential impacts to Davidson Canyon and to Cienega Creek.

5.4 Horizontal and Vertical Model Grid

The numerical, finite-difference model grid consisted of 205 rows by 169 columns by 20 layers, for a total of 692,900 cells (Figure 5-2). Of these 692,000 model cells, 433,895 cells were active. Model cells in the southwestern and southeastern portions of the model grid were located outside of the Cienega Creek watershed boundary and were designated as no flow or inactive cells (Figure 5-2).

The groundwater flow model grid was designed to: 1) maximize the accuracy of the regional model in matching water levels in existing wells; 2) increase accuracy in predicting drawdown and groundwater flow in the Open Pit area; and 3) facilitate analysis of potential impacts to Davidson Canyon and Cienega Creek.

A telescoping horizontal model grid was used to increase the simulation resolution in the pit area, while maintaining a manageable number of cells in the entire model domain. The model grid cell width was selected as 800 feet at the model domain edges, decreasing to a cell width of 200 feet in the vicinity of the Open Pit (Figure 5-2). The model grid was also aligned north-south and east-west.

The vertical groundwater flow model grid was constructed using 20 horizontal model layers with constant thicknesses except for Model Layer 1 (Table 5-1). Model Layer 1 ranged in thickness from 250 to 1,679 feet, with the thicker portions underneath the mountain ranges. Uniform thickness model layers were chosen for the other model layers to assist in numerical simulation of the mining-phase pit dewatering and post-closure pit-lake development. The physical conditions in the Project area create steep hydraulic gradients, and thinner, constant thickness model layers reduce numerical instability and improve accuracy.

Model layers intersecting the pit were assigned a thickness of approximately 150 feet. Model cells above and below the pit were assigned thicknesses between 200 and 430 feet. Elevations and thicknesses for each model layer are shown in Table 5-1. The bottom elevation of the Open Pit (3,050 feet amsl) was aligned with the bottom of Model Layer 15 to simplify construction of the drain and lake cells used to simulate dewatering and pit refilling. The vertical flow model grid discretization is illustrated on Figure 5-3. The base of the model was set at an elevation of 1,000 feet amsl. This elevation was sufficiently below the anticipated bottom of the pit so that hydraulic stresses did not encounter the bottom model boundary during pit dewatering or refilling.

Table 5-1 Model Layer Elevations and Thicknesses

| Model Layer | Top Elevation (ft amsl) | Layer Thickness (ft) |
|-------------|-------------------------|----------------------|
| 1 | 6,929 | 250 – 1,679 |
| 2 | 5,250 | 200 |
| 3 | 5,050 | 150 |
| 4 | 4,900 | 150 |
| 5 | 4,750 | 150 |
| 6 | 4,600 | 150 |
| 7 | 4,450 | 150 |
| 8 | 4,300 | 150 |
| 9 | 4,150 | 150 |
| 10 | 4,000 | 150 |
| 11 | 3,850 | 150 |
| 12 | 3,700 | 150 |
| 13 | 3,550 | 150 |
| 14 | 3,400 | 150 |
| 15 | 3,250 | 200 |
| 16 | 3,050 | 330 |
| 17 | 2,720 | 430 |
| 18 | 2,290 | 430 |
| 19 | 1,860 | 430 |
| 20 | 1,430 | 430 |

5.5 Hydrogeologic Framework

The groundwater flow model developed for the Project was based on regional geology. A 3D representation of the hydrogeologic units was created, allowing the geology to be accurately incorporated into the regional groundwater flow model grid. A detailed discussion of the hydrogeologic units and development of the 3D hydrogeologic framework model was presented in Section 4.0.

5.6 Recharge Distribution

Recharge is one of the most critical inputs to a flow model, as it prescribes the volume and location of water entering the groundwater flow system due to precipitation. Development of the initial recharge distribution is presented in this section. Modifications to the recharge distribution were made during the steady-state calibration process and are discussed in Section 6.0, “Steady-State Model Calibration”.

Changes to the calibrated recharge distribution also occurred in the different model versions (i.e., mining-phase and post-closure period) due to simulation of the Open Pit, Project facilities, and pit-lake development. These recharge distribution modifications are discussed in the mining-phase and post-closure recharge sections (Sections 5.6.2 and 5.6.3).

5.6.1 Methodology

Within the model study area, the highest precipitation rates generally occur at high elevations on low permeability bedrock, with steep slopes. While recharge occurs in these higher elevations, a significant amount of the precipitation runs off and flows down-gradient until it reaches areas with flatter slopes and higher permeability deposits. Once runoff reaches these areas, it can more readily infiltrate into the subsurface. The methodology applied to distribute recharge within the flow model domain followed this simple and observable process.

Groundwater investigations in the desert southwest commonly estimate recharge based on precipitation-elevation relationships (Maxey and Eakin, 1949; Anderson, 1995). Recharge analysis performed by M&A (M&A, 2009b; M&A, 2010a) used the precipitation-elevation relationship developed by Anderson (1995) to estimate 10,100 acre-feet per year (ac-ft/yr) recharge from precipitation for the model domain.

The methodology used for Tetra Tech's regional groundwater flow model further refined this common precipitation-elevation approach. The procedure involved using a combination of Geographic Information System (GIS) analysis, empirical surface-runoff modeling, and water-balance calculations. The procedure allowed for excess precipitation in the upland bedrock areas to be conveyed to lower elevations before infiltrating, i.e., recharging the groundwater system. The spatial redistribution of precipitation- and runoff-derived recharge was determined by modeling this process. Additional details of how the recharge estimates were obtained are provided in the Technical Memorandum titled *Groundwater Flow Model Construction and Calibration* (Tetra Tech, 2010i).

Soil, geologic, and topographic data were used to redistribute the upland area precipitation to the lower-elevation areas. Sub-watersheds or individual drainage basins within the Cienega Creek watershed were delineated based on topography. These sub-watersheds were then further subdivided into bedrock, alluvial fan, and valley floor sub-basins. Existing geologic maps were used to delineate bedrock areas and to identify the contact between bedrock and alluvial deposits. Lower elevation areas with alluvial deposits were designated as the valley floor.

Hydrologic soil group classification data were used with the Runoff Curve Number (CN) method (USDA, 1986) to calculate the threshold precipitation amount for each sub-basin that would result in surface runoff. Excess precipitation (runoff) on the bedrock areas was routed to alluvial fan areas and excess precipitation on the alluvial fan areas was routed to valley floor areas. In this manner, precipitation was numerically rerouted down-gradient to mimic the natural precipitation, runoff, and recharge processes.

Several independent investigations have also estimated total recharge over various parts of the region. These recharge estimates are identified and discussed in Section 2.0, "Conceptual Groundwater Model". These previous recharge estimates provide upper and lower bounds on the likely total recharge in the model domain. Based on these existing studies, and the investigation by M&A (2009b), an estimated total recharge of 10,100 ac-ft/yr was determined for the groundwater flow model domain. This recharge estimate was within the mid-range of reasonable estimates discussed in Section 2.0.

Water-balance calculations normalized the recharge rates for each sub-basin so that the total recharge for all of the sub-basins equaled 10,100 ac-ft/yr. The calculation results and recharge

estimates for each sub-watershed and sub-basin were developed by Tetra Tech (2010i). The initial recharge estimate of 10,100 ac-ft/yr was approximately 5.4 percent of average annual precipitation in the model domain. The recharge estimates used in the flow model ranged from 0.34 to 0.66 inches per year (in/yr) depending on the sub-watershed. Figure 5.4 shows the spatial distribution of the recharge. These normalized recharge rates were used as the initial recharge distribution in the pre-mining, steady-state, groundwater flow model. Some modifications were also made to these rates during the calibration process.

5.6.2 Mining-Phase Recharge

During the mining-phase simulation, the recharge distribution remained unchanged from the pre-mining, steady-state model (Figure 5-4). Recharge in the pit area, which was less than direct precipitation, was removed by the drain cells and included in the pit dewatering estimates. In practice, however, water ponding within the pit due to precipitation would need to be removed. The simulated dewatering estimate did not account for this volume.

No changes in recharge were simulated due to the Project facilities during the mining-phase simulation. During operations, process solutions will be contained in double-lined ponds. Any potential leakage through the bottom pond liners, or the heap leach pad liner, would be minimal. This assumption is also valid for the other lined facilities such as the Process Water/Temporary Storage (PWTS) Pond and the Settling Basin. As such, any minor seepage from these facilities was not included as recharge during the mining-phase simulation.

At closure, the PWTS Pond and Settling Basin will be removed. Liners associated with the Heap Leach Facility ponds will also be removed following closure of the heap. Closure of the heap will include drain-down management and covering the spent ore with waste rock.

Following the heap operational period, the spent ore will continue to drain into the PLS Pond for approximately three (3) years before the heap is closed. At this time, the liners will be removed from both the PLS Pond and Stormwater Pond located at the toe of the Heap Leach Pad. Depending on drain-down conditions, these ponds may be converted to treatment basins. Infiltration and seepage modeling (Tetra Tech, 2010d) predicts that the flow rate from the spent ore will be approximately ten (10) gpm at the end of the three (3) year period following the cessation of leaching. This rate is expected to decrease to 2.5 gpm after 15 years. Modeling also predicts that the spent ore will continue to drain at a decreasing rate until seepage ceases after 115 years. Drain-down reporting to the treatment basins would be a potential source of recharge. Regardless, this potential recharge source was not added to the post-closure model simulation due to its limited duration and volume. Additionally, the former heap leach facilities are predicted to be within the capture zone (hydraulic sink) of the Open Pit.

As indicated, minor seepage and negligible potential recharge associated with the lined facilities were not simulated in the mining-phase. Changes in recharge due to meteoric precipitation due to changing facility layouts during the mining-phase were also not modified from the pre-mining simulation. Adjustments to recharge in the Project facilities area from meteoric precipitation were considered in the post-closure model.

5.6.3 Post-Closure Recharge

During the post-closure period, when recovery of groundwater levels in the pit area results in formation of a pit-lake, the pit will continue to act as a groundwater sink. Although precipitation falling directly on the lake surface will recharge the lake, and by implication the groundwater system, evaporation from the lake surface will greatly exceed precipitation and other inflows, resulting in a net loss of water. Therefore, the post-closure recharge on the pit-wall area above

the final pit-lake level was set to the steady-state recharge rate and recharge below the final pit-lake level was set to zero. The detailed pit-lake water balance was simulated with MODFLOW's LAK2 package (Council, 1999) and is discussed in subsequent sections.

Post-closure recharge in the immediate Project area will be affected by placement of the Waste Rock Storage Area and the Dry Stack Tailings Facility. Previous modeling of these facilities (AMEC, 2009; Tetra Tech, 2010c; Tetra Tech, 2010d) indicated that post-closure precipitation-related recharge beneath the footprint of the Dry Stack Tailings Facility and the Waste Rock Storage Area will be zero. Consequently, the pre-mining precipitation-related recharge in those areas was removed and was replaced by recharge as described below.

The dry stack tailings will contain excess water when initially placed, which will result in recharge to the groundwater system from tailings drain-down (AMEC, 2009). Recharge resulting from tailings drain-down was distributed uniformly over the entire tailings footprint. The drain-down rate will decrease with time based on an analysis prepared by AMEC (2009, Figure 6.8). The temporal allocation of recharge from drain-down during the post-closure simulation was divided into six (6) periods: five (5) periods of 100 years each, during which the recharge from drain-down was decreased step-wise from the initial 8.4 gpm (13.6 ac-ft/yr) to zero at 500 years, and a final period after 500 years, during which there was no recharge contribution from the tailings. The dry stack tailings recharge rate shown on Figure 5-5 is the recharge rate at the start of the tailings drain-down. The drain-down curve developed by AMEC (2009) and the step-wise recharge simulated in the model is shown on Figure 5-6.

A network of flow-through drains is planned beneath the waste rock and dry stack tailings areas to direct stormwater flows down-gradient of the Rosemont Ridge Landform. The Rosemont Ridge Landform consists of the consolidated footprint of the Waste Rock Storage Area, the Dry Stack Tailings Facility, and the close Heap Leach Facility. The main segments of the flow-through drain system, which are primarily beneath the tailings, will result in recharge to the groundwater system from stormwater runoff infiltration in the buried drains (Tetra Tech, 2010c). Recharge rates in the flow-through drains were based on the results of Tetra Tech (2010c) modeling, which assigned infiltration values to each of the major segments of the drain system (N1, N2, N3, S1, S1C, and S2; Figure 5-5). Recharge from infiltration through the drain system totals 273.5 ac-ft/yr, as compared to the total pre-mining recharge of about 40 ac-ft/yr within the footprint of the Dry Stack Tailings Facility and about 208 ac-ft/yr within the footprint of the Waste Rock Storage Area. This resulted in a net recharge increase of about 25 ac-ft/yr under the dry stack tailings area.

A planned stormwater runoff diversion channel around the pit will report to a perimeter containment pond (Pond PCA-2) near the southwest edge of the Waste Rock Storage Area (Figure 5-5). Stormwater runoff infiltration in Pond PCA-2 will also be a source of recharge. An average of 56.21 ac-ft/yr of infiltration was estimated for the pond (Tetra Tech, 2010c). This recharge was distributed over the model cells containing the pond, resulting in a recharge rate of 61.1 in/yr within those cells (Figure 5-5).

Overall, the post-closure recharge in the Project facilities area will increase about 81 to 95 ac-ft/yr as compared to pre-mining conditions. The total estimated recharge in the Project area under pre-mining conditions was approximately 249 ac-ft/yr versus 330 to 343 ac-ft/yr for the post-closure condition. This recharge increase was due to recharge via the flow-through drain system, containment pond PCA-2, and drain-down from the dry stack tailings. Potential recharge resulting from drain-down seepage through the spent heap pile was not simulated (see Section 5.6.2).

5.7 Evapotranspiration

Groundwater losses due to evapotranspiration (ET) occur primarily in the reaches of Davidson Canyon and Cienega Creek where riparian vegetation is present. The ET distribution and rates developed by M&A (2009b), and discussed in Section 2.6, were assumed to be the best available ET data for model construction and calibration.

ET was simulated with MODFLOW's evapotranspiration (EVT) package. Maximum ET rates were assigned to each model cell and simulated ET values varied depending on the depth to groundwater. ET varies linearly between a location-specific maximum value that occurs when the simulated head in a model cell is at the land surface and zero when the simulated head is below an assigned extinction depth. The maximum ET rates assigned in the model are shown on Figure 5-7.

Extinction depths vary with the types of soil and vegetative cover, generally ranging from about 1.5 feet under bare conditions in sandy soil to about 27 feet under forest cover conditions in clayey soil (Shah et al., 2007). A spatial distribution of extinction depths based on plant types was not available at the time of model construction, so the extinction depth was set uniformly to 16.4 feet (5 meters) below the land surface. This depth was a mid-range value that approximated the average extinction depth over the riparian areas. The result of the linear relationship between water level and ET (when the DTW is less than the extinction depth) is that the assigned ET values represent the maximum potential ET. As the water-level decreases to the extinction depth, the simulated ET rate also decreases, reaching zero when the DTW is equal to the extinction depth.

5.8 Stream Flow

Cienega Creek has several reaches of perennial flow that are separated by dry or intermittent flow reaches (Figure 1-2). Section 2.0, "Conceptual Groundwater Model" discussed the groundwater and surface-water flow conditions in Davidson Canyon and in Cienega Creek. Mean monthly stream discharge has historically varied between zero and 9.3 cubic feet per second (cfs) at the USGS stream gages presented in Table 5-2. Davidson Canyon has one (1) reach with historical stream flow measurements (1968-1981). However, measurements at this USGS gage location have been discontinued.

The stream-flow data available from two (2) USGS gaging stations in Cienega Creek and one (1) station in Davidson Canyon Wash were evaluated for use as model calibration targets. The gaging station locations and identifications are shown on Figure 5-8. Monthly mean and median flow data from these stations are summarized in Table 5-2. The data show relatively consistent and small flows during October through June and a strong influence from high discharges during the July to September monsoon season. Only median stream flows were compared to the simulated results at each gaging station. Using median stream flows removed the influence of high flows observed during the summer monsoon season. These higher stream flows, which occur during July, August, and September, are not representative of the groundwater supported base flow.

Stream-flow measurements at non-USGS stations in Cienega Creek and Davidson Canyon were also available. For upper Cienega Creek near the Narrows, estimates of average annual stream flow ranged from 1.0 to 3.0 cfs (PAG, 1998). In lower Cienega Creek, upstream and downstream of the USGS gage, estimates of annual average stream-flow measurements ranged from 0.0 to 2.0 cfs (PAG, 1998 and PAG, 2010). There are no non-USGS flow measurements in Davidson Canyon, except for flood warning purposes near the former USGS gage (PAG, 2005).

The intermittent interaction of surface water and groundwater along Cienega Creek and Davidson Canyon was simulated using MODFLOW's Stream Flow Routing (SFR1) package (Prudic et al., 2004). The SFR package allows the groundwater system to: 1) lose water to a stream when the head in the cell containing the stream boundary is higher than the streambed or stream stage elevation; and 2) to gain water from the stream when the head in the cell is lower than the streambed or stream stage elevation. The GAGE package (Merritt and Konikow, 2000) was also used in conjunction with the SFR package to obtain simulated stream flows at the three (3) USGS gages during model calibration.

Stream channel locations were identified from the National Hydrography Dataset (USGS, 2010b), and elevations were obtained from the ten (10) meter National Elevation Dataset (NED). The minimum elevation within each model cell was used as an approximation for the streambed elevation. The resulting stream profile was then checked for any uphill stream segments (i.e., segments that gained elevation moving downstream). Streams were associated with model grid cells and their length in each cell calculated and combined with the width estimated from aerial photography and streambed hydraulic conductivity to produce streambed conductance values. A stream boundary was assigned to the model layers corresponding to the stream elevation at each cell that intersected the stream channel. Model Layers 7 through 14 contain stream cells (Figure 5-8).

Stream flows were used as calibration targets in the pre-mining, steady-state model. The model scale limited the accuracy of simulating the alluvial stream channel - aquifer interaction. The local geologic and stream-channel characteristics controlling surface flows were represented in the 800 foot x 800 foot model cells.

Table 5-2 Summary of Monthly Mean Stream Flows

| Month | USGS 09484550 Cienega Creek near Sonoita, AZ (cfs) | USGS 09484560 Cienega Creek near Pantano, AZ (cfs) | USGS 09484590 Davidson Canyon Wash near Vail, AZ (cfs) |
|---------------|--|--|--|
| Jan | 0.94 | 0.0 | 0.11 |
| Feb | 1.0 | 1.1 | 0.18 |
| Mar | 1.1 | 0.17 | 0.2 |
| Apr | 0.83 | 0.0 | 0.15 |
| May | 0.47 | 0.0 | 0.11 |
| Jun | 0.31 | 0.32 | 0.07 |
| Jul | 9.3 | 11.0 | 2.5 |
| Aug | 5.0 | 9.2 | 3.4 |
| Sep | 2.6 | 5.5 | 2.1 |
| Oct | 0.53 | 0.31 | 0.1 |
| Nov | 0.66 | 0.0 | 0.14 |
| Dec | 0.81 | 0.0 | 0.23 |
| Median | 0.885 | 0.24 | 0.165 |

Source: U.S. Geological Survey (USGS)

The stream flows provided in Table 5.2 differ from those recorded in Cienega Creek near the Pantano stream gage (USGS station ID 09484560) as provided in PAG (1998). A minimum annual flow of 608 ac-ft/yr (0.84 cfs), a median flow of 1,408 ac-ft/yr (1.9 cfs), and a maximum

flow of 4,496 ac-ft/yr (6.2 cfs) were reported in PAG (1998). The PAG flow estimates are provided for comparative purposes to the USGS gage values. However, the median USGS values were selected for the calibration targets. The calibration target stream flows used in the groundwater flow model were estimates of the groundwater contribution to the stream flow and do not consider flows in response to precipitation events, which is appropriate for evaluating impacts as a result of changes in the groundwater flow system.

5.9 Geologic Structures

Geologic mapping by the AZGS delineated several geologic structures, including faults and dikes, in the pit area and throughout upper Davidson Canyon (Ferguson, 2009; Ferguson et al., 2001, Spencer et al., 2001). One of the objectives of the aquifer testing program performed by M&A (M&A, 2009a; M&A, 2009c) was to determine if these geologic structures were barriers or conduits to groundwater flow. Due to aquifer-test limitations (e.g., small hydraulic stresses), the role of specific faults and fractures on controlling groundwater flow was not conclusively determined. Drawdown did not appear to be significantly influenced by no-flow boundaries during hydraulic testing. Faults and fractures were therefore not explicitly simulated in the groundwater flow model due to the lack of data defining their characteristics.

The north-south trending “Backbone Fault” is present along the ridge of the Santa Rita Mountains and through the western pit area. This faulting appears to have created a higher conductivity rubble zone parallel to the fault, which may enhance north-south groundwater flow. However, the Precambrian geologic units to the west of the fault have low conductivity, which would impede groundwater flow to the west. Thermal and mineral alteration in this area may have reduced the rock permeability by sealing fractures or faults. Simulation of this area is discussed further in Section 6.0, “Steady-State Model Calibration”.

The Horizontal Flow Barrier Package (HFB package) in MODFLOW was used to simulate the quartz-porphphy dike described in Section 2.2.1. The hydraulic characteristic of the dike was defined as the hydraulic conductivity divided by the width and was a required input to the HFB package. The width of the dike was assumed to be 100 feet based on the minimum measurements taken from geologic maps and field observations. The HFB was projected in the groundwater flow model from land surface to the bottom of the model. The two (2) major mapped sections of the dike were simulated. Hydraulic conductivity of the HFB was initially set to 3.28×10^{-3} ft/d, which was the initial hydraulic conductivity for the intrusive HGU (KTi). This is equivalent to a hydraulic characteristic value of 3.28×10^{-5} day⁻¹.

5.10 External Model Boundaries

Similar to the model domain, Tetra Tech used the same external model boundary locations as M&A (2009b) and M&A (2010a). No-flow boundaries represented groundwater divides on the southeastern and southwestern Cienega Basin watershed boundary. The areas southeast and southwest of these groundwater divides were designated as inactivate, no-flow cells. Constant-head cells (cell with a specified head value that is constant through time and allows for water to flow in or out of the model domain) were designated for the remainder of the active model area.

The layout of the horizontal model layers created situations where the upper layers were above land surface. These situations were remedied by assigning no-flow boundaries to the cells located above the land surface. These external model boundaries were simulated in the same manner in all three (3) of the groundwater flow models: pre-mining, mining-phase, and post-closure simulations.

The hydraulic head assigned to the constant-head boundaries was based on contoured water levels (potentiometric surface elevation) from wells within and surrounding the model domain.

Within the model domain, a modified steady-state target water-level data set was used to determine the constant-head elevations (Appendix C). For purposes of assigning constant-head elevations, modifications to the target water-level data set included removing wells with vertical hydraulic gradients and deep screened intervals that were potentially influenced by vertical gradients. The resulting data set was used to develop a potentiometric surface map that represented the water-table elevation within the model domain.

Outside of the model domain, water-level data were obtained from the ADWR Well Registry Web (ADWR, 2010b) and USGS (2010b) databases. Water-level data were obtained for the surrounding Cienega Creek, Tucson, and Upper San Pedro Basins. Although these data were not rigorously reviewed, anomalous data were removed from the data set. These additional water-level data allowed contouring outside of the model domain, which reduced edge effects and minimized errors in the constant-head elevations.

Water-level contours for the larger regional area were created by kriging the data inside and outside the model domain. The head values assigned to the constant-head boundary cells were based on the head value located at the model cell centroid, as determined from the potentiometric surface map.

5.11 Existing Groundwater Use

The effects of current groundwater pumping within the model study area were not simulated in the groundwater flow model for several reasons. The major municipal and agricultural groundwater demands are outside the boundaries of the model domain or distant from the focus area of the study, i.e., Project facilities area. Additionally, domestic pumping was not included due to the speculative and incomplete data, the likely small and dispersed nature of the pumping. Also, historic groundwater-level data do not show wide-spread declining trends in the domestic pumping areas. In summary, the inclusion of this pumping data into the groundwater flow model was considered inconsequential for purposes of predicting groundwater level changes that may result from dewatering the Rosemont Open Pit.

6.0 STEADY-STATE MODEL CALIBRATION

The calibrated pre-mining, steady-state groundwater flow model provided hydraulic properties and initial hydraulic heads for the mining-phase flow model. The steady-state model was calibrated to obtain a satisfactory match to existing water-level and stream-flow data. The calibration process of fitting the model to observed data provided confidence that the model parameters were appropriate for simulating the mining-phase and post-closure conditions. The steady-state groundwater flow model calibration and model fit are discussed in this section, and the mining-phase and post-closure model constructions are discussed in subsequent sections.

The objectives of the model calibration were to: 1) obtain appropriate model parameters that were representative of the hydrogeologic conditions; and 2) simulate current, observed water levels and stream flows. A measure of flow model accuracy and representativeness was the magnitude of the difference between observed and measured water levels, which are termed residuals. A good model fit minimizes the water-level and stream-flow residuals.

Stream flows, in conjunction with water-level measurements, were used during model calibration to reduce the non-uniqueness of the model parameters. However, stream flows were not rigorously matched due to their low base-flow rates (< 1 cfs). Stream flows in the model domain are largely controlled by the interaction of complex geology, incised stream channels, small groundwater level fluctuations, and stormwater runoff. Bedrock outcrops or faults commonly force shallow groundwater to the surface where it flows until consumed by ET or infiltrates back into alluvial deposits or fractured bedrock.

The scale of the regional model necessitated 800 foot x 800 foot model cells over most of the stream channel reaches. Based on these model cells, it was not possible to accurately represent all of the geologic complexity, stream-channel geometry, and precise water levels. Adjusting regional model parameters to accurately match low stream flows resulting from unique and isolated hydrogeologic conditions would require complexity greater than could be justified based on the available data and model resolution. Large discrepancies between observed and simulated stream flows, however, would be an indication of inaccurate model parameters and poor representation of the regional groundwater flow system.

The calibration approach consisted of iteratively using automated parameter estimation (PEST) methods (Doherty, 2010) and manual calibration to achieve the calibration objectives and the best possible model fit.

6.1 Calibration Targets and Weights

Water-level elevation data from 377 wells, 12 piezometers, and 67 springs located within the model domain were evaluated for use as water-level (head) targets for calibration of the steady-state model. The initial water-level and well data set was provided by M&A after they had re-evaluated the target data set used in their M&A (2009b) groundwater flow model. This data set had been repeatedly evaluated by M&A over the course of their investigations and was considered to be the best-available data.

Target water levels were weighted to reflect their relative value in the flow model calibration process. Water levels representative of steady-state, regional flow system conditions at specific depths were the most valuable and were assigned the highest weighting. Water-level data that was of lesser quality and ambiguous regarding the conditions being monitored were assigned lower weights. These weights were used by the parameter-estimation process when calculating the parameter values, resulting in the best model fit. Higher-weighted targets were preferentially matched over the lower-weighted targets.

Water-level targets were assigned calibration weights based on the following criteria:

- Availability and completeness of well construction information;
- Well completion interval depth and screen length;
- Water-level trends; and
- Period of water-level data.

All targets were assigned to model layers based on the well completion and water-level data. Using the elevations of the screened interval, water level, and total depth, each well was assigned to the model layer containing:

1. the midpoint of the screened interval, for wells where both the top and bottom of the screen were known;
2. the midpoint between the water level and the well's total depth, for wells where the screened interval was unknown, but the water level and total depth were known; or
3. the water level, where the screened interval and total depth were unknown.

Data from wells screened across a single model layer, and with recent water level data, were assigned the highest weights. Data from wells screened over multiple layers, lacking construction information, exhibiting strong trends or large water-level fluctuations, or with water levels measured before 1980, were assigned lower weights. Data from wells in constant-head cells of the model were assigned a weight of zero since the heads in those cells were not changed by the model parameters. Furthermore, using the target heads in those cells would have skewed the model-calibration statistics.

The target water level data set was a revised version of the target water levels used in the M&A flow model (M&A, 2009b). A significant difference was that most of the original 67 springs used in M&A (2009b) were removed as target observations in the revised data set because their seasonal flow did not represent the regional groundwater flow system. Only water-level elevations from two (2) perennial springs, Rosemont and Questa, were retained.

Rosemont and Questa Springs were considered perennial springs and assigned a weight of 0.5. This lower weight represented the uncertainty associated with the model layer where the water level associated with the spring should be simulated. Unlike a well that has a discrete screen interval, the origin of a spring's water is unknown. Ephemeral (seasonal or intermittent) springs were not retained in the target set or were assigned weights of zero.

The water-level target weighting criteria is summarized in Table 6-1. Data for the wells and springs used as steady-state calibration targets are provided in Appendix C. Steady-state calibration head target locations and weights are shown on Figure 6-1. The steady-state water-table map, developed from the target-head data and water levels from wells surrounding the model domain, is illustrated on Figure 6-2.

The median stream flows presented in Table 5-2 were used as calibration targets for the steady-state model. These targets were assigned to the three (3) model cells that corresponded to the location of the USGS stream gage stations. Weights were assigned to these flow targets for use in the parameter estimation process. Lower weights were assigned to the stream flow-targets than the water-level targets in order to equalize their relative importance. This was necessary since the flow target observations had different units than the water-level targets (i.e., cfs versus feet). A summary of the data used for the stream-flow targets are presented in Table 6-2.

Table 6-1 Weighting Criteria for Steady-State Calibration Water-Level Targets

| Group | Weight | Criteria |
|-------|--------------------|---|
| 1 | 1.0 | Screened interval known and in one (1) model layer only |
| 1 | 1.0 | Screened interval is unknown but total depth and water level are both within one (1) model layer only |
| 2 | 0.9 | Screened interval known and across two (2) model layers |
| 2 | 0.9 | Screened interval unknown and TD and WL span two (2) model layers |
| 3 | 0.8 | Screened interval known and across three (3) model layers |
| 4 | 0.5 | Perennial springs |
| 5 | 0.4 | Screened interval known and across four (4) or more model layers |
| 5 | 0.4 | Screened interval unknown and total depth and water level span three (3) or more model layers |
| 6 | 0.2 | Water level only; total depth and screen depth unknown; model layer assigned based on water-level elevation |
| 7 | 0 | Water-level time series shows range >25 feet |
| 8 | 0 | Water-level time series shows range >50 feet |
| 9 | 0 | Water level time series shows strong trend upward or downward |
| 10 | 0.5 x group weight | Water-level date before 1980 but otherwise acceptable |
| 11 | 0 | Rejected – water level time series shows large range and strong trend up or down or unexplained large recent change |
| 12 | 0 | Well located in constant-head cell; weight set to zero |
| 13 | 0.5 x group weight | Flowing well (reported water level at or above ground surface (unless pressure transducer is known to be in well - i.e., PC-2 and PC-5) |
| 14 | 0 | Intermittent springs |

Table 6-2 Steady-State Calibration Stream-Flow Targets and Weights

| Target Name | UTM X-Coordinate (NAD83, meters) | UTM Y-Coordinate (NAD83, meters) | Target Flow (cfs) | Layer | Row | Column | Weight |
|--------------------------------|----------------------------------|----------------------------------|-------------------|-------|-----|--------|--------|
| Cienega Creek near Sonoita, AZ | 540709 | 3525638 | 0.885 | 9 | 72 | 122 | 0.005 |
| Cienega Creek near Pantano, AZ | 540833 | 3539063 | 0.24 | 12 | 17 | 123 | 0.01 |
| Davidson Canyon near Vail, AZ | 533555 | 3540081 | 0.165 | 13 | 13 | 93 | 0.01 |

6.2 Calibrated Model Parameter Values

Hydrogeologic parameter values for many of the HGUs were obtained from analyzing the short-term and long-term aquifer tests conducted by M&A (M&A 2009a; M&A 2009c; M&A 2009d). Analytical methods and numerical radial flow modeling were used to estimate horizontal and vertical hydraulic conductivities. Literature review and professional judgment were used to assign initial values for HGUs that did not have parameter estimates from an aquifer test. The initial and final calibrated steady-state model parameter values are presented in Table 6-3.

Parameters that were not HGU specific, such as recharge, were modified during calibration and are discussed in detail later in this section. Constant head values and ET parameters were not modified during calibration.

Table 6-3 Steady-State Model Initial and Calibrated Parameter Values

| Zone | HGU | Initial Horizontal Hydraulic Conductivity (ft/day) | Initial Vertical Hydraulic Conductivity (ft/day) | Final Horizontal Hydraulic Conductivity (ft/day) | Final Vertical Hydraulic Conductivity (ft/day) |
|------------|--------|--|--|--|--|
| 1 | Qal | $2.39 \times 10^{+2}$ | $2.39 \times 10^{+1}$ | $8.53 \times 10^{+1}$ | $3.87 \times 10^{+1}$ |
| 2 | QTg | 8.86×10^{-1} | 8.86×10^{-2} | 7.87×10^{-1} | 5.58×10^{-1} |
| 3 | QTg1 | 2.00×10^{-2} | 2.00×10^{-3} | 1.64×10^{-1} | 1.18×10^{-2} |
| 4 | QTg2 | 2.00×10^{-3} | 2.00×10^{-4} | 1.31×10^{-2} | 6.56×10^{-4} |
| 5 | Tsp | 1.71×10^{-2} | 1.71×10^{-3} | 1.64×10^{-2} | 1.64×10^{-4} |
| 6 | Kti | 3.28×10^{-3} | 3.28×10^{-3} | 1.31×10^{-2} | 1.31×10^{-3} |
| 7 | Kv | 2.39×10^{-2} | 2.39×10^{-3} | 8.53×10^{-2} | 2.00×10^{-2} |
| 8 | Ksd | 1.28×10^{-1} | 1.31×10^{-1} | 6.56×10^{-2} | 4.92×10^{-3} |
| 9 | Pz | 2.89×10^{-2} | 6.89×10^{-2} | 2.23×10^{-2} | 1.08×10^{-2} |
| 10 | PCb | 2.82×10^{-3} | 2.82×10^{-3} | 2.38×10^{-3} | 2.38×10^{-3} |
| 11 | Pz_Pit | N/A | N/A | X - 3.28×10^{-4} Y - 3.28×10^{-3} | 3.28×10^{-3} |
| 15 | QTg_TB | N/A | N/A | 3.61×10^{-1} | 1.31×10^{-1} |
| Stream-bed | -- | 3.28 | -- | 6.56 | -- |
| Zone | HGU | Initial Conductance (day ⁻¹) | Initial Vertical Hydraulic Conductivity (ft/day) | Final Conductance (day ⁻¹) | Final Vertical Hydraulic Conductivity (ft/day) |
| HFB | QPD* | $3.28 \times 10^{-5} \text{ day}^{-1}$ | -- | $3.28 \times 10^{-4} \text{ day}^{-1}$ | -- |
| Zone | HGU | Initial Recharge (in/yr) | Initial Vertical Hydraulic Conductivity (ft/day) | Final Recharge (in/yr) | Final Vertical Hydraulic Conductivity (ft/day) |
| Rch_2 | -- | 0.35 | -- | 0.33 | -- |
| Rch_3 | -- | 0.39 | -- | 0.37 | -- |
| Rch_4 | -- | 0.43 | -- | 0.42 | -- |
| Rch_5 | -- | 0.50 | -- | 0.53 | -- |
| Rch_6 | -- | 0.63 | -- | 0.68 | -- |
| Rch_7 | -- | 0.68 | -- | 1.31 | -- |

*Quartz-porphry dike

6.2.1 Horizontal Hydraulic Conductivity

Model calibrated horizontal hydraulic conductivity (K_{xy}) values were reasonable based on estimates obtained from aquifer testing. The median, lower quartile, upper quartile, maximum and minimum horizontal hydraulic conductivity values derived from the aquifer tests are illustrated on Figure 6-3. Calibrated model values were generally within the range of measured values. The exceptions were for Quaternary units that can exhibit a wide range of hydraulic properties due to heterogeneous depositional environments. However, the calibrated hydraulic conductivity values for the Quaternary units were within the range of typical values.

The Qal K_{xy} -value was lowered during calibration to reduce the hydraulic gradient through this unit to better match water-level elevation data and stream flows. The QTg1 and QTg2 K_{xy} -values were increased from the initial values to better match water levels in Upper Cienega Basin. The initial values for these three (3) HGUs were based on short-term aquifer tests that only stressed a small portion of the aquifer near the pumping well. The changes during calibration were reasonable due to scale differences between the tests and the regional groundwater flow model. For K_{xy} -values not derived from an aquifer test (i.e., Tsp, KTi, and pCb), professional judgment was used to adjust these values during calibration.

Two (2) additional material property zones were added during model calibration. Based on hydraulic testing in test well HC-1B, the north-south trending “Backbone Fault” along the ridge of the Santa Rita Mountains was determined to be a discrete zone within relatively low permeability bedrock. This area also has steeply dipping beds with nearly vertical bedding planes that created intervals of higher vertical hydraulic conductivity and lower horizontal hydraulic conductivity perpendicular to the orientation of the bedding planes. The backbone fault and the steeply dipping beds were simulated by creating a zone for Paleozoic units in the western side of the pit area (Zone 11 – Pz_Pit). The lower x-direction hydraulic conductivity (K_x) in this zone represented heterogeneities and flow perpendicular to bedding planes that limited east-west flow. The lower x-direction hydraulic conductivity assisted in increasing water levels in the pit area closer to the observed levels. This zone also included horizontal anisotropy with higher K-values in the y-direction (K_y), which is parallel to the Backbone fault’s north-south strike. The relatively higher vertical hydraulic conductivity, due to the steeply dipping beds, was simulated by setting K_z equivalent to K_y , which are an order of magnitude higher than K_x .

Quaternary-Tertiary gravels were differentiated based on hydrographic basins. The Tucson Basin zone parameter (Zone 15 – QTg_TB) was assigned a lower hydraulic conductivity than the Cienega Creek QTg. Based on the type and size of sands and gravels observed from core and hydrogeologic data, the Tucson Basin has different lithology, hydraulic gradients, and water-level elevations than Cienega Creek Basin. The K_{xy} distributions by model layer are illustrated on Figures 6-4 through 6-23.

6.2.2 Vertical Hydraulic Conductivity

Two (2) HGUs (Ksd and Pz) were analyzed using radial flow modeling to obtain vertical hydraulic conductivity (K_z) values. Steady-state model calibrated K_z -values for Pz (0.01 and 0.003) fall within the range of values obtained from radial flow modeling (0.35 to 0.0013). The steady-state Ksd K_z -value (0.005), however, is slightly lower than values obtained from radial flow modeling (0.006 to 2.8). The higher K_z -values were required in the radial flow modeling to simulate drawdown at depth or to match drawdown at observation wells completed within the steeply dipping beds present in these HGUs near the pit. In the steady-state model, the objective was to match water-level elevation data on a regional scale, not just in the pit area. Lower K_z -values were needed to elevate water levels near the pit and to better match water levels across the model domain.

6.2.3 Hydraulic Conductivity Scale Differences

Differences between horizontal and vertical hydraulic conductivity values at a local scale (i.e., values derived from aquifer tests) versus a regional scale (i.e., values derived from steady-state model calibration) are common. Pumping during aquifer testing imposes a relatively small stress on the groundwater system. The short-term aquifer tests were typically 12-hours long and the multi-well, long-term pumping test rates were relatively low (<45 gpm). These aquifer test results are representative of small volumes of heterogeneous fractured rock. The 3D regional groundwater flow model, however, simulated a regional-scale equivalent porous medium (EPM) as described in Section 4.3.5.2, "PC-5 Radial-Model".

In the steady-state model, some K_z -values were adjusted during calibration based on professional judgment. The initial range of K_z -values was one (1) to ten (10) times lower (1:10) than the initial K_{xy} -values. In the calibrated model, K_z -values were one (1) to 100 times lower (1:100) than the K_{xy} -values. A smaller anisotropy ratio than 1:10 between the horizontal and vertical hydraulic conductivities was required in the regional groundwater flow model for four (4) HGUs (QTg1, QTg2, Ksd, and Tsp) to more accurately match water levels and hydraulic gradients throughout the model domain. The lower K_z -values, which were needed to maintain higher water levels than would be expected based on the steeply dipping HGUs in the pit area, could be due to K_x values that were not sufficiently low enough to restrict east-west groundwater flow. The distribution of K_z -values, by model layer, are also shown on Figures 6-4 through 6-23.

6.2.4 Recharge

Recharge estimates from previous investigations within the model domain ranged from 6,900 to 25,500 ac-ft/yr. This large range of estimated recharge values reflects uncertainty in the estimates. Modification of the initial recharge rates was used as a calibration tool to maintain a reasonable balance with simulated hydraulic conductivity values. However, calibration of the steady-state model required only relatively small changes to the initial recharge distribution. The total recharge calculated by the calibrated steady-state model was 9,900 ac-ft/yr, which is slightly lower than the initial total recharge of 10,100 ac-ft/yr.

The initial, steady-state, recharge distribution had 58 recharge zones due to the finely-divided recharge increments and numerous sub-basins. Preliminary model simulations indicated that this initial recharge distribution could be simplified by consolidating recharge into six (6) zones. This reduction facilitated recharge adjustments on a zone basis rather than in the individual model cells. Zones were combined that had similar values based on natural breaks in the range of initial recharge values (0.33 to 0.68 in/yr).

The most significant recharge adjustment was made in bedrock areas west and southwest of the Open Pit. This area can accommodate higher rates of recharge due to fractures and faults within the steeply-dipping bedrock. Recharge was increased from the initial estimates of about 0.51 to 0.63 in/yr to final values of about 0.68 to 1.31 in/yr, or approximately four (4) to seven (7) percent of precipitation. The simulated water levels in these areas were significantly below the observed (target) water levels when the initial recharge values were used. The increased recharge resulted in a closer fit of modeled heads to the target heads. The recharge distribution in the calibrated pre-mining, steady-state model is shown on Figure 6-24.

6.2.5 Evapotranspiration

No changes were made to evapotranspiration rates or extinction depths during model calibration. The total simulated ET depends on the extinction depth and the simulated DTW in the riparian areas. Total ET in the steady-state simulation was 5,638 ac-ft/yr. A discussion of

regional ET estimates is provided in Section 2.6 and simulation with the EVT package is discussed in Section 5.7.

6.2.6 Stream Flow

During model calibration, the streambed hydraulic conductivity was the only parameter modified as part of the SFR1 package. Streambed conductance is the streambed hydraulic conductivity multiplied by the area of the streambed divided by the streambed thickness. The amount of stream-aquifer interaction, or groundwater gains and losses with the stream, was sensitive to the streambed conductance. The initial streambed hydraulic conductivity was 3.28 ft/d and was increased by a factor of two (2) to 6.56 ft/d during calibration (Table 6-3). The increase in streambed hydraulic conductivity allowed a better match to stream flow gage data and water levels in wells completed in the Qal within the stream channels.

Stream flows in the steady-state simulation are provided in Table 6-4. Although the flows are generally higher than the observed base flows, they are of comparable magnitude and indicate adequate simulation of the flow system.

Table 6-4 Simulated Pre-Mining Steady-State Stream Flows by Reach

| Stream Segment | Simulated Pre-Mining Stream Flows | |
|----------------|-----------------------------------|-----------------------|
| | Cienega Creek (cfs) | Davidson Canyon (cfs) |
| 1 | 0.67 | |
| 2 | 1.92 | |
| 3 | 3.15 | |
| 4 | 3.71 | |
| 5 | 3.71 | |
| 6 | 3.8 | |
| 7 | 4.77 | |
| 8 | 4.95 | |
| 9 | 3.72 | |
| 10 | 2.15 | |
| 11 | | 0.22 |
| 12 | | 0.44 |
| 13 | | 0.65 |
| 14 | | 0.77 |
| 15 | | 0.67 |
| 16 | | 0.06 |
| 17 | 3.61 | |

6.2.7 Quartz-Porphyry Dike

The HFB hydraulic characteristic was adjusted during model calibration to better match water-level elevation data on the up- and down-gradient sides of the quartz-porphyry dike. The final calibrated HFB hydraulic characteristic was 3.28×10^{-4} per day, which is a significant barrier to groundwater flow. Including the HFB in the groundwater flow model allowed reasonable and consistent bedrock K-values to be simulated in the Davidson Canyon area. Simulating a more permeable HFB resulted in the model under predicting water levels up-gradient of the HFB and over predicting water levels down-gradient of the HFB. The calibrated HFB hydraulic characteristic improved the match to water levels on the up- and down-gradient sides of the dike and improved the match to the observed hydraulic gradient in Davidson Canyon.

6.3 Steady-State Calibration Statistics

Several statistical measures were calculated to assess the quality of the steady-state model calibration. These calibration statistics are summarized in Table 6-5. Unweighted and weighted statistics were reported to provide a comparison between the model fit to all water-level targets (unweighted) and those targets that were most representative of the regional groundwater flow system (weighted). The goal of the calibration was to minimize the statistical values, since lower values represent a better fit to the observed conditions.

The residual mean for the model calibration was slightly negative, indicating a slight model bias toward under predicting water levels. The difference between observed and simulated water levels was expected to be larger in a regional-scale model than in a site-scale model. The calibration statistics for the groundwater flow model indicated an acceptable model fit at this regional scale. For example, the residual standard deviation divided by the range of observations is considered acceptable if it is below ten (10) percent (Anderson and Woessner, 1992). For the steady-state model, this value was below five (5) percent for both unweighted and weighted residuals. The residual sum of squares was meaningless by itself, but was useful in comparing the sensitivity of parameters in the model calibration. A discussion of the parameter sensitivity analysis is included in Section 9.0, "Sensitivity Analyses".

The spatial distributions of weighted and unweighted residuals are illustrated on Figures 6-25 and 6-26. The minimum and maximum residuals occurred at wells where the hydraulic gradient was very steep or in flowing wells. These steep hydraulic gradients and flowing wells occurred in the Santa Rita Mountains, particularly near the Open Pit. Several wells near the Open Pit had water-level elevations near land surface or were flowing. These elevations are several hundred feet above nearby measured water levels considered to be representative of the regional groundwater flow system. Therefore, it was not possible to accurately simulate these highly variable and apparently isolated vertical gradients in the Open Pit area.

The comparison between observed and simulated water-level elevations for the steady-state model is shown on Figure 6-27. A perfect model fit would have all of the data plotting on the 1:1 line. A good model fit was indicated by the data points being well distributed above and below the 1:1 line. The model calibration showed slightly more points below the 1:1 line, indicating a small negative model bias due to simulated water levels being below the observed water levels. This bias was evident near the pit area where the model tended to under predict water levels due to the measured water levels near or above land surface. A random pattern on the observed water levels versus unweighted residuals is shown on Figure 6-28, indicating a good calibration. An accurate steady-state model tends to have unweighted residuals that are randomly distributed and do not display consistent spatial trends.

Table 6-5 Pre-Mining Steady-State Model Calibration Statistics

| Statistic | Unweighted (ft) | Weighted (ft) |
|-----------------------------|-----------------|---------------|
| Residual Mean | -1.18 | -4.47 |
| Residual Standard Deviation | 133.12 | 90.17 |
| Absolute Residual Mean | 97.61 | 55.05 |
| Residual Sum of Squares | 6.60E+06 | 9.96E+05 |
| RMS Error | 133.12 | 90.28 |
| Minimum Residual | -333.88 | -333.88 |
| Maximum Residual | 465.77 | 465.77 |
| Range of Observations | 2,886.19 | 2,886.19 |
| SD/Range as a percentage | 4.6% | 3.1% |

6.4 Steady-State Mass Balance

A summary of the steady-state model mass balance is presented in Table 6-6. Due to the steep hydraulic gradients and low permeability rocks that exist in the model domain, the PCG4/5 solver (Hydrogeologic, 2010) was critical in obtaining a stable solution that converged with approximately zero percent discrepancy between inflows and outflows. Over 60-percent of the water budget was from groundwater flow in and out of the model through the external model boundaries simulated as constant heads. There was a net flow out of the model domain through the constant head cells (Table 6.6).

Figure 6-29 compares the contoured simulated water levels to the observed water levels. The observed water-level contours included all measurements (i.e., low and high weights). The simulated contours followed the general trends displayed by the observed water-level contours. Discrepancies typically existed along drainage channels and the pit area where the model had difficulty simulating the steep hydraulic gradients.

The simulated stream flows versus the observed base flows for the USGS gages within the model domain are shown on Figure 6-30. The simulated stream flow shown on Figure 6-30 is presented as the cumulative net stream flow for each stream segment, and the amount of stream flow reporting at the model cell containing the USGS gage station. Due to variable stream channel elevation and groundwater levels, the simulated stream segments gain and lose water in a similar manner as does the observed conditions. The model over predicts stream flow in the gage reaches and likely in the other reaches. As previously discussed, small water-level changes and small stream flows that are due to localized hydrogeologic conditions are difficult for a regional-scale model to simulate. However, the simulated stream flows indicate that water levels, the 3D hydrogeologic framework, and the general flow system conditions were adequately simulated.

Simulated ET in the calibrated steady-state model was 5,638 ac-ft/yr (Table 6.6), which is approximately ten (10) percent higher than the range of ET estimated in other studies. This relatively high ET was due in part to the simulated water levels being generally higher than observed in the riparian areas. Actual ET in the model domain is probably not known within ten (10) percent due to the variability in plant types, distribution, and rates. The simulated ET is likely within the natural ET variability, indicating that the flow system was appropriately simulated.

During model development, the number of recharge zones was reduced and distinct recharge rates were assigned to each zone, rather than a range of values. Recharge was also increased in two (2) bedrock areas west and southwest of the Open Pit. These simplifications and

modifications resulted in a total recharge of 9,900 ac-ft/yr (Table 6.6) rather than the original recharge estimate of 10,100 ac-ft/yr. This small difference was insignificant relative to the large range of recharge estimates.

Table 6-6 Mass Balance Summary for Pre-Mining Steady-State Model

| Cumulative | Rate (ft³/d) | Rate (ac-ft/yr) |
|----------------------------|--------------------------------|------------------------|
| IN | 5,096,910 | 42,702 |
| Evapotranspiration | 0 | 0 |
| Recharge | 1,181,704 | 9,900 |
| Streams | 995,072 | 8,337 |
| Constant Head | 2,920,134 | 24,465 |
| OUT | 5,096,912 | 42,702 |
| Evapotranspiration | 672,391 | 5,633 |
| Recharge | 0 | 0 |
| Streams | 1,307,318 | 10,953 |
| Constant Head | 3,117,202 | 26,116 |
| IN - OUT | -2.0 | 0 |
| PERCENT DISCREPANCY | 0.00 | 0.00 |

7.0 TRANSIENT MODEL CALIBRATION

Simulating groundwater system changes over time with a predictive model requires aquifer-storage parameters. It is common practice to estimate the storage and hydraulic conductivity parameters from hydraulic tests. These parameter estimates are then adjusted in the groundwater flow model to match observed changes in water-level and flow observations over time. This process is called a “transient calibration.”

Time-varying water-level, spring flow, and/or stream flow observations based on a known groundwater system stress, such as pumping, recharge changes, ET changes, etc., are also needed for a transient calibration. It is fairly common for groundwater levels to have declining and rising trends due to variations in long-term pumping and climatic conditions. Spring flows and stream flows can also have fluctuations correlated to pumping and climatic conditions. When available, these data types are used as transient model target observations in the same manner that water-level targets are used in steady-state model calibration. The time-varying pumping is simulated and the hydraulic properties are adjusted until the model adequately reproduces the observed water-level and flow fluctuations.

Long-term water-level and flow fluctuations due to pumping or other causes, however, have not been observed within the model domain. This is largely due to the limited development, or the lack of large scale groundwater pumping in the region. A reliable and representative predictive model calibration to transient water level, spring flow, and stream flow data was therefore not possible due to the lack of transient target observations.

The long-term hydraulic tests conducted as part of the hydrogeologic characterization program did provide a transient water-level data set, albeit on a very small scale. However, calibrating the regional groundwater flow model to the long-term pumping test data presented numerous limitations (see Section 4.3.4). A transient 3D regional flow model calibration using the long-term hydraulic test was not completed, largely as a result of the small hydraulic stresses and limited areas of influence of the tests relative to the grid size of the regional groundwater flow model. The transient data were instead used to calibrate 2D radial-flow models from which the hydraulic parameters were estimated (Section 4.0) and subsequently up-scaled (hydraulic conductivity only) during the steady-state calibration process. The optimized storage parameters from the radial models were considered the best available storage parameter estimates and were therefore incorporated into the transient flow model.

7.1 Storage Parameters

Predictive transient models are time dependant and require that aquifer storage parameters be defined. Two (2) parameters are required for these transient simulations: specific yield and specific storage. Parameterization of the storage properties is discussed in Section 4.3.6, “Aquifer Storage Properties”. These simulated values were primarily developed from the transient calibration of the radial flow models to the long-term test data. The final storage parameter values for the alluvial and bedrock units are presented in Table 7-1.

Table 7-1 Storage Parameter Values Simulated in the Mining-Phase and Post-Closure Predictive Simulations

| Zone | HGU | General Aquifer Material | Specific Storage (feet ⁻¹) | Specific Yield |
|------|--------|--------------------------|--|----------------|
| 1 | Qal | Alluvium | 6.56×10^{-5} | 0.15 |
| 2 | QTg | Alluvium | 6.56×10^{-5} | 0.10 |
| 3 | QTg1 | Alluvium | 6.56×10^{-5} | 0.05 |
| 4 | QTg2 | Alluvium | 6.56×10^{-5} | 0.05 |
| 5 | Tsp | Bedrock | 9.84×10^{-6} | 0.01 |
| 6 | Kti | Bedrock | 9.84×10^{-6} | 0.01 |
| 7 | Kv | Bedrock | 9.84×10^{-6} | 0.01 |
| 8 | Ksd | Bedrock | 9.84×10^{-6} | 0.01 |
| 9 | Pz | Bedrock | 9.84×10^{-6} | 0.01 |
| 10 | PCb | Bedrock | 9.84×10^{-6} | 0.01 |
| 11 | Pz_Pit | Bedrock | 9.84×10^{-6} | 0.01 |
| 15 | QTg_TB | Alluvium | 6.56×10^{-5} | 0.10 |

The effect of storage parameter variability is discussed in Section 9.0, "Sensitivity Analysis". The sensitivity simulations bracketed a range of potential storage values, which, when coupled with the hydraulic conductivity estimates, produced a corresponding range of aquifer diffusivity that governed the rate of drawdown propagation. The long-term, post-closure simulation results, which represent steady-state conditions, are not dependant on storage parameters. Therefore, the long-term drawdown is insensitive to the storage parameter values.

8.0 PREDICTIVE SIMULATIONS

The predictive simulations utilized two (2) transient models to evaluate the interaction between the groundwater flow system and the Open Pit. The first predictive model simulated the 22-year operational period during pit dewatering. The second predictive model simulated the combined groundwater – pit-lake system beginning at the end of operations when active dewatering ceased and the pit began filling with water. This post-closure period was simulated for 1,000 years. These models were based on the calibrated pre-mining, steady-state model, but incorporated different MODFLOW packages to simulate the hydraulic stresses created by the presence of the pit.

The MODFLOW drain (DRN) package was used to simulate pit dewatering. The LAK2 package (Council, 1999) was used to simulate the pit-lake formation and the interaction between the pit-lake and aquifer in the post-closure predictive model. These models utilized the adaptive time-stepping and output control package (ATO4) and the PCG5 solver in MODFLOW-SURFACT (Hydrogeologic, 2010). For each transient model, a base-case model (“no pit simulation”) without the hydraulic stresses associated with the Open Pit was simulated for the same time period with the same solver parameters. This permitted a direct comparison of the simulated effects due to the Open Pit versus a simulated scenario without the pit.

8.1 Mining-Phase Pit Dewatering Simulation

The mining-phase model simulated the flow system’s response to pit dewatering. Relevant details from the Mine Plan of Operations (MPO) (Westland, 2007), deepening and expansion of the Open Pit, and the preliminary pit dewatering plan (Call & Nicholas Inc., 2010) were incorporated into the mining-phase model.

A combination of wells, horizontal drains, and sumps are planned for pit dewatering during the mining-phase (Call & Nicholas Inc., 2010). The combined influence of wells, horizontal drains, and sumps outlined in the dewatering plan were simulated using the drain boundary condition in MODFLOW. Drains were used for simulating the effects of dewatering the pit. The drains only removed water from the groundwater system when heads in the cells exceeded the drain elevation. The drain elevations were set below the bottom of the pit for each mining stage. Additionally, some drains were set in the pit walls to simulate continued dewatering as the pit deepened via inflow to the pit from the pit walls. Drain cells were also easily modified to account for deepening of the pit. Model cells simulated as drains are illustrated in the ultimate pit shell shown on Figure 8-1.

Based on the MPO (Westland, 2007), the mining-phase was expected to last for a period of 22-years. This operational period was subdivided into 12 phases or stress periods to simulate the progressive deepening and expansion of the Open Pit (Table 8-1; Figure 8-2). During operational years 2-21, a new Open Pit configuration was simulated every two (2) years, with the dewatering process initiated in advance of the actual excavation. This created a step-wise change in groundwater inflows as the pit was instantaneously advanced in the groundwater flow model.

Table 8-1 Mining-Phase Simulation Stress Period Set-Up

| Stress Period | Time Length (days) | Maximum Pit Depth (ft amsl) | Stress Period | Time Length (days) | Maximum Pit Depth (ft amsl) |
|---------------|--------------------|-----------------------------|---------------|--------------------|-----------------------------|
| 1 | 365 | 5,200 | 7 | 730 | 3,650 |
| 2 | 731 | 4,600 | 8 | 731 | 3,650 |
| 3 | 730 | 4,300 | 9 | 730 | 3,550 |
| 4 | 731 | 4,250 | 10 | 731 | 3,400 |
| 5 | 730 | 4,100 | 11 | 730 | 3,250 |
| 6 | 731 | 3,800 | 12 | 366 | 3,050 |
| Total | | | | 8,036 | |

The drain package was developed by intersecting the model grid with the 3D pit shells developed from the MPO for each stress period. The pit shell at the end of each stress period was used for the entire duration of the stress period (start to finish). Drains were assigned to each model layer based on the elevation determined by intersecting the grid with the pit shell. An additional 33 feet (10 meters) was subtracted from this elevation to create a more realistic cone of depression and to ensure that the pit was dewatered below the pit bottom. The drain configuration changed with increasing pit depth by lowering the drain elevations in each stress period.

Several drain-cell conductance values were tested to ensure that the drain cells would not impede groundwater discharge. Conductance was incrementally increased until the discharge stopped increasing with increasing conductance. The final drain conductance of 1,640 ft²/day (500 m²/day) was set slightly higher than necessary to ensure that there was no flow restriction. The higher conductance value did not result in numerical instability, and the mass balance error was less than one (1) percent.

Achieving full pit dewatering required additional drain cells placed throughout the entire pit volume. These “infill” drains were set at an elevation equal to an average pit low point. A total of 4,560 drain cells were used to simulate pit dewatering. Even with these additional drains, the low hydraulic conductivity of the bedrock within the pit created instances where the water did not drain from some model cells. Since the rocks within the pit were physically removed by mining, the hydraulic conductivity of these cells was increased to 6.6 ft/day to facilitate dewatering. The simulation resulted in appropriate pit dewatering with the final water level below the ultimate pit-shell.

8.1.1 Pit Inflows

Groundwater inflow rates into the Open Pit varied throughout the simulation period, primarily due to incrementally increasing the pit depth every two (2) years (Figure 8-3). Dewatering rates during operations are anticipated to be more gradual. However, since the pit advance was simulated in a step-wise manner, and water was removed at the start of each new mining-phase, dewatering rates were likely overestimated in the simulation.

As dewatering started, simulated groundwater inflow rapidly increased to approximately 475 gpm, but then decreased over the initial two (2)-year stress period to less than 300 gpm as water was removed from aquifer storage and hydraulic gradients decreased (Figure 8-3). Further pit advancement resulted in the highest simulated groundwater inflow of approximately 509 gpm during operational year 4. Inflow rates also varied depending on the transmissivity of the geologic units being excavated as illustrated by the lower inflow peak and slower changes

during operational years 5 through 7. As water was removed from storage, the peak inflows were attenuated even though the pit was increasing in depth (Figure 8-3). Groundwater inflow at the end of mining (operational year 22), when the excavation had reached a maximum depth of 3,050 feet amsl, was approximately 400 gpm.

The range of groundwater inflow rates during dewatering operations was predicted to range between 400 and 500 gpm. It is possible, however, that geologic complexities, including faults and fractures that were not discretely simulated in the groundwater flow model, could result in observed groundwater inflows that are higher or lower than this range. These simulated dewatering rates represent average groundwater inflows and do not include net precipitation (direct precipitation minus evaporation) that reaches the pit bottom.

In general, groundwater inflow to open pits having low permeability rocks with relatively low fracture density and connectivity has shown that fractures can initially yield substantial volumes of water that decrease rapidly over time. The degree to which this occurs depends on how well connected the fracture network is over large areas. The EPM flow model assumes that the fracture network is connected enough to be simulated as a porous media at the regional scale. In practice, the long-term groundwater inflow is likely to be less than the simulated rate. Variations in aquifer transmissivity and faults may result in aquifer compartmentalization.

Assuming reasonable ranges for bulk EPM hydraulic properties, and not simulating heterogeneities, may have contributed to the inability to simulate higher observed water levels in the pit area, which were under predicted in the pre-mining groundwater flow model. This may suggest that flow barriers, poorly connected fractures, or other heterogeneities contribute to increased observed water levels near the pit. Hydraulic testing in the pit area (M&A, 2009a; M&A, 2009c), however, did not result in clear evidence that faults or other discrete flow barriers impacted the observed drawdown. Well RP-3B went dry after 12 days of pumping at a rate of approximately 28 gpm (M&A, 2009c), indicating that it was testing low permeability rocks.

The assumption that the hydraulic testing used to generate the effective hydraulic conductivity values was a valid REV may not be accurate. The steady-state calibration was at least partly constrained by staying within the range of values determined from the hydraulic testing for the various HGUs. As a result, the calibrated effective permeabilities may be high relative to actual subsurface conditions, and the groundwater flow model is considered to be conservative with respect to the predicted impacts to the regional hydrogeologic and groundwater system.

8.1.2 Predicted Groundwater Level Drawdown

Dewatering of the Open Pit was simulated with drain cells that removed water from the model when the water reached a specified drain elevation (Figure 8-4). Dewatering lowered the water table below the bottom of the pit and created a cone of depression that extended away from the pit. Since drawdown propagation away from the Open Pit depended on the transmissivity and storage properties of the rock units, the cone of depression was not concentric. The furthest extent of the zone of influence (as defined by the five (5)-foot drawdown contour) at the end of the mining phase was predicted to be approximately four (4) miles east and 4.5 miles to the northeast in Model Layer 17, which was the model layer with the furthest simulated drawdown extent from the Open Pit (Figure 8-5). Drawdown expanded to the northeast partly due to the relatively low specific storage in the bedrock units.

By the end of the mining-phase, the cone of depression had expanded towards the upper reach of Davidson Canyon, but had not yet reached the quartz-porphyry dike. Rosemont Spring was near the 100-foot drawdown contour and within the large hydraulic gradient zone created by the dewatered Open Pit (Figure 8-5). It is likely that Rosemont Spring flow will cease by the end of

operations due to water-level declines and pit development. However, Rosemont Spring will also be buried under waste rock during the mining-phase. Questa Spring, located east of the Open Pit, was near the ten (10)-foot drawdown contour interval. Although this is not a significant amount of simulated drawdown, it is possible that Questa Spring will have reduced flows or will stop flowing by the end of operations. Due to the distance of Questa Spring from the Open Pit and its unknown origin, a definitive assessment of the potential impact from the planned Rosemont operation is not possible.

8.1.3 Predicted Surface-Water Flows

The simulated stream flow changes in Cienega Creek and Davidson Canyon were evaluated along specific stream segments (Figure 8-6). The five (5)-foot drawdown contour does not reach the vicinity of Cienega Creek or the perennial reach of Davidson Canyon during the 22-year operational period. Monitoring locations near Cienega Creek and Davidson Canyon also indicated that water levels in these areas were generally stable during the mining-phase, with small water-level declines (Figure 8-7). Since water levels had generally not declined, the simulated stream flows were unaffected (Figure 8-6). The global decrease in stream flow compared to the base-case simulation was less than 0.1 percent, which was within the range of model error.

8.2 Post-Closure Pit-Lake Simulation

Upon cessation of active pit dewatering, the Open Pit will begin to fill with water. The rate at which the pit fills, and the ultimate depth and stage of the pit-lake, depends on the pit-lake water balance. The pit-lake water balance describes how water flows into and out of the lake. This was simulated with the LAK2 Package (Council, 1999). The post-closure water balance for the Rosemont Open Pit can be expressed as:

$$\Delta_{\text{pit lake volume}} = I_{\text{precip}} + I_{\text{runoff}} + I_{\text{pit runoff}} + \text{GW}_{\text{inflow}} - E_{\text{pit}} - \text{GW}_{\text{outflow}} \quad (\text{Eqn. 1})$$

where:

I_{precip} is the inflow from direct precipitation falling on the lake surface;

I_{runoff} is the inflow from runoff from up-gradient drainages (no runoff from drainages beyond the pit-catchment are planned for the reclaimed, post-closure pit);

$I_{\text{pit runoff}}$ is the inflow from pit-wall runoff (the fraction of precipitation falling on the pit-walls that ultimately reaches the pit-lake);

$\text{GW}_{\text{inflow}}$ is the groundwater inflow to the pit-lake;

E_{pit} is the open water evaporation from the pit-lake surface based on a modified pan evaporation rate; and

$\text{GW}_{\text{outflow}}$ is the outflow of groundwater from the pit-lake.

Depending on the relative magnitudes of the water balance components, a pit could remain dry or a pit-lake could form. There are two (2) types of pit-lakes: terminal-sink and flow-through. A terminal-sink pit-lake has no groundwater leaving the pit (Eqn 1: $\text{GW}_{\text{outflow}} = 0$). A flow-through pit has a component of groundwater leaving the pit (Eqn 1: $\text{GW}_{\text{outflow}} > 0$).

For a terminal pit-lake to form, evaporation must be greater than the sum of precipitation, runoff, and groundwater inflow. The stabilized lake stage dictates the steady-state groundwater inflow

and the long-term drawdown associated with a perpetual pit-lake. Terminal pit-lake conditions are anticipated to form within the Rosemont Open Pit.

Due to the steep, roughly cone shaped walls of the proposed Open Pit, the initial surface area of the pit-lake will be small, but will increase as the lake stage rises. As the surface area of the pit-lake increases, so will evaporation losses. The lake level will stabilize when the evaporation rate equals the sum of the inflow components (direct lake precipitation, groundwater inflow, and pit-wall runoff).

8.2.1 Lake-Package Inputs

The LAK2 package was selected to simulate the pit-lake for the following reasons: 1) it calculates the transient pit-lake stage as it fills; 2) it determines groundwater inflow or outflows across multiple model layers; and 3) it was found to be more numerically stable than the LAK3 package (Merritt and Konikow, 2000). Application of the LAK2 package allows for coupling between the pit-lake water balance and the groundwater flow model. This allows the lake stage to vary according to the hydraulic stresses applied to the aquifer and the lake water budget. The inputs and outputs for the LAK 2 package are:

- Direct precipitation onto the lake (L/T);
- Lake evaporation (L/T);
- Runoff into the pit (L³);
- Pit wall runoff (L/T); and
- Conductance values for LAK cells (L/T).

A 3D representation of the final pit was developed (Westland, 2007) and model cells adjacent to the exterior of the pit were designated as “lake cells”. Groundwater inflow to the pit varied depending on heads in the surrounding aquifer cells, lake stage, and cell conductance. The lake cell conductance was set equal to or greater than the conductance of the adjacent aquifer material.

The bottom of the lake was set to the base of the pit at 3,050 feet amsl, which was in Model Layer 15 (Figure 8-8). The top elevations of the lake cells were set to the elevation of the pit-shell, rather than the model-cell elevation. In this way, the lake cells, stage-area, and stage-volume relationships were refined beyond the vertical discretization of the model grid. The stage-volume relationship generated by the LAK2 package was a function of the simulated lake cell areas for each layer and layer thickness. The stage-volume relationship simulated by the LAK2 package was checked against the elevation-volume relationship of the ultimate pit shells and was found to accurately represent the Open Pit. Similarly, an accurate simulation of the stage-area relationships was essential for accurately predicting evaporation, precipitation, and pit-wall runoff. The simulated and stage-area relationships for the pit, as compared to the MPO, are provided on Figure 8-9.

For the Rosemont site, precipitation was estimated to be 17.37 inches per year and annual pan evaporation was estimated to be 71.52 inches per year (Tetra Tech, 2010b). The conversion of pan evaporation to free surface lake evaporation is complex due to the heat-storage capacities between the lake and the pan. Water depth, heat-storage capacity of surrounding materials, and exposure of the pan to the sun and air influence the estimated evaporation. These factors significantly affect the energy balance, elevating warm-season average temperature and vapor pressure of the water surface of a pan relative to a lake (Dingman, 1994). The conversion from pan evaporation to lake evaporation was estimated using a pan coefficient of 0.7.

Precipitation falling on the catchment of the pit that does not infiltrate, pond, or evaporate will run off the pit-walls and flow towards the lake at the bottom of the pit. This parameter is known as the pit-wall runoff coefficient and was estimated to be 30-percent of precipitation. In practice, this parameter will vary over time as the pit fills, but 30-percent was considered a reasonable estimate for the climate at the Project site.

The input values used in the LAK2 package do not explicitly match the values presented above. Modifications were made to more accurately account for precipitation on the lake as the surface area changes during refilling. Lake stage and groundwater inflows, which are important for simulating potential impacts, are sensitive to these LAK2 inputs. The standard input for precipitation in the LAK2 package results in the precipitation rate being assigned to the entire footprint of the simulated lake catchment, which is greater than the lake's surface area as it is filling. Using the simulated lake catchment would result in over estimating precipitation since only 30-percent of the water falling on the pit-walls was estimated to reach the lake.

The precipitation input parameter was used for defining the 30-percent of precipitation falling on the pit-walls and reaching the lake (5.21 in/yr). However, 100-percent of the precipitation on the lake surface must be accounted for in the water balance. This was accomplished by accounting for the net precipitation and evaporation over the lake, as dictated by the lake surface area for each time step. The evaporation parameter was defined as a rate and only applied to the surface area of the lake. Therefore, a net average annual evaporation rate was defined as the input. This parameter was defined as the lake-evaporation rate minus 70-percent of the precipitation rate, since 30-percent of the precipitation was already applied as part of the precipitation input parameter.

$$\begin{aligned}\text{Net Lake Evaporation} &= \text{Lake Evaporation} - 0.70(\text{Precipitation}) \quad (\text{Eqn 2}) \\ &= 50.06 \text{ in/yr} - 12.16 \text{ in/yr} = 37.9 \text{ in/yr}\end{aligned}$$

The final step was assigning any runoff to the lake not already included in the precipitation value. No stormwater diversions are expected to flow into the pit from beyond the pit catchment area. Based on the ultimate pit shell, the total pit catchment area is 702.7 acres. However, the catchment simulated in the model was 501.1 acres. The area difference was due to dry model layers not being included in the LAK2 package area calculation. The lake footprint in Model Layer 3 was used for Model Layers 1 and 2, even though the pit area was increasing in Model Layers 1 and 2. Some of the precipitation falling on the pit-wall area in Model Layers 1 and 2 will flow towards the pit, so the pit-wall runoff coefficient of 30-percent was assumed. The simulated average annual runoff from the upper portion of the pit represented by Model Layers 1 and 2 was 54.3 gpm.

8.2.2 Stress Period Set-up

The pit-lake and groundwater system are expected to reach or approach steady-state conditions within a 1,000-year time period following the cessation of dewatering. Therefore, a 1,000-year simulation period was selected for the flow model. Although a simulation of this length is inherently inaccurate, it does provide an indication of the magnitude of changes over time.

The 1,000-year, post-closure simulation was divided into six (6) stress periods (Table 8-2). The stress periods were set to coincide with the transient recharge conditions associated with drain-down of the Dry Stack Tailings Facility. There were no other time-varying boundary conditions in the simulation.

Table 8-2 Post-Closure Simulation Stress Period Set-Up

| Stress Period | Time Length (years) | Maximum Time Step (days) |
|---------------|---------------------|--------------------------|
| 1 | 100 | 30 |
| 2 | 100 | 90 |
| 3 | 100 | 90 |
| 4 | 100 | 90 |
| 5 | 100 | 90 |
| 6 | 500 | 365 |

8.3 Post-Closure Phase Simulation Results

The post-closure model simulated refilling of the dewatered Open Pit, the resulting pit-lake formation, and the corresponding changes to the regional groundwater system. A groundwater divide, higher than the lake level, was predicted to form around the Open Pit, creating a terminal-sink condition. Over the long-term, the predicted terminal pit-lake will continue to consume groundwater due to the net loss of water from evaporation. This is hydrologically equivalent to removing groundwater by production wells.

Pit-lakes draw groundwater levels down most dramatically in the vicinity of the open pit with decreasing drawdown at greater distances away from the pit. The magnitude and extent of the drawdown depends in part on the pit-lake water balance, which determines the pit-lake level (lake stage) and groundwater inflow rates.

This drawdown and associated cone of depression can be advantageous by capturing potential process area contaminants and preventing their migration away from the immediate facility area. Drawdown in a regional groundwater flow system, however, can reduce base flows in streams and springs. Drawdown associated with a pit-lake will continue to expand outwards until there is sufficient capture of water from other sources to create a new stable water table. At steady-state conditions, the rate of water capture will be equal to the steady-state groundwater inflow to the pit lake. The Rosemont pit-lake water balance is discussed in Section 8.4, "Predictive Model Mass Balance".

8.3.1 Predicted Groundwater Level Drawdown

Groundwater elevations near the pit will start recovering following the cessation of dewatering. The lake stage increase will increase from a dewatered depth of approximately 33 feet below the bottom of the pit (3,050 feet amsl - 33 feet = 3,017 feet amsl) to a simulated steady-state elevation of 4,279 feet amsl, or approximately 700 feet below the pre-mining groundwater level. The post-closure steady-state conditions are anticipated between 700 to 1,000 years after the cessation of dewatering.

Despite the recovery of groundwater elevations near the pit following the cessation of dewatering, the cone of depression will continue to expand away from the Open Pit. Drawdown propagation at 20 years, 50 years, and 150 years following the cessation of dewatering is illustrated on Figures 8-10, 8-11, and 8-12. As shown on these figures, drawdown will elongate in the north-south direction, in part as a result of the bedrock's higher hydraulic conductivity as compared to the east-west direction. After 150 years, the drawdown had not yet reached Cienega Creek or the perennial reach of Davidson Canyon (Figure 18-2).

The effect of the quartz-porphphy dike on drawdown propagation became relevant 20 years after the end of dewatering (Figure 8-10). The low hydraulic conductivity of the dike hindered

drawdown propagation into the lower reaches of Davidson Canyon. Due to this natural restriction, drawdown migrated laterally along the dike toward the northwest and southeast.

The extent of the predicted groundwater drawdown continued to expand after 150 years and had reached steady-state condition by 1,000 years (Figure 8-13). Drawdown near the Open Pit was relatively stable as the 100-foot drawdown contour was nearly identical at 150 years and at 1,000 years. In contrast, the five (5)-foot drawdown contour expanded to the east and north over this same time interval, illustrating the long-time interval potentially required for the regional flow system to reach equilibrium.

The effects of groundwater inflow to a pit (hydraulic sink) may take many years to materialize and stabilize at greater distances from the pit. The time to reach equilibrium, or steady-state conditions, depends on the hydraulic diffusivity (transmissivity divided by storativity) of the aquifer and the distance from the point of measurement to the pit-lake. The relatively low diffusivity in the Rosemont model domain, therefore, required hundreds of years to reach equilibrium.

A 1,500-year post-closure simulation was also performed and indicated that the extent of the predicted groundwater drawdown was approximately the same as the 1,000-year simulation (Figure 8-14). This indicated that the maximum drawdown and new steady-state condition had been achieved within the 1,000-year post-closure period.

Simulated monitoring wells were set within the groundwater flow model to illustrate the predicted long-term drawdown near Davidson Canyon and Cienega Creek (Figure 8-7). The predicted stable drawdown at these locations, which are more than nine (9) miles from the Open Pit, also indicated that the maximum drawdown had been achieved within 1,000 years. Observation wells in Davidson Canyon predicted a maximum drawdown of about 0.25 feet (DC-1 and DC-2, Figure 8-7), which is likely less than the flow model's prediction accuracy. The greatest predicted drawdown of approximately one (1) foot was at observation location C-1 in upper Cienega Creek (Figure 8-7). Negligible drawdown was simulated in the lower reach of Cienega Creek (C-2, Figure 8-7). These drawdown magnitudes, however, would likely be indistinguishable from the larger natural groundwater-level variations as compiled by M&A (2010b).

The ten (10)-foot drawdown contour west of the Open Pit approached the model domain boundary, which was simulated with constant-head cells. The assigned heads at this boundary, which were on the edge of the basin-fill down-slope of the Santa Rita Mountains, were lower than the water levels near the Open Pit. Under the pre-mining, mining-phase, and post-closure simulations, there was flow out of the model domain at this boundary.

Drawdown during the post-closure simulation resulted in less water flowing out of the model through the constant-head cells along the west boundary. Although reduced, all cells still simulated flow out of this boundary. The flow was reduced by 52 gpm (84.5 ac-ft/yr) or approximately three (3) percent of the total outflow between the post-closure simulation and the no-pit simulation. This reduction in outflow was a form of capture by the Open Pit's hydraulic sink.

As part of the sensitivity analysis presented in Section 9.0, "Sensitivity Analysis", the western model boundary was also simulated as a no-flow boundary and as a General Head Boundary (GHB). A GHB is a head dependant boundary, whereby the flow into or out of the model domain is dependant on the difference between the assigned hydraulic head and the head in the model cell. These sensitivity simulations tested the influence of the western boundary model configuration on the predicted drawdown and boundary fluxes.

8.3.2 Predicted Surface-Water Flows and Evapotranspiration

Drawdown is expected to extend towards Davidson Canyon and Cienega Creek. Therefore, some of the groundwater that may have discharged to these drainages could be captured by the Open Pit. The predicted decrease in stream base flow was estimated by calculating the difference simulated in the post-closure groundwater flow model to that simulated without the Open Pit. The stream flow over each simulated stream segment was evaluated so that the predicted base flow changes could be determined over several parts of the entire stream length (Figure 8-15).

Conceptually, the maximum possible long-term impact to Cienega Creek, Davidson Canyon, and regional springs within the zone influenced by the Open Pit is approximately the simulated 1,000-year steady-state groundwater inflow of 230 gpm or 0.51 cfs. This groundwater inflow to the pit will be captured from various sources within the region. Sources of simulated water capture may include:

- Increased flow into the model domain;
- Decreases in stream flow;
- Decreases in riparian vegetation evapotranspiration;
- Decreases in flow out of the model domain (e.g., western model boundary); and
- Increases in recharge resulting from post-closure conditions.

The total decrease in average annual base flow along Cienega Creek after 1,000 years was simulated as 0.09 cfs, which was less than three (3) percent of the simulated base flow (Figure 8-15). The largest decreases in flow were predicted in the upper reaches of Cienega Creek (Stream segments 1 – 4, Figure 8-15). Stream flows were decreased due to slightly lower water levels and less groundwater discharging to the stream channel. Stream-flow decreases of approximately 0.01 cfs were predicted in the downstream reaches of Cienega Creek (Stream segments 8 – 10, Figure 8-15).

Although the post-closure model simulated stream flows that were higher than the median flow recorded at the USGS gage location in Davidson Canyon, the predicted change in stream flow can be used to estimate the anticipated magnitude of change due to the Project. In Davidson Canyon, the predicted change in flow was 0.01 cfs in the upper most reach (Stream segment 11, Figure 8-15). No losses were simulated in the reach identified as an Outstanding Arizona Water (PAG, 2005; Stream segment 15, Figure 8-15). These small simulated stream flow changes, however, were within the range of model error. The predicted cone of depression therefore, did not lower water levels enough to significantly affect the simulated stream flows.

Simulated water-level declines also had a negligible effect on the riparian vegetated areas along Davidson Canyon and Cienega Creek. The simulated change in riparian vegetation evapotranspiration (ET) in Davidson Canyon and Cienega Creek was approximately 14 ac-ft/yr or 0.2 percent (see Section 8.4, "Predictive Model Mass Balance"). Therefore, both ET discharge and riparian vegetation are not expected to significantly change.

Over time, water-levels will recover near the Open Pit as the pit-lake fills. In terms of post-closure conditions, the Project area springs could resume flowing as water levels rise. For example, although Rosemont Spring would be under the Rosemont Ridge Landform, there was less drawdown predicted at this location after 1,000-years than compared to the end of mining simulation (Figures 8-5 and 8-13). However, it is not possible to predict whether perched or regional springs will have resumed flows during the post-closure water-level recovery. Conversely, at the more distant Questa Spring location, the flow model predicted approximately ten (10)-feet of drawdown 50 years after the end of operations, but the drawdown increased to

over ten (10)-feet after 150 years. This increase in drawdown, compared to the end of mining, makes it more likely that Questa Spring will have reduced flows or will stop flowing over the post-closure period.

8.4 Predictive Model Mass Balance

At the end of the 22-year operational period, the simulated Open Pit and surrounding rock were completely dewatered. Groundwater inflows in the final time step (year 22), simulated as discharge through drain cells, were 650 ac-ft/yr (402 gpm) (Table 8-3). Changes to the other mass balance components were relatively minor when comparing the mining-phase simulation to the simulated pre-mining, steady-state mass balance (Table 8-3).

Drawdown propagation had not reached the streams or riparian areas in Davidson Canyon or Cienega Creek at the end of the mining-phase simulation. There was essentially no change in the net stream flow (1 ac-ft/yr) and only a one (1) ac-ft/yr (0.02 percent) decrease in ET (Table 8-3). The small simulated change in ET and lack of drawdown indicated that riparian vegetation in Davidson Canyon and Cienega Creek would remain unaffected during the mining-phase.

Groundwater flow in and out of the model's external boundaries was simulated with constant head cells. High groundwater-level elevations along the crest of the Santa Rita Mountains and in the Open Pit area resulted in outflows through the western boundary during all simulations. Outflows through the constant-head cells decreased 1,080 ac-ft/yr during the mining-phase. This was largely attributable to a 0.13 percent decrease in flow out of the western boundary (Table 8-3). Drawdown in the Open Pit area decreased the hydraulic gradient to the west, which resulted in the small decrease in outflows.

Table 8-3 Mass Balance for Predictive Simulations

| | Steady State, Cumulative (ac-ft/yr) | Mining Simulation, Cumulative (ac-ft/yr) | Mining Simulation, Final Time Step, 22 yrs (ac-ft/yr) | Cumulative Difference [Steady state - Mining Simulation] (ac-ft/yr) | Post-Closure Simulation, Cumulative (ac-ft/yr) | Post-Closure Simulation, Final Time Step, 1,000 yrs (ac-ft/yr) | Cumulative Difference [Steady state - Post-Closure Simulation] (ac-ft/yr) |
|----------------------------|-------------------------------------|--|---|---|--|--|---|
| IN | 42,702 | 42,899.0 | 42,661 | -197 | 42,305 | 42,262 | 397 |
| Storage | 0 | 839.7 | 605 | -840 | 45 | 2 | -45 |
| Evapotranspiration | 0 | 0 | 0 | 0 | 0 | 0 | 0.0 |
| Recharge | 9,900 | 9,900 | 9,900 | 0 | 10,096 | 10,092 | -196 |
| Streams | 8,337 | 8,336 | 8,335 | 1 | 8,341 | 8,342 | -4 |
| Constant Head | 24,465 | 23,823 | 23,821 | 642 | 23,824 | 23,826 | 641 |
| Drains/Lake | 0 | 0 | 0 | 0 | 0 | 0 | 0.0 |
| OUT | 42,702 | 42,906 | 42,689 | -204 | 42,307 | 42,261 | 395 |
| Storage | 0 | 474 | 362 | -474 | 40 | 2 | -40 |
| Evapotranspiration | 5,633 | 5,634 | 5,634 | -1 | 5,619 | 5,615 | 14 |
| Recharge | 0 | 0 | 0 | 0 | 0 | 0 | 0.0 |
| Streams | 10,953 | 10,954 | 10,957 | -1 | 10,909 | 10,899 | 44 |
| Constant Head | 26,116 | 25,036 | 25,087 | 1,080 | 25,348 | 25,373 | 768 |
| Drains/Lake | 0 | 809 ¹ | 650 ¹ | -809 | 391 ² | 371 ² | -391 |
| IN - OUT | 0 | -7 | -1 | -- | -2 | 0 | -- |
| PERCENT DISCREPANCY | 0 | 0 | 0 | -- | 0 | 0 | -- |

¹ Drain cells² Lake cells

The lake stage and groundwater inflow reach steady-state conditions approximately 700 years after the cessation of dewatering. At this time, the conditions reached were about 99.5 percent of the 1,000-year simulation values. The final 1,000-year time step indicated that there was very little water moving in and out of storage in the simulation (Table 8-3). Simulated groundwater inflow at 700 years was greater than 99.9 percent of inflows projected at the end of the 1,000-year simulation period. A 1,500-year simulation confirmed that the 1,000-year simulation results did not change with increasing time. The surface area of the steady-state pit lake is predicted to be about 213 acres and have a volume of approximately 95,975 acre-feet. At this stage, the pit-lake elevation will be about 4,279 feet amsl. The groundwater divide to the east of the Open Pit is about 4,680 feet amsl.

The cumulative, simulated net stream flow loss at the 1,000-year post-closure period compared to the pre-mining steady-state simulation modeled without the pit was 48 ac-ft/yr (30 gpm) or 0.4 percent (Table 8-3). Simulated ET decreased 14 ac-ft/yr (9 gpm) or 0.2 percent. Groundwater inflow to the pit-lake, simulated with lake cells, was 371 ac-ft/yr (230 gpm) in the final 1,000-year time step.

Recharge in the post-closure simulation was 196 ac-ft/yr higher than in the steady-state simulation modeled without the pit. This increase was mostly attributable to recharge simulated in the flow-through drains associated with the Rosemont Ridge Landform

8.4.1 Pit-Lake Mass Balance

Components of the pit-lake water balance at the end of the 1,000-year simulation period are summarized in Table 8-4. The predicted pit-lake water balance over the entire 1,000-year post-closure simulation is illustrated on Figure 8-16. The lake stage rose rapidly over the first 100 to 200 years and then approached a constant or steady-state level after approximately 700 years (Figure 8-16). The steady-state groundwater inflow to the pit was 230 gpm and represented the long-term water consumption rate due to the pit-lake. Groundwater inflows started low immediately after the cessation of dewatering and rapidly increased over the next ten (10)-year period before gradually decreasing to a constant rate (Figure 8-16). The largest single component of the water balance was evaporation with an outflow of 891 ac-ft/yr (Table 8-4). The step-wise increases in evaporation (Figure 8-16) were due to the step-wise increases in the pit-lake surface area. The three (3) sources of inflow that balanced evaporation were direct precipitation on the lake surface, groundwater inflow, and pit-wall runoff.

Table 8-4 Simulated Pit-Lake Water Balance 1,000 Years after End of Operations

| Inflows | Average Annual Rate (ac-ft/yr) | Average Annual Rate (gpm) |
|-------------------------|---------------------------------------|----------------------------------|
| Direct Precipitation | 308.3 | 191 |
| Groundwater Inflow | 371.2 | 230 |
| Pit-Wall Runoff | 211.4 | 131 |
| Upgradient Runoff | 0 | 0 |
| Total Inflow | 890.9 | 552 |
| Outflows | Average Annual Rate (ac-ft/yr) | Average Annual Rate (gpm) |
| Evaporation | 891.0 | 552 |
| Groundwater Outflow | 0 | 0 |
| Total Outflow | 891.0 | 552 |
| Inflow – Outflow | -0.1 | 0 |

Theory predicts that groundwater inflow will decrease exponentially after the initial surge of inflow immediately following the cessation of dewatering. Therefore, simulated groundwater inflow rates were expected to be highest after the cessation of mine dewatering, decreasing with time as the hydraulic gradient decreased. The predicted early time groundwater inflows, however, were lower than anticipated (Figure 8-16). This was largely explained by the methods used to simulate dewatering and pit refilling.

The drain elevations in the mining-phase model were set 33 feet below the pit-shell elevations in the deepest model layers to ensure that the entire pit was dewatered. This drain configuration had the effect of realistically expanding the dewatered area's footprint away from the pit shell, thus increasing the volume of rock being dewatered. The LAK2 cells simulating pit refilling, however, more closely approximated the pit shell. During the transition from the mining-phase simulation to the post-closure simulation, the dewatered model cells around the pit shell had to re-saturate before groundwater began flowing into the pit. This re-saturation process resulted in the simulated delay before inflows increased.

The volume of dewatered cells to be filled, combined with the hydraulic properties of the hydrogeologic units, determined the lag time in pit refilling. For example, lower hydraulic conductivity results in longer lag times. As the water levels initially recovered in the dewatered rock, groundwater inflows increased. However, over the long-term, the hydraulic gradient decreased and the inflow rate decreased to a steady-state rate of 230 gpm (Figure 8-16). The long-term impact of the Project on the regional groundwater system was therefore simulated as 230 gpm.

The highest post-closure groundwater inflow rate of 311 gpm occurred approximately 7.7 years after the cessation of dewatering. This was approximately 25-percent less than the groundwater inflows at the end of operations (402 gpm). This was due to the lower hydraulic gradient between the rock mass and the pit-lake over this time period. In the dewatered condition, the head difference was greater because the Open Pit was completely dewatered to an elevation below 3,050 feet amsl.

9.0 SENSITIVITY ANALYSES

Sensitivity analyses were completed on the groundwater flow model for the pre-mining steady-state, mining-phase, and post-closure simulations. The objective of the pre-mining steady-state model sensitivity analyses was to identify the model inputs that had the most impact on calibration and model fit. The objective of the predictive mining-phase and post-closure model sensitivity analyses was to determine the likely range of impacts to the regional groundwater system.

The steady-state simulation results evaluated during the sensitivity analyses were limited to the effect on the sum of square weighted residuals (SOSWR). The SOSWR is a measure of how well the model matches the target water levels. During the calibration process, the SOSWR was minimized to the greatest extent possible without simulating unrealistic conditions, such as water-levels above land surface.

The most sensitive parameters in the steady-state model were identified and then varied to determine the impact on the SOSWR. Hydraulic conductivity, recharge, stream-bed conductance, and the western model boundary were evaluated. The SOSWR for each parameter change indicated whether the change improved the statistical model fit. A lower SOSWR indicated lower residuals and a better model fit to the observed data.

The predictive model sensitivity analyses included an evaluation of how parameter changes impacted drawdown, stream flows, ET, pit inflows, and the lake stage. Predicted changes were relative to the simulation without the pit, which had the same parameter values as the predictive models. Changes were observed at the end of operations, 150 years post-closure, and 1,000 years post-closure.

Parameter changes for the two (2) predictive models included K_{xy} (horizontal hydraulic conductivity), K_z (vertical hydraulic conductivity), HFB conductance, S_s (specific storage), and S_y (specific yield). The post-closure sensitivity analysis included pit-lake precipitation, evaporation, and pit-wall runoff parameter changes that were specific to pit-lake development and not relevant to the mining-phase simulation. This set of parameters and the percent change were determined based on a review of preliminary simulation results. Parameters that were likely to influence changes in drawdown, stream flow, and ET were selected for analysis. This sensitivity analysis approach was taken since there were no regional, transient water-level observations available to statistically identify the most sensitive parameters.

9.1 Model Parameters

The same parameters were used in each of the three (3) simulations (pre-mining, mining-phase, and post-closure). Parameters were established for the HGUs, recharge, streambed conductance, and the quartz-porphphy dike simulated as an HFB. The HGU parameters included the ten (10) units in the hydrogeologic framework model, plus the Pz_Pit and QTg_TB parameters that were added during model calibration (Table 9-1). The bedrock HGU zone parameter Pz_Pit simulated the steeply dipping Paleozoic beds and the influence of the Backbone fault in the western pit area. The Pz_Pit parameter was the only zone with different values for the K_x and K_y directions. Higher north-south permeability, due to the Backbone fault, resulted in the K_y being greater than the K_x direction. The basin-fill zone parameter QTg_TB simulated the higher permeability Tucson Basin deposits in the northwest corner of the model domain.

Table 9-1 Final Hydrogeologic Unit Parameters Evaluated in the Sensitivity Analysis

| HGU Parameter | Description |
|---------------|--|
| Qal | Quaternary and Recent alluvium |
| QTg | Late Tertiary to Early Quaternary basin-fill deposits – higher permeability |
| QTg1 | Late Tertiary to Early Quaternary basin-fill deposits – lower permeability |
| QTg2 | Late Tertiary to Early Quaternary basin-fill deposits – lowest permeability |
| QTg_TB | Tucson Basin Late Tertiary to Early Quaternary basin-fill deposits – higher permeability |
| Tsp | Early to Mid-Tertiary sedimentary and volcanic units (Pantano Formation) |
| KTi | Upper Cretaceous and Early Tertiary intrusive rocks |
| Kv | Upper Cretaceous volcanic rocks |
| Ksd | Lower Cretaceous sedimentary units (Bisbee Group) |
| Pz | Paleozoic sedimentary and metamorphic formations |
| Pz_Pit | Paleozoic sedimentary and metamorphic formations near the Backbone Fault |
| pCb | Precambrian igneous and metamorphic crystalline formations |

9.2 Steady-State Parameter Sensitivity

Parameter sensitivities measure how changes in model parameters impact the computed water levels at the measured water-level locations. The PEST (Parameter ESTimation) software (Doherty, 2010) provided an overall quantification of the parameter sensitivities through a variable referred to as a composite sensitivity.

Parameter sensitivity was defined as the derivative of a predicted value, in this case groundwater level, relative to a model parameter, such as hydraulic conductivity. The sensitivity was the change in the groundwater level caused by a change in a model parameter value divided by the change in the parameter value. In the case of the hydraulic conductivity parameter, the sensitivity would have units of feet divided by the units of hydraulic conductivity, such as feet per day (ft/day). As a result, the units for composite sensitivity were different depending on which model parameter was considered. Comparing composite sensitivities among parameters required normalized values by multiplying the sensitivity by the parameter value. If the model parameter was log transformed in PEST, the log of the parameter value was multiplied by the composite sensitivity. The resulting composite scaled sensitivity had the units of feet regardless of what model parameter was being considered.

Composite parameter sensitivities are useful in identifying those parameters which may be degrading the performance of the parameter estimation process through a lack of sensitivity to model outcomes. The use of composite scaled sensitivities, in addition to normal sensitivities, assists in comparing the effects that different parameters have on the parameter estimation process when these parameters are of a different type, and possibly of very different magnitudes.

The 13 parameters with the highest composite scaled sensitivity (CSS) values for the steady-state model, plus the HFB hydraulic conductivity and the streambed hydraulic conductivity, are provided in Table 9-2. CSS indicates the importance of observations as a whole to each parameter. Modifying the parameters with relatively high CSS values will result in simulated head changes at the observation locations. Parameters were also normalized to the highest composite scaled sensitivity value (Recharge zone 2) to simplify the comparison of CSS values.

The most sensitive parameters were six (6) recharge zones and the hydraulic conductivity of seven (7) HGUs.

Table 9-2 Steady-State Model Composite Scaled Sensitivities for the Most Sensitive Parameters

| PEST Parameter Name ¹ | Parameter (Zone) | Calibrated Parameter Value | Composite Sensitivity | Composite Scaled Sensitivity (CSS) | Normalized CSS |
|----------------------------------|------------------|------------------------------|-----------------------|------------------------------------|----------------|
| r2 | Recharge (2) | 0.33 in/yr | 13.00 | 60.30 | 1.00 |
| r5 | Recharge (5) | 0.53 in/yr | 5.63 | 24.90 | 0.41 |
| kz6 | Kv (6) | 1.31 x 10 ⁻³ ft/d | 6.83 | 23.20 | 0.38 |
| r4 | Recharge (4) | 0.42 in/yr | 4.87 | 22.10 | 0.37 |
| kz11 | Pz_Pit (11) | 3.28 x 10 ⁻⁴ ft/d | 5.43 | 21.70 | 0.36 |
| r7 | Recharge (7) | 1.31 in/yr | 3.40 | 13.70 | 0.23 |
| kz8 | Ksd (8) | 3.94 x 10 ⁻³ ft/d | 4.57 | 13.30 | 0.22 |
| kx3 | QTg1(3) | 1.74 x 10 ⁻¹ ft/d | 8.80 | 11.20 | 0.19 |
| r6 | Recharge (6) | 0.68 in/yr | 2.20 | 9.51 | 0.16 |
| kx15 | QTg_TB (15) | 3.61 x 10 ⁻¹ ft/d | 9.24 | 8.85 | 0.15 |
| kz9 | Pz (9) | 1.08 x 10 ⁻² ft/d | 3.55 | 8.81 | 0.15 |
| r3 | Recharge (3) | 0.37 in/yr | 1.75 | 8.03 | 0.13 |
| kx11 | Pz_Pit (11) | 3.28 x 10 ⁻³ ft/d | 2.36 | 7.08 | 0.12 |
| Hf1 | HFB | 3.28 x 10 ⁻⁶ ft/d | 0.78 | 4.70 | 0.08 |
| St1 | Stream bed | 6.56 ft/d | 0.14 | 0.04 | 0.001 |

¹r = recharge; kz = vertical hydraulic conductivity (K_z); kx = horizontal hydraulic conductivity (K_{xy}); Hf = horizontal flow barrier (HFB); St = stream bed conductance

9.2.1 Steady-State Sensitivity Simulations

The steady-state sensitivity analyses confirmed that the steady-state calibration resulted in nearly optimal parameter values for matching water levels in the groundwater flow model. However, different values for a few model parameters did result in an improvement in the SOSWR. These parameter values, however, would have resulted in either water levels above land surface in the pCb HGU southwest of the pit or a lowering of water levels in the pit area. Simulated water levels in the calibrated model were lower than observed, so further water-level decreases were undesirable. While changing parameter-values would improve the calculated model fit, the model's representation of the overall groundwater system would be degraded.

A series of sensitivity simulations were conducted by increasing and decreasing values of the parameters identified in Table 9-2. In addition, stream-bed and HFB hydraulic conductivities were evaluated. The results of the steady-state sensitivity simulations are presented as the percent difference of the SOSWR value from the calibrated model plotted versus the multiplier used to modify the calibrated parameter value. A negative percent difference value would indicate that the change in parameter value decreased the SOSWR due to smaller differences between the observed and simulated water levels. A positive SOSWR percent difference would indicate that the change in the parameter value increased the SOSWR due to a larger difference between the observed and simulated water levels.

Most changes in K_{xy} resulted in a higher SOSWR, indicating that near optimal parameter values were chosen during calibration. Parameters and their values used in the steady-state sensitivity

analyses are provided in Table 9-3. Application of these parameter values, and the results of each steady-state model sensitivity simulation, are discussed in the following subsections.

9.2.1.1 Horizontal Hydraulic Conductivity (K_{xy}) by Zone

The sensitivity to K_{xy} for QTg1, Pz_Pit, and QTb_TB on SOSWR are shown on Figure 9-1. Increasing these parameter values increased the SOSWR, which indicated a decrease in model fit. Decreasing the K_{xy} of the Pz_Pit parameter resulted in a 2.9-percent reduction in SOSWR compared to the calibrated steady-state model. However, this reduction in K_{xy} caused water levels in the Santa Rita Mountains (pCb HGU) to rise above land surface.

9.2.1.2 Horizontal Hydraulic Conductivity (K_{xy}) by Rock Type

The sensitivity of varying K_{xy} of all basin-fill HGUs (zones 1 – 4 and 15) at the same time and the sensitivity of varying K_{xy} of all bedrock HGUs (zones 5 – 11) at the same time is shown on Figure 9-2. An increase or decrease in K_{xy} by 30-percent (i.e., a multiplier of 0.7 or 1.3) for basin-fill HGUs resulted in a higher SOWSR, indicating that near optimal parameter values were obtained during calibration. Reducing the bedrock K_{xy} values by ten (10)-percent (i.e., a multiplier of 0.9), resulted in a reduction of the SOSWR by approximately five (5) percent. However, this reduction in K_{xy} caused water levels in the Santa Rita Mountains (pCb HGU) to rise above land surface. A corresponding decrease in recharge would have been necessary to prevent simulated water levels from mounding based on the lower K_{xy} values. The groundwater flow model could not converge on a solution when the bedrock K_{xy} was decreased by more than ten (10)-percent.

Table 9-3 Sensitivity Analysis Parameter Changes for the Pre-Mining Steady-State Model

| Parameter | Property | Change |
|---------------------|---|--|
| QTg1, QTb_TB | Horizontal Hydraulic Conductivity, K_{xy} | ± 30 percent |
| Pz_Pit | Horizontal Hydraulic Conductivity, K_{xy} | -30,-50, -90 percent; +30 percent, +5x, +10x |
| Basin-fill | Horizontal Hydraulic Conductivity, K_{xy} | ± 30 percent |
| Bedrock | Horizontal Hydraulic Conductivity, K_{xy} | -30 percent, -10 percent; +30 percent |
| Kv, Ksd, Pz, Pz_Pit | Vertical Hydraulic Conductivity, K_z | -30,-50, -90 percent; +30 percent, +5x, +10x |
| Basin-fill | Vertical Hydraulic Conductivity, K_z | ± 30 percent |
| Bedrock | Vertical Hydraulic Conductivity, K_z | ± 30 percent |
| Recharge | Recharge | ± 20 percent; +40 percent |
| HFB | Hydraulic Conductivity, K | -90 percent; +10x |
| Streambed | Hydraulic Conductivity, K | -90 percent; +10x |

9.2.2 Vertical Hydraulic (K_z) Conductivity by Zone

The sensitivity of K_z for the Kv, Ksd, Pz, and Pz_Pit HGUs (zones 6, 8, 9, and 11) on SOSWR is shown on Figure 9-3. Reduction in K_z values for Kv (volcanic units) and Pz_Pit produced up to a 1.9 percent reduction in SOSWR. Reducing the Kv (zone 6) K_z caused water levels in the pit area to drop by over ten (10) feet. Reducing Pz_Pit HGU (zone 11) K_z caused water levels in the pCb HGU southwest of the pit area to rise above land surface. Increasing K_z for the Ksd HGU (zone 8) and the Pz HGU (zone 9) produced up to a 3.8 percent reduction in SOSWR. Increasing K_z in the Kv or Pz_Pit HGUs by 30-percent, however, caused water levels in the pit

area to decrease by over ten (10) feet. Although simulated water levels in the calibrated model were lower than observed, and changing parameter-values would improve the calculated model fit, the model's overall representation of the groundwater system would be degraded.

9.2.3 Vertical Hydraulic (K_z) Conductivity by Rock Type

The sensitivity of varying K_z of the basin-fill HGUs at the same time and the sensitivity of varying K_z of the bedrock HGUs at the same time is shown on Figure 9-4. An increase in K_z by 30-percent for basin-fill HGUs resulted in a minor reduction (0.2 percent) of the SOSWR. Reducing the bedrock K_z values by 30-percent resulted in a reduction of the SOSWR by approximately two (2)-percent. However, the K_z reduction caused water levels in the Santa Rita Mountains (pCb HGU) to rise above land surface.

9.2.4 Recharge

The sensitivity of simultaneously changing all recharge zones equally is shown on Figure 9-5. Increasing recharge by 20-percent reduced the SOSWR by approximately two (2)-percent. However, this increase in recharge caused water levels in the Santa Rita Mountains (pCb HGU) to rise above land surface. Decreasing recharge by 20-percent or increasing recharge by 40-percent resulted in over a 20-percent increase in the SOSWR.

9.2.5 Streambed Hydraulic Conductivity and Horizontal Flow Barrier

The sensitivity of the streambed and the quartz-porphyry dike HFB hydraulic conductivity on the SOSWR is shown on Figure 9-6. Due to their low CSS values, there was little change in SOSWR even with an order of magnitude increase or decrease of these parameter values.

9.3 Western Flow Model Boundary

Due to the proximity of the western model boundary to the Open Pit, sensitivity simulations were conducted to determine the boundary's impact on the simulation results. Two (2) alternative scenarios were tested for the western boundary, including simulating the boundary as a no-flow boundary and as a general head boundary (GHB).

9.3.1 No-Flow Boundary

In the steady-state model sensitivity analysis, the western flow model boundary was simulated as a no-flow boundary in all model layers rather than as a constant-head boundary. The SOSWR increased by 264 percent, indicating that the steady-state model calibration was extremely sensitive to changing the western boundary condition to no-flow. In the steady-state model, groundwater flows out of the western boundary through constant head cells. Converting the western boundary to no-flow cells caused water levels near this boundary to rise substantially.

The western flow model boundary was also simulated as a no-flow boundary in the mining-phase sensitivity simulation. The model was unable to converge on a solution with the no-flow boundary condition. In the mining-phase simulation, groundwater was flowing out of the model domain through the constant-head cells at this boundary and stopping this flow resulted in water-level mounding along the Santa Rita Mountains. Additionally, concurrent Open Pit dewatering in the lower model layers likely created numerical problems that could not be resolved.

9.3.2 General Head Boundary

The western model boundary was also simulated as a GHB to determine the influence of the constant-head boundary assumption on drawdown propagation. The GHB cells were assigned the same hydraulic head value as the constant-head cells. The conductance of the GHB cells was calculated by the formula:

$$\text{Conductance} = (\text{hydraulic conductivity} \times \text{cell width} \times \text{saturated thickness}) / (\text{distance to boundary})$$

The hydraulic conductivity assigned to the GHB cells was the hydraulic conductivity of the HGUs present along the western boundary. The boundary distance was assigned 2,640 feet or ½-mile west of the model boundary. This was equivalent to moving the western model boundary ½-mile to the west. If the proximity of the western model boundary to the Open Pit was significantly influencing the simulation and predictions, moving the boundary to the west would produce significantly different drawdown and western boundary fluxes. Conversely, minor changes in the drawdown and boundary fluxes would indicate that the boundary location was not significantly influencing the simulation results.

Simulating the western model boundary as a GHB resulted in a good match to the steady-state model calibration targets. The SOSWR increased by only 2.6 percent indicating a minor effect on the calibration statistics. The mining-phase and post-closure simulated drawdown contours shown on Figures 9-7, 9-8, and 9-9 are quite similar to those produced using the constant-head boundary. In the post-closure GHB simulation, the maximum drawdown propagation to the east was less than 0.1 miles and approximately 0.4 miles in Davidson Canyon. Drawdown contours at 150 years and 1,000 years propagated some distance past the western edge of the model, whereas in the constant-head simulation the drawdown contours were near the model boundary.

The significance of the drawdown contours propagating past the western boundary were evaluated by comparing groundwater inflow and outflow from both the GHB and constant-head boundaries for each simulation. None of the simulations indicated flow into the model along the western boundary with either the constant-head or GHB configurations. The GHB simulations indicated that outflow from the model decreased 0.04 percent during the 22-year operational period and decreased by 2.1 percent during the 1,000-year post-closure period relative to the simulation without the Open Pit. These small decreases in outflow were very similar to outflows simulated using the constant-head boundary. Outflow through the western model boundary during the mining-phase and post-closure period decreased by 0.13 percent and 2.2 percent, respectively, using the constant-head boundary relative to the no-pit simulation.

These sensitivity simulations indicated that drawdown propagation to the east and outflows to the west were not sensitive to whether the western boundary was simulated as a constant-head boundary or as a GHB. Additionally, the low permeability pCb HGU located west of the Open Pit, which forms the core of the Santa Rita Mountains, is a significant barrier to westerly groundwater flow.

9.4 Mining-Phase Sensitivities

The mining-phase sensitivity analyses simulated the change in drawdown, ET, and stream flows in Davidson Canyon and Cienega Creek. Values of K_{xy} (horizontal hydraulic conductivity), K_z (vertical hydraulic conductivity), S_s (specific storage), and S_y (specific yield) were increased and decreased from the values used in the predictive mining-phase model as shown in Table 9-4.

Table 9-4 Sensitivity Analysis Parameter Changes for the Mining-Phase Simulation

| Parameter | Property | Change |
|------------|---|--------------------------|
| Basin-Fill | Horizontal Hydraulic Conductivity, K_{xy} | ± 30 percent |
| Bedrock | Horizontal Hydraulic Conductivity, K_{xy} | -10 percent; +30 percent |
| Basin-Fill | Vertical Hydraulic Conductivity, K_z | ± 30 percent |
| Bedrock | Vertical Hydraulic Conductivity, K_z | -10 percent; +30 percent |
| HFB | Hydraulic Conductivity, K | ± Order of magnitude |
| All HGUs | Specific Storage, S_s | ± Order of magnitude |
| Basin-Fill | Specific Yield, S_y | ± 50 percent |
| Bedrock | Specific Yield, S_y | ± Factor of 2 |

The mining-phase model simulated 22 years of operations, and the pit advance was simulated in 12 steps of one (1) to two (2) years each. Results of the mining-phase sensitivity simulations are presented on Figures 9-10 to 9-26. Drawdown resulting from changing the parameter values in the predictive mining-phase model is also presented on these figures. There were no simulated changes in Davidson Canyon and Cienega Creek stream flows at the end of operations since drawdown had not propagated to these areas.

As previously indicated the groundwater flow model was constructed with horizontal, uniform thickness layers. Maximum drawdown extent and magnitude generally occurred in Model Layer 17, which was active across the entire model domain. Therefore, drawdown contours and comparisons between simulations were based on Model Layer 17 results.

9.4.1 Basin-Fill Horizontal Hydraulic Conductivity (K_{xy})

At the end of operations, drawdown in the predictive mining-phase model had not yet reached the quartz-porphry dike in Davidson Canyon. A 30-percent decrease in K_{xy} for all basin-fill units resulted in drawdown expanding to the northeast an additional 1,600 feet and reaching the dike (Figure 9-10). Drawdown propagation was minimal in the other directions due to this decrease. A 30-percent increase in basin-fill K_{xy} resulted in a 1,200-foot decrease in the drawdown extent to the northeast (Figure 9-11). These results indicated that drawdown was not sensitive to basin-fill K_{xy} . This was due largely to the limited extent of the basin-fill units in the higher elevation areas.

9.4.2 Bedrock Horizontal Hydraulic Conductivity (K_{xy})

The K_{xy} for all bedrock units was increased by 30-percent and decreased by ten (10)-percent for the sensitivity simulations. A 30-percent decrease in bedrock K_{xy} resulted in the mining-phase model being unable to converge to a stable solution. This indicated that the bedrock K_{xy} was a relatively sensitivity parameter in the mining-phase simulation. A ten (10)-percent decrease in bedrock K_{xy} resulted in virtually no change in drawdown propagation (Figure 9-12), but a 30-percent increase resulted in drawdown expansion in all directions (Figure 9-13). The greatest expansion was to the northeast into Davidson Canyon where drawdown was approximately 1,600 feet further than that simulated without the 30-percent increase. Drawdown expanded less than 1,000-feet in the other directions.

9.4.3 Basin-Fill Vertical Hydraulic Conductivity (K_z)

A 30-percent change in the K_z for all basin-fill units resulted in minor changes to the drawdown extent. The 30-percent decrease in K_z resulted in drawdown expanding approximately 500 feet to the northeast and southeast (Figure 9-14). The drawdown extent decreased less than 500 feet when the basin-fill K_z was increased by 30-percent (Figure 9-15).

9.4.4 Bedrock Vertical Hydraulic Conductivity (K_z)

The ten (10)-percent decrease and 30-percent increase in the K_z for all bedrock units resulted in minor changes to the drawdown extent (Figures 9-16 and 9-17). This indicated that the mining-phase model was not sensitive to the bedrock K_z at these parameter values. The mining-phase model would not converge when the bedrock K_z was decreased by 30-percent, indicating that the model was sensitive to lower bedrock K_z values.

9.4.5 Quartz-Porphry Dike Hydraulic Conductivity (K)

The hydraulic conductivity (K) of the quartz-porphry dike HFB was increased and decreased by an order of magnitude. An order of magnitude decrease in K resulted in drawdown propagation increasing approximately 1,300 feet to the northeast and expanding to and along the quartz-porphry dike (Figure 9-18). An order of magnitude increase in K resulted in drawdown receding approximately 0.5 miles in the Davidson Canyon area (Figure 9-19). These results indicated that drawdown propagation in the Davidson Canyon area was sensitive to the hydraulic conductivity of the quartz-porphry dike HFB.

9.4.6 Storage Parameters (S_s and S_y)

Specific storage (S_s) was changed in the sensitivity analysis by an order of magnitude and specific yield (S_y) was changed by either 50-percent or by a factor of two (2). Drawdown propagation was sensitive to each of these changes as shown on Figures 9-20 through 9-25. In these simulations, specific storage was changed for all units (basin-fill and bedrock) simultaneously. Specific yield was also changed for all basin-fill units simultaneously and then for all bedrock units simultaneously.

The time to reach equilibrium, or steady-state conditions, depended on the hydraulic diffusivity (transmissivity divided by storativity) of the aquifer and the distance from the point of measurement to the Open Pit. The relatively low bedrock transmissivity required hundreds of years to reach equilibrium. A decrease in storativity resulted in a relative increase in aquifer diffusivity, so drawdown propagated faster in sensitivity simulations having lower storage values.

An order of magnitude decrease in specific storage resulted in an expansion of drawdown in all directions by the end of operations (Figure 9-20). Drawdown reached and expanded along the quartz-porphry dike to the northeast and expanded 0.25 to 0.5 miles in the other directions. Conversely, increasing specific storage by an order of magnitude resulted in the drawdown extent decreasing approximately one (1) to three (3) miles (Figure 9-21).

The specific-storage estimates obtained from radial flow modeling ranged from 7×10^{-7} to 4.0×10^{-3} per foot, with a geometric mean of 9.84×10^{-6} per foot. The specific storage (9.84×10^{-6} per foot) estimate was used for all bedrock units in the mining-phase simulation. This range of specific-storage estimates indicated that higher values were possible in the Project area and that the simulated value was a relatively low estimate. The extent and magnitude of drawdown

would be over predicted in the mining-phase simulation if the simulated specific storage was lower than the effective bedrock properties.

Decreasing the specific yield of the basin-fill by 50-percent resulted in an expansion of drawdown to the northeast and southeast (Figure 9-22). An increase in the specific yield by 50-percent resulted in less propagation of drawdown (Figure 9-23). At the end of operations, the model was less sensitive to an increase in specific yield of the basin-fill than it was to a decrease.

At the end of operations, the model was also more sensitive to changes in specific yield of the bedrock units than it was to the basin-fill units. This was due to the limited amount of basin-fill units within the drawdown area. A decrease by a factor of two (2) in the bedrock's specific yield resulted in drawdown reaching and expanding along the quartz-porphyry dike (Figure 9-24). Drawdown also expanded approximately one (1) mile to the north due to the mountains consisting entirely of bedrock units. Increasing bedrock specific yield by a factor of two (2) resulted in less drawdown propagation towards Davidson Canyon and to the north (Figure 9-25). Changes in the bedrock specific yield resulted in less change to the drawdown extent to the southeast where there are near surface basin-fill units.

9.5 Post-Closure Sensitivities

The post-closure groundwater flow model simulated conditions from the end of dewatering to 1,000 years into the future. During this time, a lake is predicted to form in the Open Pit. Drawdown and changes to stream flows and ET depend, in part, on the lake stage and groundwater inflows. At 1,000 years post-closure, the groundwater system was considered to be in a steady-state condition since there was essentially no change in aquifer storage (Table 8-3) and pit-lake conditions had been stable since 700 years post-closure. Therefore, the maximum impacts were realized by the end of the 1,000-year post-closure simulation. The 1,000-year simulation was also compared to drawdown predicted at 1,500 years post-closure, and the extent of drawdown was essentially the same (Figure 9-26).

The sensitivity analysis simulated the changes due to variations in K_{xy} , K_z , S_s , S_y , pit-lake precipitation, evaporation, and pit-wall runoff (Table 9-5). Results of the post-closure sensitivity simulations are discussed in the following subsections. Drawdown, pit-lake groundwater inflows, and pit-lake stage at 150 years and at 1,000 years are presented. Simulated changes in Davidson Canyon and Cienega Creek stream flows and ET at 1,000 years are also presented for select simulations.

Table 9-5 Post-Closure Sensitivity Analysis Simulations

| Parameter | Property | Change |
|------------|--|---------------------------|
| Pit Lake | Precipitation | ± 30 percent |
| Pit Lake | Evaporation | ± 20 percent |
| Pit Lake | Pit Runoff | 20 percent; 40 percent |
| HFB | Hydraulic Conductivity, K | ± Order of magnitude |
| All HGUs | Specific Storage, S _s | ± Order of magnitude |
| Basin Fill | Specific Yield, S _y | ± 50 percent |
| Bedrock | Specific Yield, S _y | ± Factor of 2 |
| Basin Fill | Horizontal Hydraulic Conductivity, K _{xy} | ± 30 percent |
| Bedrock | Horizontal Hydraulic Conductivity, K _{xy} | -10 percent; +30 percent |
| Basin Fill | Vertical Hydraulic Conductivity, K _z | ± 30 percent |
| Bedrock | Vertical Hydraulic Conductivity, K _z | -10 percent; 30 percent |
| Recharge | Steady state distribution | Steady state distribution |

As previously indicated, the groundwater flow model was constructed with horizontal, uniform thickness layers. Maximum drawdown extent and magnitude generally occurred in Model Layer 17, which was active across the entire model domain. Therefore, drawdown contours and comparisons between simulations used Model Layer 17 results.

In the predictive post-closure simulation, drawdown expanded relative to the predictive mining-phase simulation (Figure 9-27). Drawdown also propagated to the quartz-porphry dike and elongated in the north-south direction after 150 years. Drawdown also approached the western model boundary (Figure 9-27). After 1,000 years, the five (5)-foot drawdown contour propagated one (1) to 1.75 miles past the quartz-porphry dike. At this time, the five (5)-foot drawdown contour was over six (6) miles from the perennial reaches in Davidson Canyon (Figure 9-27) and was two (2) to three (3) miles from the upper perennial reaches of Cienega Creek.

In general, sensitivity simulations that increased the lake stage relative to the predictive post-closure simulation caused groundwater inflow to decrease, which decreased drawdown propagation and long-term groundwater capture. A simulated decrease in the lake stage had the opposite effect. The lake stage rose with an increase in precipitation or pit-wall runoff and decreased with an increase in evaporation.

9.5.1 Pit-Lake Sensitivity Analysis

Lake stage and groundwater inflows at 150 years and 1,000 years are provided for the pit-lake parameter sensitivity analysis. Conceptually, the maximum possible impact to Davidson Canyon, Cienega Creek, and regional springs within the zone of influence would be based on the simulated post-closure, steady-state groundwater inflow to the pit. Drawdown associated with the pit-lake will continue to expand outwards until there is sufficient capture of water from other areas to create a new stable water table. This rate of water capture is equal to the steady-state groundwater inflow to the terminal pit-lake, which was predicted to be approximately 230 gpm.

The pit-lake parameter sensitivity analysis illustrated how changes in precipitation, evaporation, and pit-wall runoff affected the groundwater inflows and capture. The lake-package inputs for the sensitivity analysis are provided in Table 9-6. Lake stage and groundwater inflow for the sensitivity analyses are provided in Table 9-7. Evaluation of the lake stage was important since a flow-through pit-lake would occur if the lake stage reached an elevation of approximately 4,680 feet amsl. Lake stages less than 4,680 feet amsl are expected to result in a terminal hydraulic sink.

Table 9-6 Pit-Lake Parameter Values used in the Sensitivity Analysis

| Parameter | Post-Closure Model | Precipitation Increase 30-Percent | Precipitation Decrease 30-Percent | Evaporation Increase 20-Percent | Evaporation Decrease 20-Percent | Pit-Wall Runoff 40-Percent | Pit-Wall Runoff 20-Percent |
|-----------------------------|--------------------|-----------------------------------|-----------------------------------|---------------------------------|---------------------------------|----------------------------|----------------------------|
| Pan Evaporation (in/yr) | 71.52 | 71.52 | 71.52 | 85.82 | 57.22 | 71.52 | 71.52 |
| Lake Evaporation (in/yr) | 50.06 | 50.06 | 50.06 | 60.08 | 40.05 | 50.06 | 50.06 |
| Precipitation (in/yr) | 17.37 | 22.58 | 12.16 | 17.37 | 17.37 | 17.37 | 17.37 |
| Pit-Wall Runoff (in/yr) | 5.21 | 6.77 | 3.65 | 5.21 | 5.21 | 6.95 | 3.47 |
| Lake Precipitation (in/yr) | 12.16 | 15.81 | 8.51 | 12.16 | 12.16 | 10.43 | 13.90 |
| Pit-Wall Catchment (acres) | 201.6 | 201.6 | 201.6 | 201.6 | 201.6 | 201.6 | 201.6 |
| Pit-Wall Runoff Coefficient | 0.3 | 0.3 | 0.3 | 0.3 | 0.3 | 0.4 | 0.2 |
| Pan Evaporation Coefficient | 0.7 | 0.7 | 0.7 | 0.7 | 0.7 | 0.7 | 0.7 |

Table 9-7 Simulated Pit-Lake Stage and Groundwater Inflow Resulting from Pit-Lake Parameter Sensitivity Analysis

| Parameter | Post-Closure Model | | Pit-Lake Evaporation Decrease 20-Percent | | Pit-Lake Evaporation Increase 20-Percent | |
|--------------------------|--------------------|-------|--|-------|--|-------|
| Post-closure (years) | 150 | 1,000 | 150 | 1,000 | 150 | 1,000 |
| Lake Stage* (feet amsl) | 4,093 | 4,279 | 4,154 | 4,429 | 4,035 | 4,150 |
| Groundwater Inflow (gpm) | 259 | 230 | 252 | 196 | 265 | 248 |

*Pit-lake flow-through elevation is approximately 4,680 feet amsl

Table 9-7 Simulated Pit-Lake Stage and Groundwater Inflow Resulting from Pit-Lake Parameter Sensitivity Analysis (continued)

| Parameter | Pit-Wall Runoff Coefficient 20-Percent | | Pit-Wall Runoff Coefficient 40-Percent | | Pit-Lake Precipitation Decrease 30-Percent | | Pit-Lake Precipitation Increase 30-Percent | |
|--------------------------|--|-------|--|-------|--|-------|--|-------|
| | 150 | 1,000 | 150 | 1,000 | 150 | 1,000 | 150 | 1,000 |
| Post-closure (years) | 150 | 1,000 | 150 | 1,000 | 150 | 1,000 | 150 | 1,000 |
| Lake Stage* (feet amsl) | 4,039 | 4,232 | 4,141 | 4,344 | 4,012 | 4,150 | 4,166 | 4,392 |
| Groundwater Inflow (gpm) | 264 | 239 | 253 | 218 | 266 | 248 | 251 | 208 |

*Pit-lake flow-through elevation is approximately 4,680 feet amsl

Changes in stream flows at 1,000 years post-closure were also evaluated as part of the sensitivity analysis. Stream flows in the post-closure model were subtracted from the sensitivity simulation stream flows to determine the change due to parameter variation. Simulated changes in stream flow of 0.02 cfs were considered within the model error.

The following subsections present changes to the post-closure model based on specific parameter values varied during the sensitivity analysis.

9.5.1.1 Pit-Lake Precipitation

Direct precipitation on the pit-lake was varied by 30-percent from the post-closure model rate of 17.37 inches/year. An increase or decrease in precipitation had minimal effect on the five (5)-foot contour after 150 years, but there was considerable change after 1,000 years (Figures 9-28 to 9-31). The decrease in precipitation resulted in drawdown propagating 0.5 miles in Davidson Canyon after 1,000 years and less propagation in the other directions. The increase in precipitation resulted in the five (5)-foot drawdown contour receding approximately one (1) mile in Davidson Canyon. The ten (10)-foot and 100-foot contours also receded significantly (Figure 9-30) due to increased precipitation. These changes in drawdown propagation were due to changes in the lake stage.

The lake stage varied between 4,012 and 4,392 feet amsl due to the change in precipitation (Table 9-7). Terminal pit-lake conditions were still predicted for the 30-percent change (increase and decrease) in precipitation. Based on the predicted groundwater elevation east of the pit after 1,000 years, the lake stage would have to rise an additional 288 feet before a flow through condition would exist under this precipitation condition. The groundwater divide east of the Open Pit is estimated to be at an elevation of 4,680 feet amsl. Groundwater inflows varied from 208 to 266 gpm (Table 9-7) based on a 30-percent increase and a 30-percent decrease in precipitation, respectively.

A 30-percent decrease in pit-lake precipitation resulted in a 0.01 cfs decrease in stream flows in Cienega Creek and no change in Davidson Canyon (Table 9-8). Increasing precipitation resulted in a 0.01 to 0.02 cfs increase in upper Cienega Creek stream flows and no change in lower Cienega or Davidson Canyon.

Simulated ET was not sensitive to changes in pit-lake precipitation. There was less than a 0.1-percent change in ET resulting from the 30-percent change in precipitation (Table 9-9).

**Table 9-8 Cumulative Change in Stream Flow for Pit-Lake
Parameter Sensitivity Simulations**

| Stream Segment | Cumulative Change in Post-Closure (1,000 yrs) Relative to Pre-Mining Model | | Pit-Lake Evaporation | | | |
|----------------|--|-----------------------|----------------------|-----------------------|---------------------|-----------------------|
| | | | Decrease 20 Percent | | Increase 20 Percent | |
| | Cienega Creek (cfs) | Davidson Canyon (cfs) | Cienega Creek (cfs) | Davidson Canyon (cfs) | Cienega Creek (cfs) | Davidson Canyon (cfs) |
| 1 | -0.02 | | 0.01 | | 0.00 | |
| 2 | -0.05 | | 0.01 | | -0.01 | |
| 3 | -0.06 | | 0.02 | | -0.01 | |
| 4 | -0.08 | | 0.02 | | -0.01 | |
| 5 | -0.08 | | 0.02 | | -0.01 | |
| 6 | -0.08 | | 0.02 | | -0.01 | |
| 7 | -0.08 | | 0.02 | | -0.01 | |
| 8 | -0.08 | | 0.02 | | -0.01 | |
| 9 | -0.08 | | 0.02 | | -0.01 | |
| 10 | -0.09 | | 0.02 | | -0.01 | |
| 11 | | -0.01 | | 0.00 | | 0.00 |
| 12 | | -0.01 | | 0.01 | | 0.00 |
| 13 | | -0.01 | | 0.01 | | 0.00 |
| 14 | | -0.01 | | 0.01 | | 0.00 |
| 15 | | -0.01 | | 0.01 | | 0.00 |
| 16 | | 0.00 | | 0.00 | | 0.00 |
| 17 | -0.09 | | 0.03 | | -0.01 | |

**Table 9-8 Cumulative Change in Stream Flow for Pit-Lake
Parameter Sensitivity Simulations (continued)**

| Stream Segment | Pit-Wall Runoff | | | | Pit-Lake Precipitation | | | |
|----------------|----------------------------------|-----------------|----------------------------------|-----------------|------------------------|-----------------|---------------------|-----------------|
| | Decrease 10 Percent ¹ | | Increase 10 Percent ² | | Decrease 30 Percent | | Increase 30 Percent | |
| | Cienega Creek | Davidson Canyon | Cienega Creek | Davidson Canyon | Cienega Creek | Davidson Canyon | Cienega Creek | Davidson Canyon |
| 1 | 0.00 | | 0.00 | | 0.00 | | 0.00 | |
| 2 | 0.00 | | 0.01 | | -0.01 | | 0.01 | |
| 3 | -0.01 | | 0.01 | | -0.01 | | 0.01 | |
| 4 | -0.01 | | 0.01 | | -0.01 | | 0.02 | |
| 5 | -0.01 | | 0.01 | | -0.01 | | 0.02 | |
| 6 | -0.01 | | 0.01 | | -0.01 | | 0.02 | |
| 7 | -0.01 | | 0.01 | | -0.01 | | 0.02 | |
| 8 | -0.01 | | 0.01 | | -0.01 | | 0.02 | |
| 9 | -0.01 | | 0.01 | | -0.01 | | 0.02 | |
| 10 | -0.01 | | 0.01 | | -0.01 | | 0.02 | |
| 11 | | 0.00 | | 0.00 | | 0.00 | | 0.00 |
| 12 | | 0.00 | | 0.00 | | 0.00 | | 0.00 |
| 13 | | 0.00 | | 0.00 | | 0.00 | | 0.00 |
| 14 | | 0.00 | | 0.00 | | 0.00 | | 0.00 |
| 15 | | 0.00 | | 0.00 | | 0.00 | | 0.00 |
| 16 | | 0.00 | | 0.00 | | 0.00 | | 0.00 |
| 17 | -0.01 | | 0.01 | | -0.01 | | 0.02 | |

¹ Runoff coefficient = 20 percent

² Runoff coefficient = 40 percent

**Table 9-9 Simulated Change in Evapotranspiration Resulting from
Pit-Lake Sensitivity Analysis**

| Simulation | Evapo- transpiration | Difference from Post-Closure Model | |
|-------------------------------|-------------------------|------------------------------------|---------|
| | ac-ft/yr | ac-ft/yr | Percent |
| Post-Closure | 5,618.8 | -- | -- |
| Evaporation -20 Percent | 5,624.6 | -5.8 | -0.10 |
| Evaporation +20 Percent | 5,615.8 | 3.0 | 0.05 |
| Precipitation -30 Percent | 5,615.8 | 3.1 | 0.05 |
| Precipitation +30 Percent | 5,623.0 | -4.2 | -0.07 |
| Runoff Coefficient 20 Percent | 5,617.1 | 1.7 | 0.03 |
| Runoff Coefficient 40 Percent | 5,621.1 | -2.2 | -0.04 |

9.5.1.2 Pit-Lake Evaporation

Similar to the precipitation sensitivity simulations, drawdown was not sensitive to evaporation changes after 150 years. Substantial changes, however, were apparent after 1,000 years (Figures 9-32 to 9-35). A 20-percent decrease in evaporation resulted in the five (5)-foot drawdown contour retreating 0.5 to 1.5 miles after 1,000 years (Figure 9-33). The ten (10)-foot drawdown contour retreated approximately three (3) miles in the upper part of Davidson Canyon. A 20-percent increase in evaporation resulted in the five (5)-foot drawdown contour propagating an additional 0.5 miles into Davidson Canyon and approximately 0.25 miles to the southeast after 1,000 years (Figure 9-35).

The lake stage varied between 4,035 and 4,429 feet amsl due to the change in evaporation (Table 9-7). A terminal pit-lake condition was therefore still predicted for a 20-percent change (increase and decrease) in evaporation. Based on the predicted groundwater elevations east of the pit after 1,000 years, the lake stage would have to rise an additional 250 feet before a flow through condition would exist. Groundwater inflows varied from 196 to 265 gpm (Table 9-7) based on a 20-percent decrease and a 30-percent increase in evaporation, respectively.

A 20-percent decrease in pit-lake evaporation resulted in a 0.01 to 0.02 cfs increase in Cienega Creek stream flows and a 0.01 cfs increase in most segments of Davidson Canyon (Table 9-8). An increase in evaporation resulted in a 0.01 cfs decrease in stream flows in Cienega Creek and no change in Davidson Canyon. These small changes in stream flow were close to the model error. Therefore, these simulations predicted little to no impact on stream flows due to a 20-percent change in evaporation.

Simulated ET was not sensitive to changes in pit-lake evaporation. There was a 0.1-percent change in ET resulting from the 20-percent change in evaporation (Table 9-9).

9.5.1.3 Pit-Wall Runoff

The post-closure model simulated pit-wall runoff with a 30-percent of precipitation coefficient. The sensitivity analysis used 20- and 40-percent coefficients, which resulted in less runoff inflow and more runoff inflow than the predictive post-closure model. Drawdown predictions at 150 years had minimal changes relative to the predictive post-closure model and changes of less than 0.5 miles after 1,000 years (Figures 9-36 to 9-39). The pit-lake water balance was less sensitive to changes in pit-wall runoff than it was to changes in evaporation.

The pit-lake stage varied between 4,039 and 4,344 feet amsl due to changes in the pit-wall runoff coefficient (Table 9-7). A terminal pit-lake condition was therefore still predicted for a ten (10)-percent change (increase and decrease) in the pit-wall runoff coefficient. Based on the predicted groundwater elevations east of the pit after 1,000 years, the lake stage would have to rise an additional 336 feet before a flow through condition would exist. Groundwater inflows varied from 218 to 264 gpm (Table 9-7) based on a 10-percent increase and a 10-percent decrease in pit-wall runoff, respectively.

A pit-wall runoff coefficient of 20-percent resulted in a 0.01 cfs decrease in Cienega Creek stream flows and no change in Davidson Canyon (Table 9-8). A pit-wall runoff coefficient of 40-percent resulted in a 0.01 cfs increase in stream flows in Cienega Creek and no change in Davidson Canyon.

Simulated ET was not sensitive to changes in the pit-lake runoff coefficient. There was a minimal 0.04-percent change in ET resulting from the ten (10)-percent change in the runoff coefficient (Table 9-9).

9.5.2 Basin-Fill Horizontal Hydraulic Conductivity (K_{xy})

A 30-percent decrease in basin-fill K_{xy} resulted in drawdown propagation to the northeast after 150 years and propagation of approximately 0.35 miles in all directions after 1,000 years (Figures 9-40 and 9-41). The 30-percent increase in basin-fill K_{xy} resulted in drawdown receding about 1,300 feet at 150 years and about 2,400 feet at 1,000 years in Davidson Canyon (Figures 9-42 and 9-43).

9.5.3 Bedrock Horizontal Hydraulic Conductivity (K_{xy})

The groundwater flow model would not converge with a 30-percent decrease in bedrock K_{xy} . A ten (10)-percent decrease in bedrock K_{xy} , however, resulted in no change in drawdown at 150 years (Figure 9-44) and a slight increase in drawdown after 1,000 years (Figure 9-45). A 30-percent increase in bedrock K_{xy} resulted in drawdown receding slightly at 150 years (Figure 9-46) and about 4,000 feet at 1,000 years in Davidson Canyon (Figure 9-47).

9.5.4 Basin-Fill Vertical Hydraulic Conductivity (K_z)

A 30-percent decrease in basin-fill K_z (Figures 9-48 and 9-49) and a 30-percent increase (Figures 9-50 and 9-51) resulted in no change in drawdown extent at 150 years and 1,000 years. Therefore, the post-closure model was not sensitive to changes in basin-fill K_z .

9.5.5 Bedrock Vertical Hydraulic Conductivity (K_z)

The post-closure model would not converge with a 30-percent decrease in bedrock K_z . A ten (10)-percent decrease in bedrock K_z , however, resulted in very little change in drawdown at 150 years and 1,000 years (Figures 9-52 and 9-53). A 30-percent increase in bedrock K_z resulted in drawdown propagating slightly at 150 years (Figure 9-54) and 1,000 years (Figure 9-55).

9.5.6 Quartz-Porphry Dike Hydraulic Conductivity (K)

Decreasing the quartz-porphry dike hydraulic conductivity (K) by an order of magnitude caused the drawdown to propagate laterally along the quartz-porphry dike at 150 years (Figure 9-56). After 1,000 years, the drawdown receded approximately one (1) mile in Davidson Canyon (Figure 9-57). Increasing the hydraulic conductivity by an order of magnitude caused the five (5)-foot drawdown contour to propagate to the down-gradient side of the quartz-porphry dike at 150 years (Figure 9-58). The ten (10)-foot drawdown contour, however, receded approximately one (1) mile at 150 years. After 1,000 years, the five (5)-foot contour propagated less than 0.5 miles in Davidson Canyon and the ten (10)-foot contour had reached the quartz-porphry dike (Figure 9-59). The five (5)-foot drawdown contour was approximately six (6) miles from the perennial stream reach in Davidson Canyon at 1,000 years.

9.5.7 Storage Parameters (S_s and S_y)

Although specific storage (S_s) and specific yield (S_y) are sensitive parameters in predictive models, their influence on drawdown propagation decreases as the groundwater system approaches steady-state conditions.

The post-closure model was most sensitive to changes in storage values over the first 100 to 200 years. Following the cessation of dewatering, the groundwater system near the Open Pit recovered during this time even as drawdown continued to propagate away from the pit. As the

groundwater system approached steady-state conditions after 700 years, the influence of aquifer storage greatly diminished.

An order of magnitude decrease in specific storage for all HGUs resulted in drawdown propagation of approximately 0.25 miles after 150 years (Figure 9-60). However, after 1,000 years the drawdown extent was virtually the same as in the predictive post-closure model (Figure 9-61).

An order of magnitude increase in specific storage for all HGUs resulted in drawdown receding from two (2) miles to over three (3) miles after 150 years (Figure 9-62). After 1,000 years, the drawdown extent was at least 0.25 miles less than the predictive post-closure model (Figure 9-63). Therefore, simulating higher aquifer specific storage than those used in the predictive post-closure model resulted in significantly less drawdown after 150 years. Additionally, the lower aquifer diffusivity resulted in drawdown propagation being slower than predicted. However, the post-closure, steady-state conditions predicted after 1,000 years were not significantly different.

The specific storage sensitivity results indicated that the predictive post-closure model had a relatively low specific storage value that approached an upper limit for drawdown propagation. Drawdown propagation increases with decreasing S_s since there is less water available in storage. The extent and magnitude of drawdown is therefore over predicted if the simulated specific storage is lower than the effective aquifer storage.

Results of the sensitivity analysis on the specific yield parameters were similar to the specific storage simulations. The most significant changes in drawdown occurred in the 100- to 200-year range following the cessation of dewatering. Also, the influence of specific yield decreased as the groundwater system approached steady-state conditions. Specific yield was evaluated individually for the basin-fill HGUs and for the bedrock HGUs.

After 150 years, decreasing the basin-fill specific yield by 50-percent resulted in drawdown propagating an additional 0.5 miles in Davidson Canyon and less than one (1) mile to the southeast of the Open Pit (Figure 64). This change in specific yield did not modify the predicted drawdown extent after 1,000 years, when the groundwater system was predicted to be in a steady-state condition (Figure 9-65).

A 50-percent increase in the basin-fill specific yield resulted in drawdown receding over 0.5 miles to the southeast (Figure 9-66). The five (5)-foot contour did not change in Davidson Canyon, but the ten (10)-foot contour receded by over 0.5 miles after 150 years. After 1,000 years, the specific yield change did not change the predicted drawdown extent (Figure 9-67).

Decreasing the bedrock specific yield by a factor of two (2) resulted in drawdown propagating 0.5 to 0.75 miles after 150 years, but no change after 1,000 years (Figures 9-68 and 9-69). Increasing the bedrock specific yield by a factor of two (2) decreased the drawdown extent after 150 years, but no change after 1,000 years (Figures 9-70 and 9-71).

9.5.8 Facility Area Recharge

The distribution of recharge in the Project facilities area in the predictive post-closure model accounted for increased infiltration and ultimately recharge due to the flow-through drains, containment pond PCA-2, and dry stack tailings drain down. Infiltration due to the flow-through drains and pond PCA-2 was based on a Technical Memorandum titled *Rosemont Infiltration Analysis – Revised* (Tetra Tech, 2010c).

A sensitivity simulation was conducted to determine the drawdown extent, ET changes, and pit-lake predictions based on using a total recharge value of 9,900 ac-ft/yr versus 10,092 ac-ft/yr used in the predictive post-closure model. The recharge value of 9,900 ac-ft/yr was used in the

pre-mining steady-state simulation without the Open Pit. This value is 191.6 ac-ft/yr less than the recharge at the end of the predictive post-closure model.

Although the difference in total recharge was less than two (2)-percent, the post-closure model was sensitive to this change due to the location of the recharge. The 191.6 ac-ft/yr decrease in recharge near the Open Pit resulted in the simulated drawdown after 1,000 years propagating three (3) miles in Davidson Canyon and one (1) to 1.5 miles toward the upper reaches of Cienega Creek (Figures 9-72 and 9-73).

Based on the modified recharge of 9,900 ac-ft/yr, the lake stage was 23 feet lower and the groundwater inflows were ten (10) gpm less after 1,000 years than in the predictive post-closure model (Table 9-10). With higher recharge in the Project area, the post-closure simulation resulted in larger hydraulic gradients due to groundwater mounding and greater groundwater inflows even though the lake stage was higher than the 9,900 ac-ft/yr recharge simulation.

Stream flows decreased 0.02 to 0.11 cfs in some stream segments due to the modified recharge of 9,900 ac-ft/yr (Table 9-11, column C) as compared to the predictive post-closure model decreases of 0.02 to 0.09 cfs (Table 9.11, column B; using 10,092 ac-ft/yr recharge). Davidson Canyon stream flows decreased from 5.2- to 16.7-percent relative to the simulated pre-mining base flow while Cienega Creek stream flows decreased from 3.4- to 8.4-percent (Table 9-11, column E). Compared to the simulated pre-mining base flow (Table 9.11, column A; using 9,900 ac-ft/yr recharge), the predictive post-closure model showed decreases of 0.02 to 0.09 cfs (Table 9.11, column B) using the 10,092 ac-ft/yr recharge value.

In the steady-state, recharge sensitivity simulation (using 9,900 ac-ft/yr), ET decreased 23 ac-ft/yr or 0.4 percent relative to the post-closure model using the 10,092 ac-ft/yr recharge value.

Table 9-10 Simulated Change in Pit-Lake Stage and Groundwater Inflows Resulting from Recharge Sensitivity Analysis

| Parameter | Post-Closure Model (10,092 ac-ft/yr) | | Steady-State Recharge (9,900 ac-ft/yr) | |
|-----------------------------|---|-------|---|-------|
| | 150 | 1,000 | 150 | 1,000 |
| Post-closure (years) | 150 | 1,000 | 150 | 1,000 |
| Lake Stage (feet amsl) | 4,093 | 4,279 | 4,087 | 4,256 |
| Groundwater Inflow (gpm) | 258.9 | 230.2 | 249.5 | 220.0 |

Note: The pit-lake flow-through elevation is approximately 4,680 feet amsl.

Table 9-11 Cumulative Change in Stream Flow for Recharge Sensitivity Simulation

| Stream Segment | (A) Simulated Pre-Mining Stream Flows | | (B) Change in Post- Closure (1,000 yrs) Relative to Pre-Mining Model | | (C) Change in Steady-State Recharge Simulation (1,000 yrs) Relative to Post-Closure Model | | (D) Total Change for Steady-State Recharge Simulation (1,000 yrs) Relative to Pre-Mining Model | | (E) Percent Change for Steady- State Recharge Simulation (1,000 yrs) Relative to Pre-Mining Model | |
|----------------|---|-----------------------------|--|--|---|--|---|--|---|---------------------------------|
| | Cienega Creek (cfs) | Davidson Canyon (cfs) | Cienega Creek (cfs) ² | Davidson Canyon (cfs) ² | Cienega Creek (cfs) ² | Davidson Canyon (cfs) ² | Cienega Creek (cfs) ² | Davidson Canyon (cfs) ² | Cienega Creek (Percent) | Davidson Canyon (Percent) |
| 1 | 0.67 | | -0.02 | | -0.02 | | -0.04 | | -6.0 | |
| 2 | 1.92 | | -0.05 | | -0.05 | | -0.10 | | -5.2 | |
| 3 | 3.15 | | -0.06 | | -0.06 | | -0.13 | | -4.1 | |
| 4 | 3.71 | | -0.08 | | -0.08 | | -0.16 | | -4.3 | |
| 5 | 3.71 | | -0.08 | | -0.08 | | -0.16 | | -4.3 | |
| 6 | 3.8 | | -0.08 | | -0.08 | | -0.16 | | -4.2 | |
| 7 | 4.77 | | -0.08 | | -0.08 | | -0.17 | | -3.6 | |
| 8 | 4.95 | | -0.08 | | -0.08 | | -0.17 | | -3.4 | |
| 9 | 3.72 | | -0.08 | | -0.08 | | -0.17 | | -4.6 | |
| 10 | 2.15 | | -0.09 | | -0.10 | | -0.18 | | -8.4 | |
| 11 | | 0.22 | | -0.01 | | -0.01 | | -0.02 | | -9.1 |
| 12 | | 0.44 | | -0.01 | | -0.03 | | -0.04 | | -9.1 |
| 13 | | 0.65 | | -0.01 | | -0.03 | | -0.04 | | -6.2 |
| 14 | | 0.77 | | -0.01 | | -0.03 | | -0.04 | | -5.2 |
| 15 | | 0.67 | | -0.01 | | -0.03 | | -0.05 | | -7.5 |
| 16 | | 0.06 | | 0.00 | | -0.01 | | -0.01 | | -16.7 |
| 17 | 3.61 | | -0.09 | | -0.11 | | -0.20 | | -5.5 | |

¹ Change relative to simulated base flows in steady-state, pre-mining simulation.

² Cumulative change in stream flow.

9.6 Sensitivity Analysis Summary

An extensive sensitivity analysis was completed on the three (3) groundwater simulations. The pre-mining steady-state conditions, mining-phase conditions, and the post-closure conditions were evaluated for their sensitivity to model parameter value changes. Sensitivity analysis parameters included horizontal and vertical hydraulic conductivity, hydraulic conductivity of the quartz-porphphyry dike, specific storage, specific yield, and recharge. Additionally, parameters specific to the pit-lake development in the post-closure model were evaluated to determine the sensitivity to changes in precipitation within the pit catchment, evaporation, and pit-wall runoff. The sensitivity analysis yielded the following key conclusions:

- Aquifer storage parameters were highly sensitive over the first 200 years (Figures 9-62 through 9-71) and resulted in:
 - Drawdown propagating up to one (1) mile based on lower storage values;
 - Drawdown receding up to three (3) miles based on higher storage values; and
 - No significant affects to the model results were seen after 700 years based on modified storage values.
- Post-closure simulation with 20-percent decrease in evaporation resulted in:
 - Drawdown receding up to 1.3 miles (Figure 9-35); and
 - Rising water levels near stream channels (Figure 9-74).
- Post-closure simulation with decrease in pit-area recharge (191.6 ac-ft/yr) (Figures 9-72, 9-73, 9-75; Table 9-11) resulted in:
 - Cienega Creek flow decreasing 3.4 - 8.4 percent relative to simulated steady-state base flow;
 - Davidson Canyon flow decreasing 5.2 - 16.7 percent relative to simulated steady-state base flow;
 - ET decreasing 42 ac-ft/yr (0.7 percent) relative to the steady-state simulation; and
 - Drawdown propagation increasing up to three (3) miles in Davidson Canyon and up to 1.5 miles in upper Cienega Creek.
- Simulation of the Western Model Boundary sensitivity (Figures 9-7, 9-8, 9-9) resulted in the following:
 - Except for the no-flow scenario, water flowed out of the model domain through this boundary in all simulations at all times (i.e., heads in the domain were higher than the assigned boundary head values);
 - Using a no-flow boundary resulted in water levels above land surface and non-convergence; and
 - Virtually the same outflows and drawdown were predicted whether the boundary was simulated as a constant-head or as a general-head boundary.

The sensitivity analysis indicated that the final model parameter values were sufficiently understood and appropriate, which resulted in generally conservative impact predictions. The range of potential impacts to the regional groundwater flow system are relatively well constrained, as demonstrated by the range of presented pit inflows, drawdown, ET, and stream flows. Long-term simulation results were most sensitive to decreases in pit-lake evaporation and changes in recharge in the pit area due to stormwater infiltration.

10.0 DISCHARGE IMPACT AREA ANALYSIS

As part of this modeling study, a Discharge Impact Area (DIA) analysis was also completed. Arizona Administrative Code (A.A.C.) R18-9-A202(A)(8)(c)(viii),(xi), and (xii) requires a project applicant to provide an assessment of the potential for a discharge to cause the leaching of pollutants from surface soils or vadose materials, to develop a map of the DIA, and to discuss the criteria and methodologies used to determine the DIA.

As described in Arizona Revised Statutes (A.R.S.) §49-201, the DIA is the potential areal extent of pollutant migration, as projected on the land surface, resulting from a discharge from a facility. The boundary of the DIA is the point at which the pollutant, because of dilution, dispersion, adsorption, or degradation, reaches a level that is indistinguishable from ambient concentrations by standard test methods.

This report section documents the results of a particle tracking analysis for the mining-phase and post-closure models used to assess the DIA.

10.1 Analysis Approach

A step-wise approach was undertaken for analyzing and defining the DIA. The post-closure groundwater flow simulations predict that a pit-lake will form and will be a perpetual hydraulic sink. The capture zone of the pit was determined by using particle-tracking simulations. A capture zone that encompassed all of the Project facilities would ensure that any potential contaminant would flow into the terminal pit-lake. In this case, there would be no possible contaminant migration down-gradient of the facilities. However, if the capture zone was not shown to encompass all of the Project facilities, the potential would exist for contaminants to migrate down-gradient.

Should Project facilities fall outside the capture zone, a water quality comparison would be necessary between the potential Project-induced recharge water and down-gradient groundwater. If the potential existed to negatively impact groundwater quality, fate and transport modeling would then be used to predict the impacted area, or DIA.

10.2 Mine Facilities and Changes in Hydrogeologic Conditions

Dewatering of the Open Pit will lower groundwater levels in the pit area. When pit dewatering is discontinued after 22 years of active operations, the pit will naturally refill with groundwater, pit-wall runoff, and precipitation and a lake will form within the pit. High evaporation rates will create a terminal hydraulic sink, and surrounding groundwater will continually flow into the pit or pit-lake (Section 8.0). A groundwater divide will form due to the pit-lake level being lower than the surrounding water table. A “capture zone” will be created with groundwater inside this zone flowing into the pit and groundwater outside the zone flowing past or away from the pit.

Project operations will locally alter recharge to the groundwater system. Runoff generated up-gradient of the facilities will be channeled beneath the Waste Rock Storage Area and Dry Stack Tailings Facility in flow-through drains or detained in ponds adjacent to the upstream side of the Waste Rock Storage Area (Tetra Tech, 2010c). Recharge will occur in these ponding areas and in the flow-through drains. Other potential smaller-volume, Project-related recharge sources are described more completely in a Technical Memorandum titled *Potential Source Volumes and Chemical Makeup for Area-Wide Fate and Transport Modeling – Rosemont Copper Project* (Tetra Tech, 2010m). Potential recharge sources with flow rates greater than zero are listed in

Table 10.1 and shown on Figure 10-1. One of these sources is drain-down from the Dry Stack Tailings Facility (AMEC, 2009; Tetra Tech, 2010d).

Table 10-1 Potential Mining-Related Sources of Groundwater Recharge

| Source Name | Latitude (UTM NAD 83 Northing - ft) | Longitude (UTM NAD 83 Easting - ft) | Period of Recharge (Years) | Water Source | Rate |
|--|---|---|----------------------------------|------------------------|---------------------------|
| Dry Stack Tailings Facility | 31° 50' 18.52" (11,556,944.78) | 110° 43' 51.40" (1,723,940.74) | 1 - 500 | Drain-down | 13.56 ac-ft/yr maximum |
| Flow-Through Drains | 31° 50' 18.52" (11,556,944.78) | 110° 43' 51.40" (1,723,940.74) | Starting year 1, permanent | Runoff Infiltration | 273.5 ac-ft/yr |
| Process Water Temporary Storage Pond | 31° 50' 9.80" (11,556,056.78) | 110° 44' 27.39" (1,720,839.83) | 1 – 10 | Leakage | 0.00012 ac-ft/yr |
| Primary Settling Basin | 31° 50' 23.78" (11,557,468.36) | 110° 44' 28.51" (1,720,739.47) | 1 – 22 | Leakage | 0.0206 ac-ft/yr |
| Raffinate Pond | 31° 50' 15.09" (11,556,589.72) | 110° 44' 35.99" (1,720,096.29) | 1 – 10 | Leakage | 0.00012 ac-ft/yr |
| PLS Pond | 31° 49' 32.20" (11,552,261.31) | 110° 44' 12.44" (1,722,137.55) | 1 – 10 | Leakage | 0.00012 ac-ft/yr |
| Heap Leach Pad (Phase 1) ¹ | 31° 49' 23.93" (11,551,418.85) | 110° 44' 48.37" (1,719,041.03) | 1 – 10 | Leakage | 0.063 ac-ft/yr |
| Heap Leach Pad (Phase 2) ² | 31° 49' 23.93" (11,551,418.85) | 110° 44' 48.37" (1,719,041.03) | 11 – 115 | Drain-down | 16.14 ac-ft/yr maximum |
| Pond PCA-2 | 31° 48' 37.2661" (11,546,700) | 110 45' 15.6377" (1,716,700) | Starting year 1, permanent | Runoff Infiltration | 56.21 ac-ft/yr |

¹ Phase 1: Approximately seven (7) years of active leaching plus three (3) years of drain-down after cessation of leaching with leak-collection system and double-lined PLS pond in-place.

² Phase 2: Post-closure phase for the heap when it is covered with waste rock, undergoing drain-down, and liner has been removed from the PLS and Stormwater Ponds and drain-down seepage passes through treatment basins.

10.3 Particle-Tracking Simulations

Particle tracking was used to determine the extent of the pit-lake capture zone and whether Project induced recharge was predicted to flow away from the pit-lake and down-gradient of the facilities. Particle-tracking was completed on the mining-phase and post-closure groundwater flow models.

Particle-tracking was completed using the MODPATH code (Pollock, 1994) as modified by HydroGeoLogic (2010) to be compatible with MODFLOW-SURFACT. MODPATH uses the output from MODFLOW-SURFACT to compute 3D flow paths for imaginary “particles” of water moving through the simulated groundwater flow system. The cell-by-cell flows computed in MODFLOW-SURFACT during each time step of the model were used in MODPATH to calculate the movement of the particles within and between the finite-difference model grid cells for each time step of the simulation. The MODPATH output provided the path lines followed by each particle throughout the simulation.

10.3.1 Particle-Tracking Model Input Parameters

The aquifer property input parameters, starting heads, hydraulic stresses, and model stress periods used in the MODPATH-SURFACT simulations were left unchanged from those used in the MODFLOW-SURFACT models. MODPATH-SURFACT, however, required one (1) additional aquifer property, effective porosity, which was not necessary in the other flow model simulations.

Effective porosity affects the groundwater velocity and therefore the travel times of contaminants within the aquifer, but not the paths traveled by the contaminants. Effective porosities of the HGUs present within the model domain typically ranged from less than one (1) percent to a few percent for limestone and some metamorphic rocks, to as much as 40-percent for unconsolidated sediments (Walton, 1988; Weight and Sonderegger, 2001). An effective porosity of 0.01 (1 percent) was assigned as representative of the hydrogeologic units in the groundwater flow model. This relatively low effective porosity resulted in high groundwater velocities and long groundwater travel distances for the 1,000-year simulation period. These groundwater travel distances were considered an upper bound and the predicted distances traveled by the particles could be less if the effective porosity of the bedrock is greater than predicted.

10.3.2 Particle Starting Locations

The starting locations and starting times for each particle were provided as input to MODPATH-SURFACT. For this modeling task, it was necessary to track the particle paths through both the mining-phase and the post-closure periods. The initial particle starting locations were specified for the mining-phase model, and their final locations at the end of the mining-phase were imported as starting particle locations in the post-closure phase. The starting locations for the 61 particles assigned to the mining-phase model are listed in Table 10-2.

Table 10-2 Particle Starting Locations

| Particle No. | Model Layer | UTM Northing (ft) | UTM Easting (ft) | Particle No. | Model Layer | UTM Northing (ft) | UTM Easting (ft) |
|--------------|-------------|-------------------|------------------|--------------|-------------|-------------------|------------------|
| 1 | 4 | 11,546,713 | 1,716,629 | 32 | 5 | 11,557,152 | 1,721,771 |
| 2 | 4 | 11,549,877 | 1,716,064 | 33 | 5 | 11,557,352 | 1,722,342 |
| 3 | 4 | 11,549,500 | 1,716,875 | 34 | 5 | 11,557,552 | 1,722,914 |
| 4 | 4 | 11,549,123 | 1,717,687 | 35 | 5 | 11,557,752 | 1,723,485 |
| 5 | 4 | 11,548,746 | 1,718,498 | 36 | 5 | 11,557,951 | 1,724,056 |
| 6 | 4 | 11,548,369 | 1,719,309 | 37 | 5 | 11,558,151 | 1,724,627 |
| 7 | 4 | 11,547,992 | 1,720,120 | 38 | 5 | 11,558,351 | 1,725,199 |
| 8 | 4 | 11,547,615 | 1,720,931 | 39 | 5 | 11,558,551 | 1,725,770 |
| 9 | 4 | 11,547,238 | 1,721,743 | 40 | 5 | 11,558,751 | 1,726,341 |
| 10 | 4 | 11,546,861 | 1,722,554 | 41 | 5 | 11,558,951 | 1,726,912 |
| 11 | 4 | 11,546,484 | 1,723,365 | 42 | 6 | 11,559,157 | 1,720,846 |
| 12 | 5 | 11,554,016 | 1,719,792 | 43 | 6 | 11,559,302 | 1,721,414 |
| 13 | 5 | 11,553,813 | 1,720,297 | 44 | 6 | 11,559,448 | 1,721,982 |
| 14 | 5 | 11,553,610 | 1,720,803 | 45 | 6 | 11,559,594 | 1,722,551 |
| 15 | 5 | 11,553,407 | 1,721,308 | 46 | 6 | 11,559,739 | 1,723,119 |
| 16 | 5 | 11,553,204 | 1,721,814 | 47 | 6 | 11,559,885 | 1,723,688 |
| 17 | 5 | 11,553,002 | 1,722,319 | 48 | 6 | 11,560,031 | 1,724,256 |
| 18 | 5 | 11,552,799 | 1,722,825 | 49 | 6 | 11,560,176 | 1,724,824 |
| 19 | 5 | 11,552,596 | 1,723,331 | 50 | 6 | 11,560,322 | 1,725,393 |

Table 10-2 Particle Starting Locations (Continued)

| Particle No. | Model Layer | UTM Northing (ft) | UTM Easting (ft) | Particle No. | Model Layer | UTM Northing (ft) | UTM Easting (ft) |
|--------------|-------------|-------------------|------------------|--------------|-------------|-------------------|------------------|
| 20 | 5 | 11,552,393 | 1,723,836 | 51 | 6 | 11,560,468 | 1,725,961 |
| 21 | 5 | 11,552,190 | 1,724,342 | 52 | 5 | 11,550,314 | 1,721,488 |
| 22 | 5 | 11,555,764 | 1,721,154 | 53 | 5 | 11,550,177 | 1,721,805 |
| 23 | 5 | 11,555,572 | 1,721,748 | 54 | 5 | 11,550,040 | 1,722,122 |
| 24 | 5 | 11,555,381 | 1,722,342 | 55 | 5 | 11,549,903 | 1,722,439 |
| 25 | 5 | 11,555,189 | 1,722,936 | 56 | 5 | 11,549,765 | 1,722,757 |
| 26 | 5 | 11,554,998 | 1,723,531 | 57 | 5 | 11,549,628 | 1,723,074 |
| 27 | 5 | 11,554,807 | 1,724,125 | 58 | 5 | 11,549,491 | 1,723,391 |
| 28 | 5 | 11,554,615 | 1,724,719 | 59 | 5 | 11,549,354 | 1,723,708 |
| 29 | 5 | 11,554,424 | 1,725,313 | 60 | 5 | 11,549,217 | 1,724,025 |
| 30 | 5 | 11,554,233 | 1,725,907 | 61 | 5 | 11,549,080 | 1,724,342 |
| 31 | 5 | 11,554,041 | 1,726,501 | -- | -- | -- | -- |

The particles in the mining-phase simulation were placed in lines forming cross sections through the Waste Rock Storage Area and the Dry Stack Tailings Facility, where the potential recharge sources would be located. Due to Open Pit dewatering, the water table dropped below some model cells, which caused the cells to become inactive for the remainder of the particle-tracking simulation. Particles were therefore placed vertically in the uppermost cells that remained active throughout the simulations, either at the water table or at the top of the uppermost model layer that remained at least partially saturated throughout the mining-phase simulation. This resulted in some particles being placed below the initial, pre-mining water table, which was necessary to allow tracking of the movement of those particles throughout the simulation.

10.3.3 Particle Tracking Simulation Results

Particle-tracking simulation results are illustrated on Figures 10-2 and 10-3 and show the combined particle tracks for the mining-phase and post-closure simulations on a local scale (Figure 10-2) and on a regional scale (Figure 10-3). Figure 10-2 shows the locations of the various potential Project-related recharge sources listed in Table 10-1 and the boundary of the Open Pit's groundwater capture zone. Although the capture zone exists on all sides of the Open Pit, only the down-gradient side of the Open Pit, where the potential Project-related recharge sources are located, was relevant to the analysis.

The particle tracks and capture zone boundary were used to differentiate the Project-related recharge sources lying within the capture zone from those outside the capture zone. Recharge originating from sources within the capture zone will flow into the Open Pit or into the post-closure pit-lake. Therefore, these sources do not have the potential to impact groundwater quality outside the capture zone. Conversely, water originating from sources outside the capture zone could ultimately flow into areas beyond the Project site, and therefore may have the potential to affect groundwater quality.

The pit capture zone included all of the Project-related recharge sources except for portions of the Dry Stack Tailings Facility and portions of the flow-through drain system (Figure 10-2). The Process Water Temporary Storage (PWTS) Pond, Primary Settling Basin, Raffinate Pond, PLS Pond, Pond PCA-2, and Heap Leach Pad are completely contained within the pit capture zone, and any seepage water from those facilities will flow into the Open Pit or pit-lake. Therefore, only the portions of the Dry Stack Tailings Facility and the flow-through drain system lying

outside the pit capture zone will have the potential to affect down-gradient groundwater quality. The majority of the Waste Rock Storage Facility is also located within the anticipated capture zone. Regardless, no seepage is expected from the Waste Rock Storage Area under average annual climate conditions (Tetra Tech, 2010d).

Potential recharge entering the groundwater system from the Project facility area located outside the pit capture zone will generally travel to the north and northwest, down-gradient of the Project area (Figure 10-3). A slight spreading of the particle tracks north of the Project area is anticipated based on variations in aquifer properties and hydraulic gradients.

10.4 Groundwater Quality Evaluation

Particle-tracking simulation results indicate that groundwater beneath portions of the Dry Stack Tailings Facility, and from portions of the flow-through drain system, are expected to migrate off site. Groundwater samples collected within and immediately adjacent to the particle tracking area located outside of the capture zone were evaluated to determine background groundwater quality. Data were available for 50 groundwater-quality analyses collected from 11 wells and one (1) spring (M&A, 2009a). The locations of the wells and spring are shown on Figure 10-4. A summary of the analytical data is presented in Table 10-3.

Groundwater quality varies over the Project area and over the model domain. A statistical evaluation of the water-quality data within the predicted flow paths provided a representation of the natural variability. Understanding the natural water-quality variability formed the basis for subsequent evaluation of potential impacts. The standard deviation provided a measure of background water quality variability. The mean and the 95-percent upper confidence limit (95% UCL) on the mean provided a measure of the central tendency or representative water quality. Both the mean and 95% UCL fall within the range of expected natural groundwater quality variability.

Table 10-3 Summary of Background Groundwater Quality Data

| Parameter | Maximum | Minimum | Mean | Standard Deviation | 95-% UCL |
|--|---------|---------|--------|--------------------|----------|
| Calcium, mg/L | 130 | 7 | 63.7 | 33.63 | 73.0 |
| Magnesium, mg/L | 46.7 | 1.7 | 12.4 | 11.6 | 15.7 |
| Sodium, mg/L | 157 | 10 | 71.8 | 40.1 | 82.9 |
| Potassium, mg/L | 7.5 | 0.8 | 1.6 | 1.17 | 1.9 |
| Bicarbonate, mg/L | 10,361 | 109 | 277.6 | 139.3 | 316.2 |
| Carbonate, mg/L | 14.4 | 1 | 5.9 | 4.2 | 7.1 |
| Total Alkalinity as CaCO ₃ , mg/L | 840 | 90 | 231.7 | 113.7 | 263.2 |
| Chloride, mg/L | 57 | 3.7 | 19.4 | 13.2 | 23.1 |
| Sulfate, mg/L | 390 | 3 | 111.4 | 102.9 | 139.7 |
| Nitrate + Nitrite as Nitrogen, mg/L | 4.88 | 0.01 | 0.8 | 1.34 | 1.2 |
| Fluoride, mg/L | 1.5 | 0.2 | 0.6 | 0.36 | 0.7 |
| Hardness as CaCO ₃ , mg/L | 516.8 | 25 | 228.4 | 129.2 | 268.9 |
| Total Dissolved Solids, mg/L | 750 | 210 | 430.4 | 140.3 | 469.3 |
| pH (Lab) , std. units | 8.7 | 7.6 | 8.2 | 0.26 | 8.3 |
| Arsenic, mg/L | 0.028 | 0.0003 | 0.0073 | 0.009 | 0.0097 |
| Barium, mg/L | 0.116 | 0.008 | 0.060 | 0.029 | 0.068 |
| Molybdenum, mg/L | 0.090 | 0.004 | 0.023 | 0.026 | 0.030 |
| Selenium, mg/L | 0.0033 | 0.0001 | 0.0008 | 0.0007 | 0.0010 |

mg/L = milligrams per liter

Note: Background groundwater quality was calculated using data for samples from wells G-35, HC-4A, HC-4B, HV-1, HV-2, P-899, RP-2A, RP-2B, RP-2C, RP-3A, RP-3B, and Sycamore Spring.

10.4.1 Facilities Area Recharge Water Quality

Potential Project-related recharge within and immediately adjacent to the particle tracking area located outside the capture zone will be a mixture of drain-down water from the Dry Stack Tailings Facility and water infiltrating from the flow-through drains system. The overall quality of the recharge is therefore expected to be proportionate to the quality of the individual sources and their respective rates.

The drain-down rate from the entire Dry Stack Tailings Facility will reach a maximum of 13.56 ac-ft/yr during years 18 through 22 of Project operations (AMEC, 2009). Since approximately 74-percent of the Dry Stack Tailings Facility is located outside the predicted capture zone, the maximum recharge rate is predicted to be 10.09 ac-ft/yr (Table 10-4). After mine closure, anticipated in year 22, the recharge rate is expected to decrease until reaching zero in approximately 500 years.

The average recharge rate due to infiltration from the flow-through drain system will total 273.5 ac-ft/yr based on average annual precipitation (Tetra Tech, 2010c). Based on the lengths of the various drain segments located outside the capture zone, and the flow rates through those segments (Tetra Tech, 2010c), the infiltration rate from the flow-through drain system is anticipated to average 222.8 ac-ft/yr.

The predicted water quality of the anticipated groundwater recharge from the Dry Stack Tailings facility drain-down and from the flow-through drain system (Tetra Tech, 2010d; Tetra Tech, 2010m) is shown in Table 10-4 as the “combined recharge from the tailings and drains.” The parameter concentrations presented in Table 10-4 for the “combined tailings and drains” recharge were calculated using the maximum drain-down rate from the dry stack tailings of 8.4 gpm (Figure 5-6). Since the drain-down rate from the dry stack tailings will decrease over time, and subsequently comprise less of the total recharge, the quality of the recharge from the “combined tailings and drains” is expected to improve from that shown in Table 10-4.

Table 10-4 Summary of Water Quality Data for Project-Related Sources and Background Groundwater

| Parameter | Recharge from Dry Stack Tailings Drain-Down | Recharge from Flow-Through Drains Infiltration | Combined Recharge from Tailings and Drains | Background Groundwater | |
|--|---|--|--|------------------------|---------|
| | | | | Mean | 95% UCL |
| Rate, ac-ft/yr | 10.09 max. | 222.8 | 232.9 max. | -- | -- |
| Calcium, mg/L | 188 | 8.69 | 18.1 | 63.7 | 73.0 |
| Magnesium, mg/L | 19.61 | 0.88 | 1.86 | 12.4 | 15.7 |
| Sodium, mg/L | 26.5 | 5.29 | 6.40 | 71.8 | 82.9 |
| Potassium, mg/L | 9.35 | 0.83 | 1.28 | 1.6 | 1.9 |
| Bicarbonate, mg/L | 0.909 | | | 277.6 | 316.2 |
| Carbonate, mg/L | | | | 5.9 | 7.1 |
| Total Alkalinity as CaCO ₃ , mg/L | 0.206 | | | 231.7 | 263.2 |
| Chloride, mg/L | 3.98 | 0.88 | 1.04 | 19.4 | 23.1 |
| Sulfate, mg/L | 559 | 6.34 | 35.3 | 111.4 | 139.7 |
| Nitrate + Nitrite as Nitrogen, mg/L | 0.001 | 0.5 | 0.47 | 0.8 | 1.2 |
| Fluoride, mg/L | 2.37 | 0.17 | 0.28 | 0.6 | 0.7 |
| Hardness as CaCO ₃ , mg/L | | | | 228.4 | 268.9 |
| Total Dissolved Solids, mg/L | 810 | 23.7 | 64.9 | 430.4 | 469.3 |
| pH (Lab) , std. units | 5.87 | 7.42 | 7.34 | 8.2 | 8.3 |
| Arsenic, mg/L | ND | 0.0052 | | 0.0073 | 0.0097 |
| Barium, mg/L | 0.017 | 0.0029 | 0.0035 | 0.060 | 0.068 |
| Molybdenum, mg/L | 0.076 | ND | | 0.023 | 0.030 |
| Selenium, mg/L | 0.006 | ND | | 0.0008 | 0.0010 |

ac-ft/yr = acre-feet per year mg/L = milligrams per liter
 UCL = upper confidence limit ND = not detected

Bold = dry stack tailings drain-down water concentrations higher than background groundwater concentrations

For comparison, the mean and 95% UCL for the background groundwater quality are also shown in Table 10-4. The concentrations in the water infiltrating from the flow-through drains were shown not to exceed the mean background groundwater concentrations. The anticipated concentrations of magnesium, potassium, sulfate, fluoride, total dissolved solids, molybdenum and selenium (shown in bold in Table 10-4) in the dry stack tailings drain-down water are higher than those in the background groundwater. However, the anticipated concentrations in the

combined recharge water were below those in the background groundwater for all analyzed parameters.

10.5 Discharge Impact Analysis Conclusions

Particle-tracking model results show that pit dewatering during operations and evaporation from the anticipated post-closure pit-lake will create a groundwater capture zone extending approximately $\frac{3}{4}$ to $1\frac{1}{4}$ miles east, northeast, and southeast of the margin of the Open Pit (Figure 10-2). The groundwater capture zone will include all of the potential Project-related recharge sources except for portions of the Dry Stack Tailings Facility and portions of the flow-through drain system. Groundwater within the capture zone will flow into the pit or into the pit-lake. Therefore, the potential recharge sources located within the capture zone do not have the potential to impact down-gradient groundwater quality.

Portions of the Dry Stack Tailings Facility and portions of the flow-through drain system are located outside the pit capture zone. Particle-tracking simulations show that groundwater recharge from potential Project-related sources located outside the capture zone will generally flow north and northwest beyond the Project area (Figures 10-2 and 10-3).

The quality of the combined recharge from the Dry Stack Tailings Facility and flow-through drain system is anticipated to have concentrations that are below those in the background groundwater for all analyzed parameters. Consequently, the potential Project-related recharge sources are not anticipated to impact the down-gradient groundwater quality. The DIA is therefore appropriately established coincident with the Pollutant Management Area (PMA) as illustrated in the aquifer protection permit (APP) application (Tetra Tech, 2009). Since the down-gradient water quality is not predicted to be altered due to the Project-related recharge, fate and transport modeling was not performed as part of the DIA analysis.

11.0 SUMMARY AND CONCLUSIONS

Extensive hydrogeologic data were analyzed and used to prepare a detailed hydrogeologic conceptual model, a hydrogeologic framework model, and a numerical groundwater flow model of the proposed Rosemont Project. The objective of these models was to predict potential impacts on the hydrologic system from the Project, including groundwater-level lowering (drawdown), surface-water flows, riparian vegetation, springs, and groundwater quality.

11.1 Open Pit

Dewatering of the proposed Open Pit will result in groundwater levels being lowered to approximately 3,020 feet amsl, which is about 2,200 feet below the pre-mining water level in the main Project area. The projected bottom of the pit is 3,050 feet amsl. Dewatering the pit will create drawdown in the regional groundwater system, propagating outward from the Open Pit. Dewatering effects will be most dramatic in the vicinity of the Open Pit, decreasing rapidly away from the pit. Drawdown is predicted to propagate through the groundwater flow system for hundreds of years following the cessation of dewatering.

After dewatering ceases, the Open Pit will naturally refill with water and a pit-lake will form. Due to the high evaporation rate of the Rosemont area, the pit-lake is expected to be a terminal hydraulic sink, with groundwater flowing toward the pit. The equilibrium lake stage (level) was predicted to be 4,279 feet amsl. Flow-through conditions, or a non-terminal pit-lake, would exist should the lake stage reach an elevation of 4,680 feet amsl. However, none of the sensitivity model runs predicted that the lake stage would reach this elevation.

A new steady-state or equilibrium condition in the regional groundwater flow system is anticipated 700-1,000 years after the end of operations and active dewatering. Drawdown 1,000 years into the post-closure period is indicated by the five (5)-foot contour interval shown on Figure 8-13. This drawdown contour is predicted to extend up to 7.5 miles east of the Open Pit and 6.2 miles to the northeast in Davidson Canyon. Simulated monitoring wells indicated that water-level declines would be approximately one (1) foot near upper Cienega Creek, approximately 0.25 feet or less near the Outstanding Arizona Water (OAW) reach in Davidson Canyon, and negligible in lower Cienega Creek. After 1,000 years post-closure, the steady-state groundwater inflow to the pit is anticipated to be 230 gpm. Inflows to the pit during active dewatering were estimated to be up to 500 gpm and a maximum of 311 gpm during the post-closure period.

11.2 Stream Flows

Impacts to stream flows in Davidson Canyon and Cienega Creek during operations were negligible and indiscernible compared to the flow model accuracy. Under post-closure conditions, a total decrease in average annual base flow along Cienega Creek, 1,000 years following the cessation of dewatering, was predicted to be 0.09 cfs, which was less than three (3) percent of the simulated base flow. The predicted flow change in Davidson Canyon was 0.01 cfs in the upper most reach after 1,000 years. However, no losses were simulated in the reach identified as an Outstanding Arizona Water.

Sensitivity analysis results indicated that higher stream flow losses are possible given the uncertainty associated with various model parameters. The most sensitive parameter affecting potential base flow reductions in Davidson Canyon and Cienega Creek was a decrease in recharge in the Project facilities area. This decrease in the Project facilities area recharge resulted in base flow reductions of 8.4 percent and 16.7 percent for Cienega Creek and

Davidson Canyon, respectively. In addition to recharge, pit-lake evaporation was also one of the most sensitive parameters in terms of modeling water-level drawdown.

Drawdown due to the Project can only impact stream flows if there is a hydraulic connection between the stream channels and the regional groundwater system. The complex, local geology along Davidson Canyon and Cienega Creek largely controls where groundwater discharges to the stream channels. Several studies and existing data indicate that the stream channels are largely hydraulically disconnected from the regional groundwater system. However, Davidson Canyon and Cienega Creek were modeled assuming they were hydraulically connected to the regional groundwater system. Although model predictions indicated base flow reductions, changes in flow may not materialize over these reaches depending on the localized geologic controls affecting the stream channels and groundwater system.

11.3 Riparian Vegetation

As with the minor predicted base-flow declines in Davidson Canyon and Cienega Creek, water-level declines in the predictive model indicated a negligible effect on the riparian vegetated areas along Davidson Canyon and Cienega Creek. The predicted change in riparian vegetation evapotranspiration in Davidson Canyon and Cienega Creek was approximately 14 ac-ft/yr or 0.2 percent of the 5,633 ac-ft/yr total. Additionally, these impacts are distant from the Open Pit and would materialize over hundreds of years, potentially giving the riparian vegetation time to adjust to the relatively minor changes in groundwater conditions.

11.4 Local and Regional Springs

Based on the groundwater flow modeling and the interpretation of the available hydrogeologic data, the following conclusions regarding springs in the model study area can be drawn:

- Local springs in close proximity to the Open Pit will likely be affected by pit dewatering. The degree of these impacts will in large part be dependent on whether the local spring source is hydraulically connected to fractures yielding flow to the Open Pit;
- Rosemont Spring will be covered by the Waste Rock Storage Area and will likely have terminated flows;
- Questa Spring is not expected to be impacted during operations, but will likely have reduced or terminated flows in the post-closure period;
- Helvetia Spring is likely to have reduced or terminated flows in the post-closure period, assuming that it has a regional groundwater source;
- The available geologic evidence suggests that Davidson Spring is unlikely to be impacted, but model results indicate flows associated with this spring could be impacted if connected to the regional groundwater flow system; and
- Nogales Spring and Little Nogales Spring are not expected to be impacted.

11.5 Groundwater Quality

Based on the pit dewatering and the formation of terminal pit-lake conditions during the post-closure period, a groundwater capture zone will form around the pit and extend underneath most of the Project facilities. Particle tracking indicated that potentially impacted seepage from facilities within the capture zone will flow back to the Open Pit or pit-lake.

Project facilities not within the predicted capture zone include part of the Dry Stack Tailings Facility and flow-through drains. Flow-through drains pass stormwater from watershed areas up-gradient of the Project facilities to the down-gradient side, mainly passing underneath the Dry Stack Tailings Facility.

Based on the contributing volumes, the water quality of the combined dry stack tailings seepage and potential infiltration due to the flow-through drain system was predicted to have a water quality with lower concentrations of all analyzed parameters than the background groundwater quality. Therefore, the Project is not anticipated to impact the quality of down-gradient groundwater sources. Regardless, down-gradient groundwater monitoring will be performed as part of Arizona's aquifer protection permit (APP) program and contingency plans will be developed should permit conditions be exceeded. An APP application for the Project has been submitted to ADEQ (Tetra Tech, 2009).

11.6 Conclusions

A geologically based numerical flow model was developed to simulate impacts to the regional groundwater flow system associated with the planned Rosemont Project and the development of an Open Pit. A pre-mining, steady-state model was developed and calibrated using existing water level and stream flow measurements. The calibrated pre-mining groundwater flow model was used as the starting condition for a mining-phase model, which modeled the incremental expansion and dewatering of the Open Pit, including the propagation of drawdown through the regional groundwater flow system. Upon cessation of pit dewatering, a post-closure model was developed to simulate pit refilling and its effect on drawdown propagation.

The bedrock units in the proposed Open Pit area have low permeabilities, which result in relatively small groundwater seepage rates during both mining operations and in the post-closure period when a pit-lake is expected to form. As a result, the predicted groundwater level drawdown associated with the Project is relatively small, particularly as it relates to distant ecologically sensitive areas in lower Davidson Canyon and Cienega Creek.

Base flows in Davidson Canyon and Cienega Creek were assumed to be hydraulic connected to the regional groundwater flow system in the groundwater flow model even though studies performed in the area have indicated that these flows are often associated with local geologic controls (e.g., bedrock highs or constrictions of shallow, alluvial flow systems) and not the regional system. Despite the conservative modeling approach, the simulated impacts to these areas were relatively minor and would take hundreds of years to develop.

Sensitivity analyses were performed on the parameters used in the predictive models to reflect potential uncertainty in selected values. Simulation results, however, did not significantly change from the predictive model results.

12.0 REFERENCES

- Anderson, Mary P. and Woessner, William W. (1992). *Applied Groundwater Modeling, Simulation of Flow and Advective Transport*. Academic Press, Inc.
- Anderson, T.W. (1995). *Summary of the Southwest Alluvial Basins, Regional Aquifer System Analysis, South-Central Arizona and Parts of Adjacent States*: U.S. Geological Survey Professional Paper 1406-A, pp. A1-A33.
- Anderson, T.W. (1972). *Electric-analog analysis of the hydrologic system, Tucson basin, southeastern Arizona*: U.S. Geological Survey Water-Supply Paper 1939-C.
- Arizona Department of Environmental Quality (ADEQ) (2008). *Regulatory Review Council Approves ADEQ Standards to Protect Arizona Waters from Pollution*. (News Release dated December 3, 2008).
- Arizona Department of Water Resources (ADWR) (2010a). *Securing Arizona's Water Future, Cienega Creek Basin*.
http://www.azwater.gov/azdwr/StatewidePlanning/RuralPrograms/OutsideAMAs_PDFs_for_web/Southeastern_Arizona_Planning_Area/Cienega_Creek_Basin.pdf;
(Downloaded September 24, 2010)
- ADWR (2010b). Well Registry Web. Online link:
<https://gisweb.azwater.gov/waterresourcedata/WellRegistry.aspx>
- ADWR (2009). *Community Water Systems in the Cienega Creek Basin, 2008 Annual Water Use Reporting Summary*; 4 p.
<http://www.azwater.gov/azdwr/StatewidePlanning/Drought/documents/CCK.pdf> (Downloaded September 27, 2010)
- ADWR (2006). *Arizona Water Atlas, Volume 3, Southeastern Arizona, Section 3.3 Cienega Creek Basin*. Draft report. 36 p.
- ADWR (1994). *Arizona Water Resources Assessment, Vol. II, Hydrologic Summary*.
- AMEC Earth & Environmental, Inc. (2009). *Dry Stack Tailings Storage Facility, Final Design Report*. Prepared for Rosemont Copper Company. Report dated April 15, 2009.
- Arizona Water Commission (1972). *Study of the adequacy of the water supply, proposed Empire Ranch Development*. prepared by P.S. Osborne and P.C. Briggs, July 7, 1972, 41 p.
- Bear, J., (1972). *Dynamics of fluids in porous media*. Environmental science series. Elsevier, Amsterdam, 784 p.
- Boggs, J.M. (1980). *Impact of future groundwater development in Cienega Creek area, Pima, Cochise, and Santa Cruz Counties, Arizona*: Master of Science Thesis, Department of Hydrology and Water Resources, University of Arizona, May 2, 1980.

- Bota, L. (1997). *Modeling of groundwater flow and surface/groundwater interaction for upper Cienega Creek basin*: Master of Science Thesis, Department of Hydrology and Water Resources, University of Arizona, July 25, 1997.
- Call & Nicholas Inc., (2010). *Dewatering Plans for the Proposed Rosemont Open Pit Mine*. Technical Memorandum to Fermin Samorano, Rosemont Copper Company. Technical Memorandum Dated March 11, 2010.
- Chong-Diaz, D., (1995). *Modeling of stream aquifer interaction in lower Cienega Creek basin using a finite element technique*: Master of Science Thesis, Department of Hydrology and Water Resources, University of Arizona, May 1995.
- Council, Gregory W. (1999). A Lake Package for MODFLOW (LAK2), Documentation and User's Manual Version 2.2, 137 p.
- CTECH Development Corporation (2010). *Mining Visualization System (MVS) Software*. Kaneohe, HI.
- Cooper, H.H. and C.E. Jacob, 1946. *A generalized graphical method for evaluating formation constants and summarizing well field history*, Am. Geophys. Union Trans., vol. 27, pp. 526-534.
- Dingman, S.L. (1994). *Physical Hydrology*. Upper Saddle River, NJ: Prentice Hall.
- Doherty, J. (2010). PEST: Model-Independent Parameter Estimation, version 12, Watermark Numerical Computing.
- Drewes, H. (1980). *Tectonic map of southeast Arizona*: U.S. Geological Survey, Miscellaneous Investigations Series Map I-1109, 1980.
- Drewes, H. (1972a). *Cenozoic Rocks of the Santa Rita Mountains, Southeast of Tucson, Arizona*: U.S. Geological Survey Professional Paper 746, 66 p.
- Drewes, H. (1972b). *Structural Geology of the Santa Rita Mountains, Southeast of Tucson, Arizona*. U.S. Geological Survey Professional Paper 748. 35 p.
- Drewes, H. (1971). *Mesozoic Stratigraphy of the Santa Rita Mountains, Southeast of Tucson, Arizona*: U.S. Geological Survey Professional Paper 658-C, 1971, 81 p.
- Ellett, W.J., (1994), *Geologic controls on the occurrence and movement of water in the lower Cienega Creek basin*: Master of Science Thesis, Department of Hydrology and Water Resources, University of Arizona, December 16, 1994.
- Ferguson, C.A. (2009). *Bedrock Geologic Map of the Northern Part of the Empire Ranch 7 ½' Quadrangle, Pima County, Arizona*: Arizona Geological Survey Open-File Report OFR-09-05, scale 1:24,000.
- Ferguson, C.A., Youberg, A., Gilbert, W.G., Orr, T.R., Richard, S.M. and Spencer, J. (2001). *Geologic Map of the Mount Fagan 7.5' Quadrangle, Eastern Pima County, Arizona*. Arizona Geological Survey Digital Geologic Map 11. November 2001.

- Ferguson, C.A. Johnson, B.J., Pearthree, P.A., Spencer, J.E., Shipman, T.C., and Cook, J.P., (2009), *Geologic map of the Helvetia 7.5' quadrangle, eastern Pima County, Arizona*: Arizona Geological Survey Open-File Report 09-06 (OFR 09-06), September 2009.
- Finnell, T.L. (1971) *Preliminary geologic map of the Empire Mountains quadrangle, Pima County, Arizona*: U.S. Geological Survey Open-File Report 71-0106.
- Freethy, G.W. and T.W. Anderson (1986). *Predevelopment hydrologic conditions in the alluvial basins of Arizona and adjacent parts of California and New Mexico*: USGS Hydrologic Investigations Atlas-HA664.
- Geraghty & Miller, Inc. (1970). *Ground water report, Empire Ranch property, Pima and Santa Cruz Counties, Arizona*: Report No. 70, July 1970.
- Grahn, Howard, 1995. *A Hydrogeochemical Evaluation of the Lower Cienega Creek Sub-basin, Pima County, Arizona*. Thesis, University of Arizona, Department of Hydrology and Water Resources.
- Harshbarger and Associates (1975). *Analysis of groundwater development program in the Empire Ranch area: preliminary draft report*. Prepared for Anamax Mining Company, July 7, 1975.
- Horton, J.L., Kolb, T.E., and Hart, S. (2001). *Physiological Response to Groundwater Depth Varies Among Species and with River Flow Regulation*. Ecological Applications, Vol. 11, p. 1046-1059.
- Harris Environmental Group, URS Corporation and Ducan & Associates (2000). *Riparian Vegetation Mapping and Classification, Sonoran Desert Conservation Plan – Final Report*. Prepared for Pima County Government. December 2000.
- HydroGeoLogic, Inc. (2010). *MODFLOW-SURFACT Software (Version 3.0)*. Herndon, Virginia, HydroGeoLogic, Inc. 548 pp.
- Johnson, B.J., and Ferguson, C.A., 2007, *Geologic map of the Rosemont area, northern Santa Rita Mountains, Pima County, Arizona (DGM-59)*: Arizona Geological Survey, January 2007.
- Knight, E.L. (1996) *A water budget and land management recommendations for upper Cienega Creek basin*: Master of Science Thesis, Department of Hydrology and Water Resources, University of Arizona.
- Leenhouts, J.M., Stromberg, J.C., and Scott, R.L. (2006). *Hydrologic requirements of and consumptive ground-water use by riparian vegetation along the San Pedro River, Arizona*: U.S. Geological Survey Scientific Investigations Report 2005-5163.
- Long, J., Remer, J., Wilson, C., and Witherspoon, P. (1982). *Porous media equivalents for networks of discontinuous fractures*. Water Resources Research, 18(3): p. 645-658.
- Maddock III, T. and K.J. Baird (2003). *A riparian evapotranspiration package for MODFLOW-96 and MODFLOW-2000*: University of Arizona Department of Hydrology and Water Resources, Research Laboratory for Riparian Studies, HWR No. 02-03.

- Mason, D.A., and Bota, L. (2006). *Regional groundwater flow model Tucson Active Management Area, Tucson, Arizona: Simulation and application*. Arizona Department of Water Resources Model Report No. 13.
- Maxey, G.B. and Eakin, T.E., (1949). *Groundwater in the White River Valley, White Pine, Nye, and Lincoln counties, Nevada*. Water Resources Bulletin No. 8, State of Nevada, Office of the State Engineer.
- Merritt, Michael L. and Konikow, Leonard F. (2000). *Documentation of a Computer Program to Simulate Lake-Aquifer Interaction Using the MODFLOW Ground-Water Flow Model and the MOC3D Solute-Transport Model*, U.S. Geological Survey Water-Resources Investigations Report 00-4167
- Montgomery & Associates, Inc. (M&A) (2010a). *REVISED REPORT - Groundwater Flow Modeling Conducted for Simulation of Proposed Rosemont Pit Dewatering and Post-Closure. Rosemont Project , Pima County, Arizona*. Prepared for Rosemont Copper Company. Report dated August 30, 2010.
- M&A (2010b). *Comparison of Natural Fluctuation in Groundwater Level to Provisional Drawdown Projections, Rosemont Mine*. Prepared for Rosemont Copper Company. Technical Memorandum to Jamie Sturgess (Rosemont Copper Company). Technical Memorandum dated March 1, 2010.
- M&A (2009a). *Results of Phase 2 Hydrogeologic Investigations and Monitoring Program, Rosemont Project, Pima County, Arizona*. Prepared for Rosemont Copper Company. Report dated February 26, 2009.
- M&A (2009b). *Groundwater Flow Modeling Conducted for Simulation of Proposed Rosemont Pit Dewatering and Post-Closure. Rosemont Project , Pima County, Arizona*. Prepared for Rosemont Copper Company. Report dated October 28, 2009.
- M&A (2009c). *Analysis of Long-Term, Multi-Well Aquifer Test – November 2008 through January 2009, Rosemont Project, Pima County, Arizona*. Prepared for Rosemont Copper Company. Report dated October 28, 2009.
- M&A (2009d). *Results of Drilling, Construction, and Testing of Four Pit Characterization Wells, Rosemont Project*. Prepared for Rosemont Copper Company. Report dated August 7, 2009.
- M&A (2009e). *Groundwater Flow Modeling Conducted for Simulation of Rosemont Copper's Proposed Mine Supply Pumping, Sahuarita, Arizona*. Prepared for Rosemont Copper Company. Report dated April 30, 2009.
- M&A (1985). *Water Adequacy Report, Stage One Development, Empirita Ranch Area, Pima County, Arizona*.
- Oppenheimer, J.M., and Sumner, J.S., (1980), *Depth to bedrock map, basin and range province, Arizona*: University of Arizona, Laboratory of Geophysics, Scale 1:1,000,000.
- Pima Association of Governments (PAG) (2010). *Pima County's Cienega Creek Natural Preserve; Surface Water and Groundwater Monitoring Project – PAG Annual Report*;

- Fiscal Year 2008 - 2009*. Prepared for the Pima County Regional Flood Control District. Dated January 2010.
- PAG (2005). *Unique Waters Nomination – Davidson Canyon*. Dated December 2005.
- PAG (2003a). *Contribution of Davidson Canyon to Baseflows in Cienega Creek*. Dated November 2003.
- PAG (2003b). *Geologic Influences on the Hydrology of Lower Cienega Creek*. Dated December 2003.
- PAG (1998). *Summary And Evaluation Of Cienega Creek Surface Water And Groundwater Monitoring Program. Final Report*. Prepared for Pima County Flood Control District, Volume I, February 1998, 138 pp.
- Pima County (2000) *Springs in Pima County, Sonoran Desert Conservation Plan*, May 2000. Draft Memorandum dated May 23, 2000. Prepared for the Pima County Board of Supervisors.
- Pima County Department of Transportation and Flood Control District, 1993. *Hydrologic Availability and Use of Streamflows at the Cienega Creek Natural Preserve, Pima County, Arizona*. Prepared for an in-stream flow permit from Arizona Department of Water Resources (Application No. 33-89090).
- Pool, D.R., and Dickinson, J.E., (2007), *Ground-water flow model of the Sierra Vista Subwatershed and Sonoran portions of the Upper San Pedro Basin, southeastern Arizona, United States, and northern Sonora, Mexico*: U.S. Geological Survey Scientific Investigations Report 2006-5266. 48 pp.
- Pollock, D.W. (1994). *User's Guide for MODPATH/MODPATH-PLOT, Version 3: A particle tracking post-processing package for MODFLOW, the U. S. Geological Survey finite-difference ground-water flow model*. U. S. Geological Survey Open-File Report 94-464.
- Prudic, D.E., Konikow, L.F., and Banta, E.R. (2004). A new stream-flow routing (SFR1) package to simulate stream-aquifer interaction with MODFLOW-2000: U.S. Geological Survey Open-File Report 2004-1042, 95 p.
- Roudebush, Eric Mitchell (1996), *The Influence of Bedrock on Perennial Streamflow in the Upper Cienega Creek Basin*, Pima County, Arizona, May 1996, M.S., Hydrology, advisor: L.G. Wilson.
- Shah, N., M. Nachabe and M. Ross (2007). *Extinction Depth and Evapotranspiration from Ground Water under Selected Land Covers*. Ground Water, vol. 45, no. 3, pp. 329 – 338.
- Shafroth, D.W., (1968), *Stratigraphy of some Cretaceous formations of southeastern Arizona*: Southern Arizona Guidebook III, Arizona Geological Society, March 1, 1968.
- Slack, Donald C. and Martin, Edward C. (1999). *Irrigation Water Requirements Of Wine Grapes In The Sonoita Wine Growing Region Of Arizona*. University of Arizona, College of

- Agriculture 1999 Wine Grape Research Report, Editors: *Linda Nunan*, and *Michael W. Kilby*, November 1999. http://ag.arizona.edu/pubs/crops/az1148/az1148_3.pdf
- Spencer, J.E., Ferguson, C.A., Richard, S.M., Orr, T.R., Pearthree, P.A., Gilbert, W.G., and Krantz, R.W. (2001). *Geologic map of the Narrows 7½" quadrangle and the southern part of the Rincon Peak 7½" quadrangle, eastern Pima County, Arizona* (DGM-10): Arizona Geological Survey, September 2001, revised May 2002.
- Tetra Tech (2010a). *Davidson Canyon Hydrogeologic Conceptual Model and Assessment of Spring Impacts*. Prepared for Rosemont Copper Company. Report Dated July 2010.
- Tetra Tech (2010b). *Site Water Management Update, Volumes 1-5, Rosemont Copper Project*, Report Dated April 2010.
- Tetra Tech (2010c). *Rosemont Infiltration Analysis - Revised*. Technical Memorandum to Kathy Arnold (Rosemont Copper Company). Technical Memorandum Dated April 5, 2010.
- Tetra Tech (2010d). *Infiltration, Seepage, Fate, and Transport Modeling Report – Revision 1*. Prepared for Rosemont Copper Company. Report Dated August 2010.
- Tetra Tech (2010e). *Baseline Regulatory (100-Yr) Hydrology and Average-Annual Runoff, Rosemont Copper Project*. Technical Memorandum to Kathy Arnold (Rosemont Copper Company). Technical Memorandum Dated March 4, 2010.
- Tetra Tech (2010f). *Post-Mining Regulatory (100-Yr) Hydrology and Average-Annual Runoff, Rosemont Copper Project*. Technical Memorandum to Kathy Arnold (Rosemont Copper Company). Technical Memorandum Dated March 5, 2010.
- Tetra Tech (2010g). *Hydraulic–Property Estimates*. Technical Memorandum to Kathy Arnold (Rosemont Copper Company). Technical Memorandum Dated July 9, 2010.
- Tetra Tech (2010h). *Hydrogeologic Framework Model*. Technical Memorandum to Kathy Arnold (Rosemont Copper Company). Technical Memorandum Dated July 3, 2010.
- Tetra Tech (2010i). *Groundwater Flow Model Construction and Calibration*. Technical Memorandum to Kathy Arnold (Rosemont Copper Company). Technical Memorandum Dated July 26, 2010.
- Tetra Tech (2010j). *Predictive Groundwater Flow Modeling Results*. Technical Memorandum to Kathy Arnold (Rosemont Copper Company). Technical Memorandum Dated July 30, 2010.
- Tetra Tech (2010k). *Rosemont Groundwater Flow Model Sensitivity Analyses*. Technical Memorandum to Kathy Arnold (Rosemont Copper Company). Technical Memorandum Dated August 17, 2010.
- Tetra Tech (2010l). *Rosemont Geochemical Pit Lake Predictive Model Summary*. Technical Memorandum to Kathy Arnold (Rosemont Copper Company). Technical Memorandum Dated August 24, 2010.

- Tetra Tech (2010m). *Potential Source Volumes and Chemical Makeup for Area-Wide Fate and Transport Modeling – Rosemont Copper Project*. Technical Memorandum to Kathy Arnold (Rosemont Copper Company). Technical Memorandum Dated August 23, 2010.
- Tetra Tech (2009). *Aquifer Protection Permit Application – Rosemont Copper Company. Submitted to the Arizona Department of Environmental Quality. February 2009.*
- Theis, C.V., 1935. *The relation between the lowering of the piezometric surface and the rate and duration of discharge of a well using groundwater storage*, Am. Geophys. Union Trans., vol. 16, pp. 519-524.
- Travers, B.C., and Mock, P.A., (1984), *Groundwater modeling study of the upper Santa Cruz basin and Avra Valley in Pima, Pinal and Santa Cruz Counties, Southeastern Arizona*: Arizona Department of Water Resources model report (unnumbered).
- United States Department of Agriculture (USDA) (1986). *Urban Hydrology for Small Watersheds*. Technical Release 55 (TR-55) Second Edition. Natural Resources Conservation Service, Conservation Engineering Division.
- United States Department of Commerce National Climatic Data Center (NCDC, 2009). NCDC Climate Data Online, Santa Rita Exp Range, AZ, COOP ID 027596, May 1950 to February 2010 Daily Precipitation Data. Online link:
<http://cdo.ncdc.noaa.gov/pls/plclimprod/poemain.cdobystn>.
- United States Department of the Interior (USDIO) (2008). *Biological Opinion on Aquatic Species Conservation at the San Pedro Riparian and Las Cienegas National Conservation Areas, Arizona*. Prepared for Field Office Manager, Tucson Field Office, Bureau of Land Management, Tucson, Arizona U.S. Fish and Wildlife Service Memorandum Dated December 31, 2008.
- United States Geological Survey (USGS) (2010a) National Map Seamless Server, 2010. 1/3" National Elevation Dataset (NED). Online link:
<http://seamless.usgs.gov/website/seamless/viewer.htm>.
- USGS (2010b). Well Data. Online link:
<https://gisweb.azwater.gov/waterresourcedata/GWSI.aspx>
- Wardrop (2005). *Technical Report on the Rosemont Property, Pima County, Arizona*. Prepared for Augusta Resource Corporation.
- Walton, W.C. (1988). *Practical Aspects of Ground Water Modeling – Third Edition*. Worthington, Ohio: National Water Well Association. 587 pp.
- Weight, W.D. and J.L. Sonderegger (2001). *Manual of Applied Field Hydrogeology*. New York: McGraw-Hill. 608 pp.
- WestLand Resources Inc. (WestLand) (2010). *Onsite Riparian Habitat Assessment*. Prepared for Rosemont Copper Company. Report Dated April 2010.
- WestLand Resources, Inc. (2007). *Rosemont Project Mine Plan of Operations*. Prepared for Augusta Resource Corporation. Report Dated July 11, 2007.

Wilson J. L., and Guan, H., (2004). *Mountain-Block Hydrology and Mountain-Front Recharge. Groundwater Recharge in a Desert Environment: The Southwestern United States.* edited by Small, E., 2005. Climate Controls on Diffuse Groundwater Recharge in Semiarid Environments of the Southwestern United States. *Water Resources Research*, Vol. 41, W04012.